MAPPING CLIMATE AND DISTURBANCE REFUGIA FOR CONSERVATION OF WHITEBARK PINE

by

Stephen John Huysman

A thesis submitted in partial fulfillment
of the requirements for the degree

of

Master of Science

in

Biological Sciences

MONTANA STATE UNIVERSITY
Bozeman, Montana

August 2025

ACKNOWLEDGEMENTS

I would like to express my sincere gratitude to my family, friends, and graduate cohort for their unwavering support throughout my master's studies. Thank you to my advisor, Dr. David Thoma, who tirelessly and enthusiastically worked with me developing my research ideas, troubleshooting issues with my analyses, and reviewing my writing. Dr. Danielle Ulrich and Dr. Brian Smithers also contributed their valuable knowledge throughout the process and their feedback on my thesis drafts helped make me a better science communicator. Thank you to Dr. Mike Tercek, who served as unofficial committee member and was a steady source of sage advice about science and navigating life in graduate school. I am appreciative of my lab colleagues Teo Rautu, Jess Harris, Lou Duloisy, Sean Hoy-Skubik, Franklin Alongi, and Katie Sparks for their friendship and camaraderie. Thank you to Kristin Legg for all your work behind the scenes and for constantly finding me new opportunities to advance my scientific and professional development. Lastly, I am grateful for the unwavering support from my wife, Su, whose assistance made it possible to navigate the challenges of graduate school. This work would not be possible without funding from the National Park Service Inventory and Monitoring Program, ORISE fellowship program, the Northern Rockies Conservation Cooperative (NRCC), and the Sara Amasa Madsen Conservation Biology Graduate Scholarship.

TABLE OF CONTENTS

TABLE OF CONTENTS – CONTINUED

TABLE OF CONTENTS – CONTINUED

LIST OF TABLES

Table Page

LIST OF FIGURES

Figure Page

LIST OF FIGURES – CONTINUED

Figure Page

LIST OF FIGURES – CONTINUED

Figure Page

ABSTRACT

Whitebark pine (*Pinus albicaulis* Engelm.) is a keystone species of montane ecosystems in western North America, where it plays an important role supporting wildfire and other vegetation. It is experiencing a rapid decline primarily due to white pine blister rust (*Cronartium ribicola* J.C.Fisch.), an invasive fungal disease, as well as other threats including increasing wildfire severity and frequency as well as climate change which exacerbates these threats. To protect this iconic tree species, land managers need to understand how climate influences these threats across the species' range and identify locations where conservation efforts are likely to succeed.

My research analyzes climate impacts on threats to whitebark pine across multiple spatial scales. Broad-scale models are used to predict wildfire ignition danger and white pine blister rust infection hazard across large areas of the western United States. At fine scales, I used a high-resolution water balance model to identify small, favorable planting sites that may offer protection from projected drought stress for seedlings.

My findings reveal that climate strongly influences both wildfire ignition danger and white pine blister rust infection, with specific moisture and temperature conditions promoting these threats. Projections indicate that climate change will generally increase the risk for these disturbances, although patterns of this change vary geographically. The high-resolution water balance analysis reveals that despite climate projections showing extreme drought, small-scale microrefugia exist where local terrain and soil features could provide protection from drought stress.

This work provides valuable, climate-informed tools for whitebark pine conservation. The models and maps can help land managers identify areas projected to face lower long-term risks from both wildfire and white pine blister rust. These refugia can be targeted for conservation actions, such as planting disease-resistant seedlings, improving the likelihood of successful establishment and survival, thus enhancing efforts to conserve this iconic species in a changing climate.

INTRODUCTION

Whitebark pine and climate change

Whitebark pine (*Pinus albicaulis* Engelm.) is a foundational and keystone species of high-elevation ecosystems in the Western U.S. and is prized for its ecological services as a nurse tree for other high-elevation plant species, as an important source of protein and fat for wildlife such as the grizzly bear (*Ursus arctos horribilis* Linnaeus, 1758), and for its aesthetic value to outdoor recreationists (Tomback et al., 2001). Climate has a pervasive influence on the fate of whitebark pine at all of its life stages from germination through establishment, growth, and reproduction. It grows in high-elevation subalpine environments where plant growth is often temperature-limited, but its growth and development are influenced by other aspects of climate as well. Additionally, its primary agents of mortality have known links to climate.

In the past half-century, whitebark pine has experienced a precipitous decline due to agents of mortality such as white pine blister rust (*Cronartium ribicola* J.C.Fisch.), mountain pine beetle (*Dendroctonus ponderosae* Hopkins), and wildfire. As of 2016, over half of all standing whitebark pine are dead (Goeking and Izlar, 2018). Due to this rapid decline, and the ongoing threats the species faces, it was given threatened status under the Endangered Species Act in 2023 (Levin, 2022).

White pine blister rust has become the primary biotic driver of mortality in whitebark pine because it attacks trees before they reach reproductive age as well as reducing the reproductive capacity of older trees through "topping" — die-back of the upper crown of trees where seed cones are concentrated (Shanahan et al., 2016). The disease is believed to have optimal windows of temperature and moisture that promote infection. For example,

in the Greater Yellowstone Ecosystem (GYE) infection is driven by an interaction between temperature and humidity during August and September, when the disease transmits from alternate hosts to whitebark pine (Thoma et al., 2019b). Due to the existential threat posed by white pine blister rust, outplanting of white pine blister rust resistant seedlings has become a primary strategy of whitebark pine restoration efforts (Tomback et al., 2022). When selecting planting sites for these seedlings two scales of potential climate impacts must be considered: the regional climate context and the microclimate that may exacerbate or ameliorate the effects of regional climate change on seedling establishment and growth.

Whitebark pine has a complex relationship with wildfire. Recently burned areas are a natural regeneration niche for the species, because wildfire clears the landscape of competing vegetation and its primary dispersal agent Clark's nutcracker (*Nucifraga columbiana* Wilson 1811) selects these areas to cache whitebark pine seeds, where some are left uneaten and able to grow (Lorenz et al., 2011). However, because whitebark pine takes around 50 years to reach cone-bearing age (Tomback et al., 2001), newly established stands are at risk of burning before they are old enough to produce cones and successfully reproduce. Increases in wildfire severity and frequency are projected due to drought and increased fuel aridity (Abatzoglou and Williams, 2016), which threatens the ability of whitebark pine to regenerate.

Other climate-driven disturbance agents of whitebark pine include mountain pine beetle. Outbreaks of mountain pine beetle are accelerated by increases in temperature, where accumulation of growing degree days can lead to semivoltine populations becoming univoltine (Bentz et al., 1991, 2016). In the GYE, climate projections show the potential for widespread mountain pine beetle outbreaks and associated increases in whitebark pine mortality (Buotte et al., 2016). Mountain pine beetle and other climate-driven mortality agents were not addressed in the present study and warrant future research.

Knowledge gaps and rationale for this study

Our ability to effectively manage whitebark pine in the face of climate change is limited by knowledge gaps regarding its sensitivity to climate and climate-driven disturbance agents. While the climatic sensitivities of some of these disturbance agents have been studied, these studies are typically local to regional in scope, preventing broader scale assessment of the impacts of climate change or requiring extrapolation of the model to make inferences in other regions. For instance, the climatic drivers of white pine blister rust infection in whitebark pine have been studied in the GYE (Thoma et al., 2019b) and the Sierra Nevada in California (Dudney et al., 2021), with somewhat divergent conclusions. However, to my knowledge, similar studies have not been conducted across broader scales in the Western US and Canada despite white pine blister rust's widespread distribution in North America and presence virtually everywhere that whitebark pine is found (United States Forest Service).

A common approach to understand any species's potential responses to climate change is to use a species distribution model (SDM). This technique models a bioclimatic envelope for the species based on the climate across its current distribution and use the model to estimate changes to its distribution based on climate projections. In the GYE, this approach revealed the potential for large reductions in suitable habitat for whitebark pine by the end of the century (Chang et al., 2014). However, the SDM approach has limits. For one, SDMs assume that species are in equilibrium with the climate in their current distribution; however, this assumption has flaws when considering a slow-growing species such as whitebark pine which can live 400 to 1,000 years, and therefore an individual tree may have become established under a far different climate from what it experiences today (Tomback et al., 2001). Additionally, SDMs only consider the bioclimatic envelope for whitebark pine, but not the climate sensitivities for its biotic (e.g., white pine blister rust) and abiotic (e.g., wildfire) disturbance agents, nor how climate change may alter interactions between whitebark pine

and those disturbances.

Scale mismatches between existing climate data and spatial and temporal scales that influence whitebark pine and its mortality and disturbance agents also presents challenges for effective management. The relatively coarse spatial scale of gridded climate data products exceeds the physical scale of individual organisms and can result in a mismatch between the scale of climate predictors and biological responses (Moudrý et al., 2023). Scale has been described as the "central problem in ecology" (Levin, 1992), and failure to account for spatial scale may be a source of apparent discord between ecological studies that are actually in agreement (Hernández, 2020). For example, SDMs are sensitive to the scale of climate data used to train them and make projections, with markedly different estimates of habitat suitability predicted depending on the scale of climate data used as input (Franklin et al., 2013). Previous studies relied on gridded climate data at resolutions of 800 m or greater, thus the fine scale responses to climate change mediated by site characteristics like slope, aspect, or soil properties were not explicitly considered.

Fire in whitebark pine stands has historically been less abundant than in lower elevation forests where fuel loads are higher. However, the thin bark of whitebark pine makes it susceptible to even low-intensity fires. This makes the geography of wildfire in the future especially important for determining suitable locations for planting rust resistant seedlings.

Thesis structure

This research aims to improve whitebark pine conservation efforts and management strategies under a changing climate by quantifying climate-disturbance relationships at multiple spatial scales and making projections of how these relationships might change under future climates. The following three chapters present manuscripts prepared for submission to a peer-reviewed journal documenting individual research projects aiming to quantify relationships between whitebark pine, some of its major threats, and climate change.

Chapter 2 presents a wildfire ignition danger rating system for the Middle Rockies ecoregion based on accumulation of dryness over short (three-day) periods is presented. The performance of the various climate indicators accumulated over varying widths of time to predict wildfire ignitions in the ecoregion is assessed. Percentiles of three-day rolling sum of climatic water deficit (CWD), a measure of dryness that indicates drought stress in plants, and vapor pressure deficit (VPD), a direct measure of atmospheric dryness, were the top performing classifiers of wildfire ignitions. Projections of future wildfire danger in the Middle Rockies Ecoregion are made with the goal of identifying wildfire refugia for whitebark pine — locations where wildfire potential is low enough to allow whitebark pine seedlings planted today to establish and reach reproductive maturity with low chance of mortality from wildfire.

Chapter 3 analyzes the broad-scale climatic drivers of white pine blister rust infection across whitebark pine's range in the contiguous United States. A novel dataset was assembled for this study consisting of long-term white pine blister rust monitoring data that assesses disease presence in whitebark pine from multiple public land management agencies. Spatially-explicit models estimating probability of white pine blister rust infection were fit using climate averages during August and September. Projections of future disease hazard across whitebark pine's distribution in CONUS were made.

Finally, chapter 4 presents a high-resolution water balance model that can be used as a tool to identify suitable microclimates for planting WPB. The high-resolution water balance model downscales coarser climate data to a 1 m resolution using topoedaphic factors (slope, aspect, and soil water holding capacity) to provide high-resolution plant-relevant measures of climate. The model was used for a case study at Burroughs Creek in Shoshone National Forest, Wyoming, USA where whitebark pine seedlings were planted in 2024 following wildfire. The model was able to identify small-scale terrain features that could minimize future drought stress, even when coarser-scale climate assessments were unfavorable. These features are evidence of climatic microrefugia — terrain features that create locally favorable climates

that are decoupled from unfavorable regional climate (Dobrowski, 2011).

The work presented here provides tools to understand the potential responses of whitebark pine and several of its major disturbance agents at biologically relevant scales to inform conservation strategies under a changing climate.

WILDFIRE REFUGIA FOR WHITEBARK PINE IN THE GREATER YELLOWSTONE ECOSYSTEM

Contribution of Authors and Co-Authors

Manuscript in Chapter 2

Author: Stephen John Huysman

Contributions: Implemented the study design. Developed scripts used for analysis. Drafted the manuscript.

Co-Author: David P. Thoma

Contributions: Conceived initial study design and consulted in direction of analysis. Reviewed manuscript drafts.

Co-Author: Mike Tercek

Contributions: Developed gridded water balance dataset used for this analysis. Consulted in implementation and troubleshooting of methods.

Co-Author: Danielle E. Marias Ulrich

Contributions: Reviewed manuscript drafts.

Co-Author: Brian V. Smithers

Contributions: Provided review of methodology. Reviewed manuscript drafts.

Manuscript Information

Stephen J. Huysman, David P. Thoma, Mike Tercek, Danielle E. M. Ulrich, Brian V. Smithers

Status of Manuscript:
_X_ Prepared for submission to a peer-reviewed journal
____ Officially submitted to a peer-reviewed journal
____ Accepted by a peer-reviewed journal
____ Published in a peer-reviewed journal

Abstract

A wildfire ignition danger rating system for the Middle Rockies ecoregion is presented. Percentiles of rolling sums or means of climate indicators were evaluated for their ability to predict ignitions at a range of rolling window widths from 1 to 31 days prior to ignition. Percentiles of 3-day rolling sums of Climatic Water Deficit (CWD) and Vapor Pressure Deficit (VPD) were the best performing predictors of wildfire ignition (days with or without wildfire ignition) in the Monitoring Trends in Burn Severity (MTBS) database. We rated wildfire ignition danger by modeling the proportion of wildfires that ignited when CWD or VPD were at or below certain percentiles and comparing current local conditions to this proportion to determine if conditions on a given day are dry enough to burn. We project wildfire ignition danger on forest cover in the Greater Yellowstone Ecosystem to identify the potential for persistence of wildfire refugia as potential management targets for tree species such as whitebark pine (*Pinus albicaulis* Engelm.). These projections show increased wildfire danger across the GYE by end-century (2070–2099) in both RCP4.5 and RCP8.5 emissions scenarios and the persistence of wildfire refugia is only likely under the lower-emissions RCP4.5 scenario. We compare the timing of ignition of the historical Valley Complex wildfire in the Middle Rockies ecoregion to the percentile of 3-day rolling sum of CWD and indices of the widely used National Fire Danger Rating System (NFDRS) and show that our approach compares favorably with the NFDRS.

Introduction

Much of the landscape of the western United States is shaped by wildfire, which alters the composition of plant communities, affects wildlife habitat, and can threaten human life and communities. Wildfire severity and frequency have increased in recent years as a result of anthropogenic climate change (Abatzoglou and Williams, 2016; Boer et al., 2017; Littell

et al., 2016; Running, 2006). Increased frequency and severity of drought conditions drives these shifts, through changes such as earlier snow melt (Tercek and Rodman, 2016) and increased summer temperatures (Running, 2006). In addition to these direct links to climate, wildfire occurrence and severity also depend on non-climatic factors such as fuel load and ignition (McKenzie and Littell, 2017).

Understanding drivers of wildfire danger over short and long time scales is necessary for managing plant and animal species and implementing wildfire management activities such as prescribed burns and fire restrictions. Short-term wildfire danger impacts decision making such as allocation of resources for fire preparedness and response, prescribed burn windows, land use restrictions to minimize wildfire ignition risks, and evacuation plans for inhabited areas. Over longer periods of time, wildfire can result in extensive changes to the landscape such as changes in plant community structure such as converting to different forest types under certain conditions (Coop et al., 2020). At the same time, most ecosystems of the western US require fire regimes of a certain intensity and frequency to maintain their dominant vegetation long-term (Agee, 1998; Paysen et al., 2000).

Long-term wildfire danger models can inform management activities such as reforestation with long-lived tree species, such as whitebark pine (*Pinus albicaulis* Engelm.). Whitebark pine can take 50 years or longer to reach mature, cone-bearing age (Tomback et al., 2001), so successful restoration plantings require that the trees avoid wildfire-related mortality for at least that long. Current whitebark pine planting efforts often target recently burned areas, with the implicit assumption that these areas will remain suitable into the future (Keane et al., 2012). However, climate projections show increasing aridity and wildfire frequency which limits windows of time for establishment, threatening the persistence of even fire-adapted tree species (Jackson et al., 2009; Turner et al., 2022). Production of whitebark pine seedlings for restoration is an expensive and labor-intensive process, requiring identifying white pine blister rust resistant parent trees, collecting seeds, growing seedlings in a nursery, screening

seedlings for rust resistance, and growing them for at least 2 years before outplanting, with a cost of approximately $1,980 to $2,400 USD per ha planted (Tomback, 2011; Tomback et al., 2022). Optimal use of this limited and costly resource can be facilitated by selecting sites that are less likely to burn before these seedlings reach reproductive age.

Climate directly affects wildfire ignition potential by controlling fuel moisture content, and also has an indirect long-term role by shaping plant communities and fuel loads (Littell et al., 2016). Wildfires occur when there is simultaneously dry fuel and an ignition source (e.g., a lightning strike); thus, wildfire occurrence in the western U.S. may be limited by either fuel or climate. A gradient of climatic conditions across the region determines fuel accumulation and fuel moisture, resulting in moisture-limited systems with ample fuel but conditions often too wet to burn (e.g., Middle Rockies, Pacific Northwest) and fuel-limited systems producing insufficient fuel for large fires even when dry conditions exist (e.g., arid southwestern US) (Littell et al., 2018; Meyn et al., 2007). Surface fires are primarily carried by dead fuels, and metrics averaged over windows of time longer than it takes these fuels to dry may have weaker correlation with ignition (Riley et al., 2013). Large wildfires develop when there is spatial continuity of available fuel and conditions dry enough to burn (Miller and Urban, 2000). Atmospheric dryness plays a role in large wildfire formation, by creating burnable conditions even in mesic forests that might otherwise act as barriers to spread (Cawson et al., 2024).

Currently, managers predict wildfire risk to inform decision making using wildfire danger rating systems such as the National Fire Danger Rating System (NFDRS). The NFDRS was first created in 1972 to standardize estimates of wildfire potential across the U.S. and has supported operational decision making around wildfire danger for over 50 years (Jolly et al., 2024; Zacharakis and Tsihrintzis, 2023). The NFDRS incorporates modules for weather, fuel moisture models, and fuel models to estimate indices of wildfire danger ignition—ignition component (IC), spread component, burning index (BI), and energy release component

(ERC)—which are integrated to create a severe fire danger index (SFDI) that indicates potential for extreme fire events (Jolly et al., 2024, 2019). These indices are used separately to assess danger from different aspects of fire behavior such as ignition potential or intensity, or together as the SFDI which provides a simple index to interpret overall fire risk which is shared with the public as "low" to "severe" fire danger signs posted on US National Forest lands. Historically, the NFDRS required complex manual inputs and was sensitive to parameter calibration, sometimes requiring field measurements to optimize performance (Jolly et al., 2024). While the NFDRS was originally intended for use with point weather station data, recent improvements to the NFDRS have removed the need for manual inputs of fuel dryness and attempt to make the system more compatible with gridded climate data allowing for broader and spatially explicit assessments of fire danger. Despite these improvements, spatially explicit estimates of fire potential using widely available gridded climate datasets remain computationally intensive (Farguell et al., 2025).

The climatic water balance provides biologically relevant indicators of plant productivity and water availability that have demonstrated associations with plant distributions across spatial scales (Stephenson, 1998, 1990), plant productivity (Thoma et al., 2016, 2020), plant water need (Thoma et al., 2019a), amphibian occupancy and wetland hydroperiod (LaFrance et al., 2024; Ray et al., 2022), and streamflow (Thoma et al., 2020). Climatic water deficit (CWD), a measure of evaporative demand not met by available water, has been demonstrated to be a strong predictor of wildfire ignitions in the Southern Rockies ecoregion, where percentiles of 14-day rolling sums of measures of atmospheric dryness (climatic water deficit (CWD) and vapor pressure deficit (VPD)) were used to develop a wildfire ignition danger rating system for the ecoregion (Thoma et al., 2020). This system of assessing wildfire ignition danger is analogous to the IC of the NFDRS. Both CWD and VPD had similar performance as binary classifiers of ignition—that is, categorizing days into one of two outcomes, wildfire ignition occurred or no ignition occurred based on thresholds

of percentile of 14-day rolling sums of the variables. Thoma et al. (2020) recommend the use of CWD over VPD in this region because of its ease of calculation and availability in gridded climate datasets for historical and projected time periods such as the National Park Service 1 km gridded water balance product (Tercek et al., 2023, 2021b). Wildfire ignition danger is determined by comparing the rolling sum of CWD on a given day to the historical distribution of rolling sums of CWD on days that a wildfire ignition occurred. As such, it is a system that compares CWD on a given day to conditions that were actually dry enough to burn. The climate-driven nature of this ignition danger rating system facilitates the creation of long-term projections of wildfire ignition danger compared to other commonly used wildfire danger rating systems such as the NFDRS, which requires inputs that are either not available or difficult to simulate for future time periods such as wind speed and non-climatic inputs related to fuel load and moisture. In addition, its use of water balance variables that are consistent with other biophysical processes facilitates interpretation more easily than less biologically relevant indicators of fire danger such as the energy release component (ERC).

This research builds on a straightforward wildfire ignition danger rating system developed for the Southern Rockies ecoregion (Thoma et al., 2020). It evaluates methods applied in the Middle Rockies ecoregion based on Thoma et al. (2020). In that study, wildfire ignition danger is determined based on dryness which is estimated as the percentile of rolling sum of climatic water deficit. We examine the assumption made by Thoma et al. (2020) that 14-day rolling windows of measures of atmospheric dryness (CWD or VPD) optimally predict wildfire ignitions and examine rolling window widths from 1 to 31 days. We also modify the percentile ranking algorithm used by Thoma et al. (2020) to improve sensitivity of the system to low levels of dryness and spatial continuity of mapped projections of wildfire ignition danger. We assess the performance of our system versus the NFDRS by comparing the timing of ignition of the historical Valley Complex (Coyote) fire with the percentile of rolling sum of CWD and NFDRS indices. Finally, we create maps of wildfire ignition danger that can be

used in conservation planning, such as selection of sites that could serve as wildfire refugia for whitebark pine.

Methods

Climate, fire, and vegetation data

Historical wildfire occurrence data in the Middle Rockies ecoregion (Omernik, 1987) from 1984 through 2020 were retrieved from the Monitoring Trends in Burn Severity (MTBS) database which collects information on wildfires occurring in the United States that are 404.5 hectares (1000 acres) or larger and provides polygons for each wildfire showing the extent of burned area (Eidenshink et al., 2007). A total of 417 fires were included in the analysis, ranging in size from 405.9 to 228,051.3 hectares.

Vegetation cover for each fire polygon was determined using the 2020 "Existing Vegetation Type" (EVT) from the LANDFIRE database (Rollins, 2009). For each fire polygon in the MTBS dataset, the statistics tool in QGIS (QGIS Development Team, 2024) was used to determine majority EVT by pixel count. Each fire polygon was classified as "forest" cover type if the majority of pixels in the polygon were "Tree" (n = 110) cover type or "non-forest" (n = 307) cover type if the majority of pixels were "Herb", "Sparse", or "Shrub". This method assumes that the cover type before the wildfire was the same as the EVT in the 2020 LANDFIRE database. Thus, in the present analysis, cover type was assumed to be unchanged before and after fire and no wildfire-driven conversion of cover type occurred (Coop et al., 2020).

We compared climate and water balance variables representing energy and moisture as predictors of wildfire ignition (Table 1). For each fire polygon, a centroid point was determined using the "pole of inaccessibility" method in QGIS to ensure that the centroid point was inside the burned polygon. Daily time series for historical climate variables representing measures of heat and moisture from 1979 through 2020 at 4 km resolution (Average temperature

Indicator	Abbreviation	Units	Sum/mean	Source	Note
Average temperature	T	°C	mean	gridMET	
Average relative humidity	RH	%	mean	gridMET	
Average relative dryness	RD	%	mean	Derived	RD = 100 − RH
Vapor pressure deficit	VPD	kPa	mean	gridMET	
Actual evapotranspiration	AET	mm	sum	NPS	
Climatic water deficit	CWD	mm	sum	NPS	
Soil moisture	SOIL	mm	mean	NPS	
Soil water deficit	SWD	mm	mean	Derived	SWD = WHC − SOIL
Rain	RAIN	mm	sum	NPS	
Growing degree days	GDD	°C	sum	Derived	Base temperature of 5.5 °C

Table 1. Indicators of climate assessed as classifiers of ignition and the abbreviations used to refer to them in this work. Each indicator was normalized to the local historical conditions of the wildfire centroid pixel by taking the percentile of rolling sums or means of the variables. Rolling sums were calculated for flux variables which describe movement of water and rolling means were calculated for state variables which describe the current conditions of the system. Rolling calculations were made at windows of 1, 3, 5, 7, 9, 11, 14, 21, and 31 days. The data source of the variable is indicated as gridMET if from the gridMET or MACA datasets, NPS if from the NPS 1 km Gridded Water Balance product, or derived if calculated *ad hoc* for this analysis from variables sourced from one those two data sets.

(T, $^{\circ}C$), average relative humidity (RH, $\%$), and vapor pressure deficit (VPD, Pa) were retrieved from the gridMET gridded climate dataset (Abatzoglou, 2013) for each centroid point determined for each historical wildfire. The complement of RH (100 - RH) was used to determine Relative Dryness (RD, $\%$), to allow direct comparison of magnitude with other indicators. Historical water balance variables actual evapotranspiration (AET, mm), climatic water deficit (CWD, mm), soil moisture (SOIL, mm), and rain (RAIN, mm) were obtained from the 1 km National Park Service gridded water balance product (Tercek et al., 2021b), which uses gridMET climate data as inputs. Soil water holding capacity (WHC, mm) for the top 100 cm of the soil profile were obtained from the US Natural Resources Conservation Service Soil Survey Geographic Database (SSURGO) product (Soil Survey Staff, 2024). Soil water deficit (SWD, mm) was calculated as WHC - SOIL. Growing degree days (GDD, $^{\circ}C$) were calculated from gridMET average daily temperature using a base temperature of 5.5 °C, a temperature below which little biological activity occurs (McMaster and Wilhelm, 1997).

Historical climate data were obtained from gridMET to facilitate the creation of long-term projections of fire danger using the Multivariate Adaptive Constructed Analogs (MACA) climate data source (Abatzoglou and Brown, 2012). The MACA dataset is statistically downscaled from General Circulation Models (GCMs) using gridMET historical meteorological data, which allows for seamless comparisons between historical gridMET and future MACA projections without further bias correction (Tercek et al., 2023).

Normalizing climate indicators

We identified potential predictors of wildfire ignition from the suite of climate indicators derived from climate and water balance variables (Table 1). To represent accumulation of dryness over time preceding ignition dates, we computed rolling sums or means ("rolling values") using the R `zoo` package (Zeileis and Grothendieck, 2005) for each variable. Variables were categorized as "state" variables if they describe the current condition of the system or "flux" variables if they describe movement of water, heat, or a substance through the system (Dingman, 2015; Wang et al., 2019). Rolling means were calculated for state variables: RD, VPD, T, SOIL, SWD. Rolling sums were computed for flux variables: RAIN, AET, CWD, GDD. Rolling calculations were made at windows of 1, 3, 5, 7, 9, 11, 14, 21, and 31 days to represent varying durations and magnitudes of drying that precede wildfire ignitions.

The percentile rank of each n-day rolling values of the indicators was determined to normalize variables to the local historical conditions for each centroid pixel. The percentile rank counts the total number of values less than each observation, and divides that value by the number of observations minus 1. This transformation develops a relative indicator of climate from the percentile rather than the absolute magnitude, which is more difficult to estimate accurately due to variation in factors that were not modeled such as differences in stomatal resistance between vegetation types or incorrect model parameterization from climate and soil properties data from published sources but with unknown accuracy at

local scales. This is a similar transformation of climate or weather data to the percentile calculations of ERC and BI in the NFDRS, which captures the spatial and temporal context of the variables and places them on comparable scales (Jolly et al., 2019). Normalizing metrics of drought and fire danger indices in this way improves correlations with large wildfire occurrence and burned area in the Western US, reducing the effect of confounding factors (Riley et al., 2013).

Daily rolling values were positively skewed with large numbers of zeroes and near-zero values (e.g., CWD was zero for many days during the winter). This created a disjointed distribution of percentiles, where days with a rolling sum of zero have a percentile of zero, and any value for climatic water deficit meaningfully greater than zero would have a percentile that is much larger than zero, i.e., around 40, with no percentile values in between (Figure 1). This caused all fires to occur at or above the 90th percentile, with the result that our model had poor sensitivity to detect ignition danger based on CWD. In order to reduce the disjointedness of the percentile values and prevent a situation where spatial projections of wildfire danger using our method have unrealistically sharp boundaries across pixels (leading to an appearance of "speckling" when the data are viewed spatially), we applied the following adjustments to the rolling values before calculating percentiles using the `percent_rank` function from the R package `dplyr` (Wickham et al., 2019):

1. Round all values to 1 decimal precision.

2. Remove zeroes from the time series.

3. Remove duplicate values so there are no repeating values.

These adjustments also removed the need for determining a fire season based on calendar dates as in Thoma et al. (2020). Since days with a rolling sum of 0 mm of CWD would have low to no fire danger, our model determines the fire season based only on days with non-zero

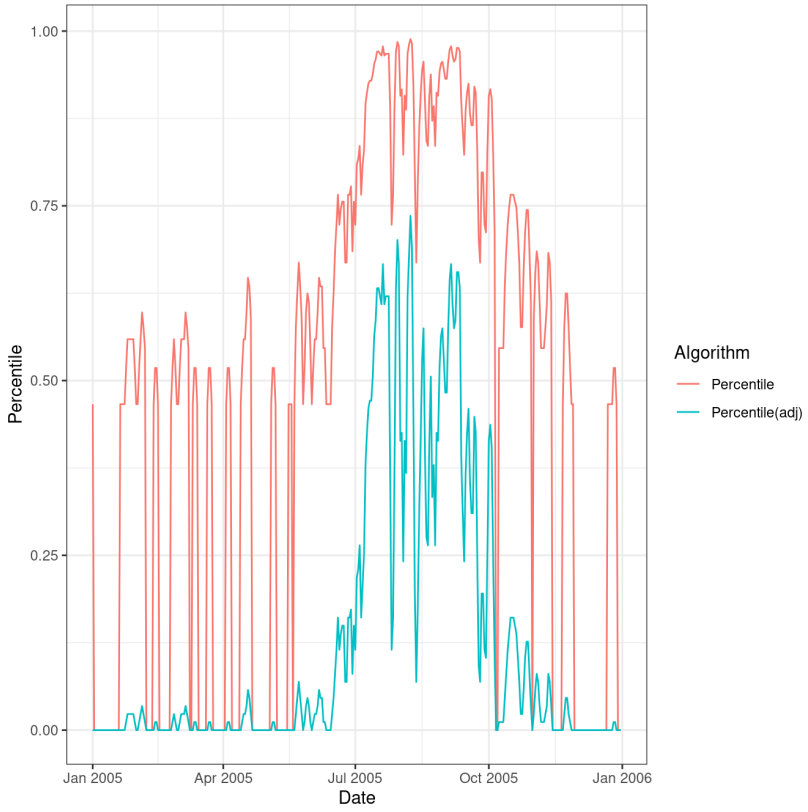

Figure 1. Percentile of 3-day rolling sum of CWD for `WY44445104060198507 27` wildfire centroid pixel for 2005, showing results of original percentile calculation (`dplyr::percent_rank()` function in R (pink) and adjusted percentile calculation described in our methods (blue). Without adjustments, percentile values jump between 0 for a 3-day rolling sum of CWD of zero and approximately 0.45 or greater for 3-day rolling sum of CWD greater than zero. With adjustments, the percentile values are continuous from 0 to 1.0, giving the model higher sensitivity to lower levels of dryness, indicated by the increased range in percentile values observed over the year (excluding the disjoint region in percentile values in the original percentile algorithm).

CWD (or other climatic variables) instead of a range of calendar dates (i.e., May 1st through October 31st).

Climatic classifiers of wildfire ignition

We determined the best classifier of ignition as the climate variable and rolling window with the highest Area Under the Curve (AUC) of the Receiver Operating Characteristic (ROC) curve. The ROC curve represents the performance of a binary classifier (ignition or no

ignition) by plotting the trade-off between true- and false-positive rates at varying thresholds of classification (Figure 2, Pontius and Parmentier (2014)). Because misclassification (false negative) of fire danger under the driest conditions has the potential to be more costly than misclassifications under wetter conditions where fires are likely to be less severe, performance is also assessed using the partial AUC (pAUC). $pAUC_{0.1}$ and $pAUC_{0.2}$ were assessed, which represent the AUC for the range of false positive rates from 0 to 0.1 and 0 to 0.2, respectively. The pAUC values represent the classification performance under the driest conditions that resulted in wildfire ignitions in the MTBS database. Higher pAUC values indicate better classification performance under these driest conditions.

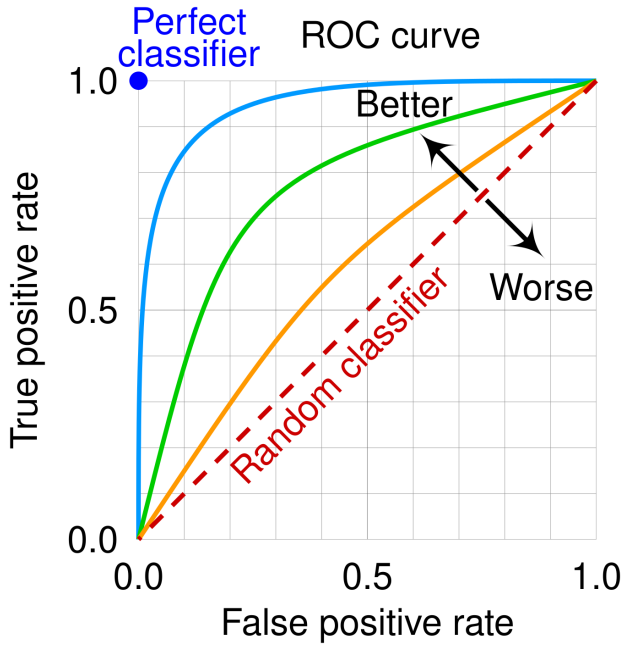

Figure 2. Receiver Operating Characteristic (ROC) curve showing true and false positive rates. Performance of a random classifier is shown by the diagonal line which is analogous to predicting ignition using a coin flip. Three example classifiers are shown in blue, green, and orange. The best possible classification performance is represented by the point in the upper left of the plot, which has 100% sensitivity (no false negatives) and 100% specificity (no false positives).
Image Source: cmglee, MartinThoma, CC BY-SA 4.0, via Wikimedia Commons

Comparison with other indices of fire danger

We compared our best performing classifier of ignition to indices included in the NFDRS: 100-hr fuels (FM100), 1000-hr fuels (FM1000), burning index (BI), and energy release component (ERC). FM100 and FM1000 are inputs to the ignition component (IC) of the NFDRS, and should be most analogous to our model of wildfire ignition hazard (Jolly et al., 2024). While the IC incorporates other measures besides fuel moisture, such as wind speed and the spread component, gridded values for IC that could be retrieved for a point of interest could not be located so the readily available FM100 and FM1000 grids were used as a proxy for the IC. Others have found that the NFDRS metrics FM10, FM100, and VPD gave similar results to IC when assessing the degree to which climate anomalies drive wildfire ignitions (Jorge et al., 2025). Daily time series from 1979-01-01 to 2021-12-31 for these indices calculated using gridMET were retrieved from Northwest Knowledge Network (Northwest Knowledge Network, 2025) for the centroid polygon (Latitude 46.09374°, Longitude -113.8503°) of the Valley Complex (Coyote) fire (MTBS ID: `MT4609711384420000731`) which ignited on 2000-07-31. This fire was selected because its burned area (8336.9 ha) is approximately the mean burned area for forest cover in the Middle Rockies in the MTBS database (8222.4 ha). Pairwise correlations were calculated for all variables using the `corrplot` function from the R `GGally` package (Schloerke et al., 2024).

Wildfire danger rating

Once the best classifier of ignition and the optimal window of time were determined, an ignition danger rating system was developed. Wildfire danger is assessed by modeling the proportion of historical wildfires that ignited at or below a given percentile of dryness. A third-degree polynomial curve was fit to the empirical cumulative distribution function (eCDF) to estimate the cumulative distribution function of wildfire ignitions versus the percentile of water balance variables at ignition. This allowed us to convert a given level of

dryness to a statement of wildfire danger that indicates the proportion of historic wildfires that burned at or below that level of dryness. The polynomial function used to estimate the eCDF provides a continuous function used to map percentile of dryness to proportion of historical wildfires and also allows for portable implementation of the system because it is a simple mathematical relationship. Figures 10a and 10b illustrate the process of converting a proportion of historic wildfires to the level of dryness at or below which they ignited, which can be used as a threshold of dryness to determine danger of wildfire ignition. This threshold can be tuned based on risk tolerance and specific management objectives. For example, a risk-averse manager might prepare for wildfires at lower dryness levels if they are wary of how often historical wildfires occurred at those levels.

Projections of fire danger in the Greater Yellowstone Ecosystem

We used this system to map wildfire ignition danger for forest cover for 20-year periods to the end of the century in the Greater Yellowstone Ecosytem (GYE), a subset of the Middle Rockies ecoregion. Spatial data was processed using the R package `terra` (Hijmans, 2024) and plotted using `ggplot` (Wickham, 2016) with `tidyterra` (Hernangómez, 2023). Projections are limited to the GYE and only made for forest cover types with the goal of identifying wildfire refugia for whitebark pine in the GYE. Projections of wildfire ignition danger in forest cover types are made for all pixels in the GYE, even those that may not currently have forest cover. This extrapolation of model predictions allows for projections of fire danger in areas where forest may be established through outplanting in places that are currently unforested.

Long-term projections of wildfire ignition danger were developed for 12 GCMs from the Multivariate Adaptive Constructed Analogs (MACA) gridded climate data product (Abatzoglou and Brown, 2012). We used a threshold of 0.35 percentile of 3-day rolling sum of CWD to quantify a threshold of fire danger. This percentile was chosen because it represents

GCM
BNU-ESM
CanESM2
CCSM4
CNRM-CM5
CSIRO-Mk3-6-0
GFDL-ESM2G
HadGEM2-CC365
inmcm4
IPSL-CM5A-LR
MIROC5
MRI-CGCM3
NorESM1-M

Table 2. GCMs used to make projections of wildfire danger in the Middle Rockies ecoregion. A total of 12 GCMs were included. Ensemble projections of wildfire ignition danger were made using the mean days above a fire danger threshold for both RCP4.5 and RCP8.5 emissions scenarios for all GCMs.

the level of dryness at or below which 10% of historical wildfires ignited. Therefore, levels of dryness above this 0.35 percentile represent the levels of dryness at which the vast majority (90%) of historical wildfires ignited and we consider these conditions high danger of wildfire ignition (Figure 10a). Days with projected 3-day rolling sums of CWD above this threshold were categorized as high danger of wildfire ignition. The number of days categorized as high danger of wildfire ignition for each year were summed for each pixel to determine total number of days at danger of wildfire ignition per year. Long-term fire danger was characterized by averaging days above this percentile threshold for each year in near-term (2023–2040), mid-term (2041–2060), and late-century (2081–2099) projection periods for each pixel.

Results

Historical fire season & frequency in the Middle Rockies ecoregion

Of the 417 historical wildfires larger than 405 hectares (1,000 acres) in the Middle Rockies ecoregion from 1984–2020, 110 wildfires occurred in forest and 307 wildfires occurred

Cover	n	Mean area (ha)	Min area (ha)	Max Area (ha)	SD (ha)
Forest	110	8222.4	416.0	228051.3	26807.1
Non-forest	307	5118.8	405.9	122792.6	11860.8

Table 3. Areal statistics for wildfires classified as forest and non-forest in the MTBS database.

in non-forest cover types (Figure 3). The largest forest wildfire was 563,527 acres and the largest non-forest wildfire was 303,427 acres. The mean forest wildfire size was 8,222.4 ha and the mean non-forest wildfire size was 5,118.8 ha (Table 3)

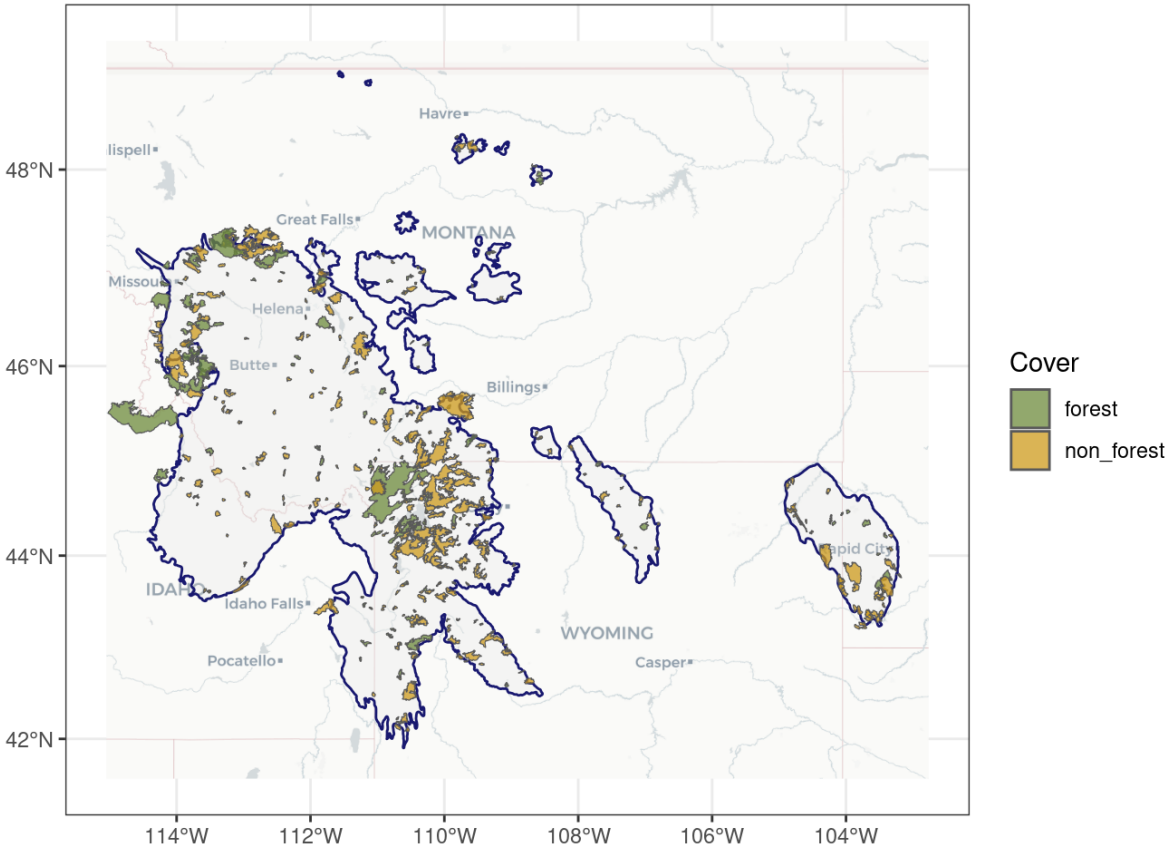

Figure 3. MTBS wildfire polygons larger than 405 hectares occurring on forest and non-forest cover types in the Middle Rockies Level III Ecoregion (dark blue outline) between 1984 and 2020. Basemap attribution: © OpenStreetMap contributors © CARTO

Wildfires in forest-cover types occurred between day of year (DOY) 93 and 289. Non-forest wildfires occurred between DOY 6 and 350. Fire ignition DOYs had similar seasonal

distributions in both forest and non-forest vegetation types (Figure 4). The mean DOY of ignition was 217.6 for forest and 215.4 for non-forest wildfires, with no evidence of difference in mean ignition DOY between the groups (Welch Two Sample t test: $t_{264.83}$=0.60794, P=0.5437).

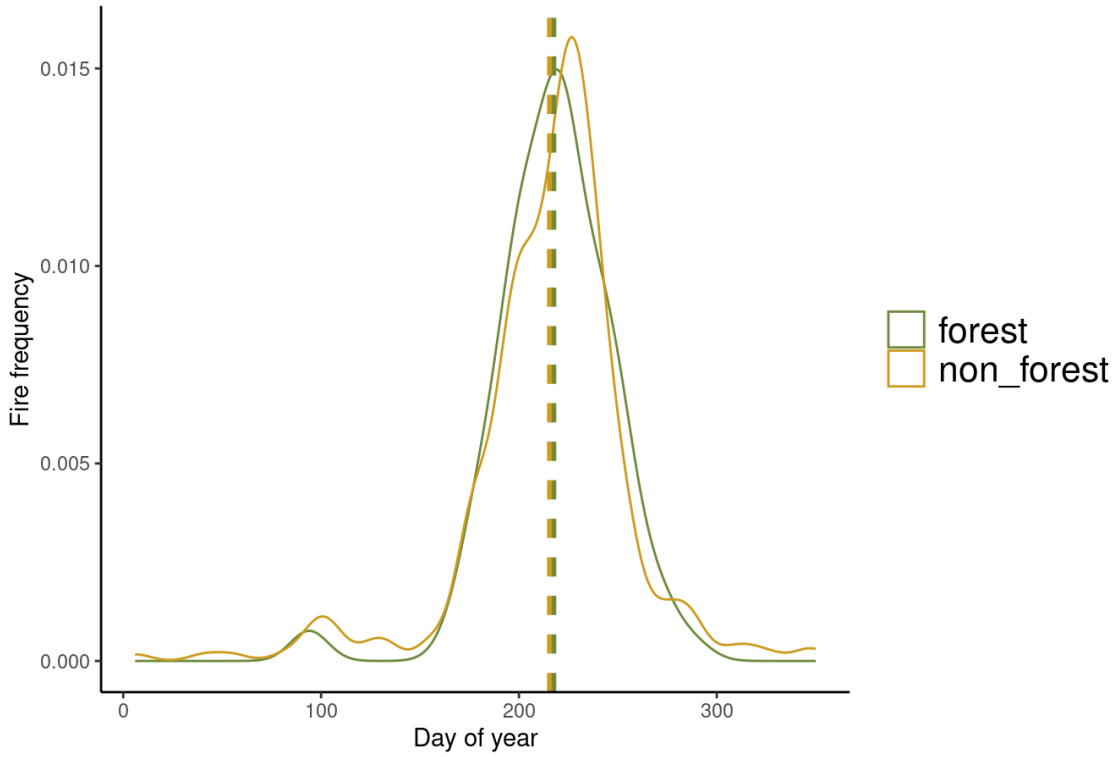

Figure 4. Density plot of fire frequency by day of year, for forest and non-forest cover types. Vertical dashed lines show mean day of ignition ($\mu_{\text{forest}} = 218$, $\mu_{\text{non-forest}} = 215$).

The classifiers of wildfire ignition tested here were distributed differently between days that experienced a wildfire ignition or not in the MTBS database (Figure 5). There is evidence that wildfires occurred more often on days with higher percentile values of the rolling values of climate indicators (or lower values for SOIL). However, the distribution of RAIN is dominated by low percentile values whether an ignition occurred or not.

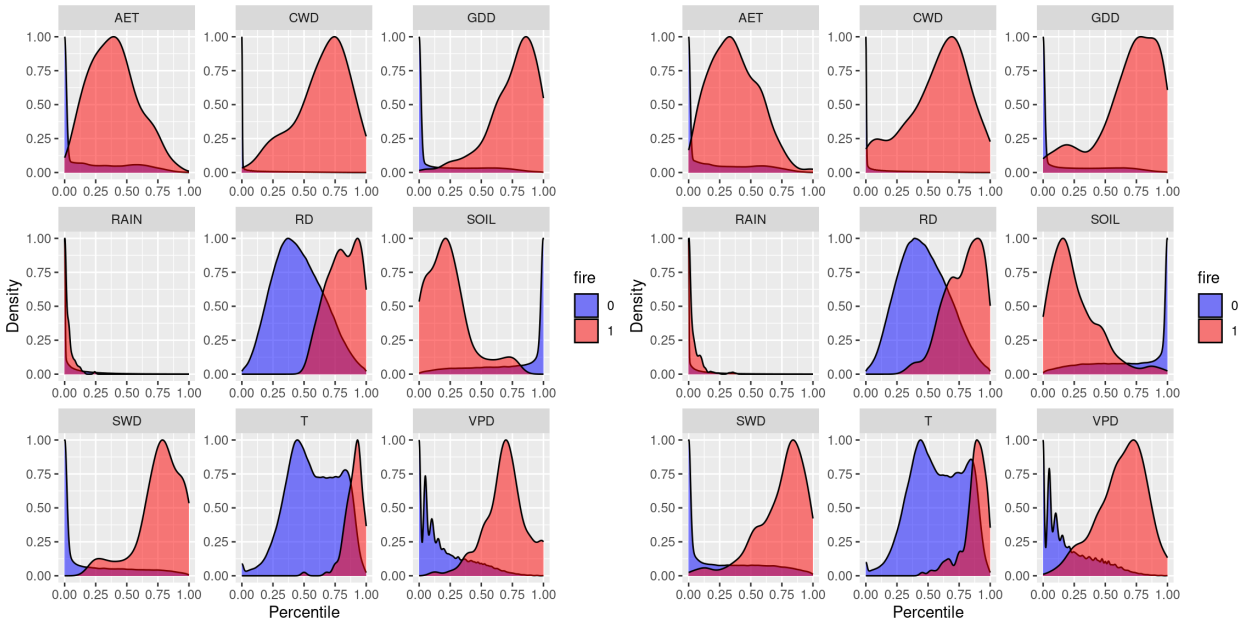

(a) Non-forest (b) Forest

Figure 5. Density plots showing distribution of percentiles for 3-day rolling values on days with wildfire ignition (fire = 1) or no wildfire ignition (fire = 0) recorded in the MTBS database. Higher wildfire densities at higher climate variable percentiles indicate better ignition predictors, while lower wildfire densities at lower percentiles reduce confusion with ignition. This combination is evaluated by the AUC. Plot densities are scaled from 0 to 1 so that fire and non-fire distributions are on the same scale.

Climatic classifiers of wildfire ignition

Measures of atmospheric dryness (CWD, VPD, RD) were consistently the best overall classifiers of ignition as measured by overall AUC at all rolling window widths compared to the other climatic measures (TEMP, SOIL, GDD, SWD, RAIN, AET). For forest cover types, the variable and rolling window width that gave the best overall classification of fire ignition (i.e., the highest AUC value) were CWD with a 3-day window (Figure 7). For non-forest cover types, the best overall predictors were VPD with a 1-day window (i.e., daily VPD) and CWD with a 3-day window. However, among measures of atmospheric dryness (CWD, VPD, RD), rolling window width appears to have minimal effect on overall ability to classify ignition, with RD, VPD, and CWD having similar AUC values for the rolling windows examined and

overlapping AUC confidence intervals. As similar performance can be expected from these variables, selecting any one can be justified based on practical requirements such as data availability or ease of computation.

Rolling window width

The different rolling window widths tested had similar performance as measured by AUC and pAUC for most of the variables examined (Figure 7). AUC values for CWD and VPD were relatively constant across all rolling window widths, however, pAUC values showed evidence of decreasing classification performance for these variables as rolling window length increased. SOIL and SWD had identical performance (Figures 6 & 7) and showed a decreasing pattern for all AUC and pAUC measures as rolling window length increased. AET showed increasing classification performance as rolling window length increased.

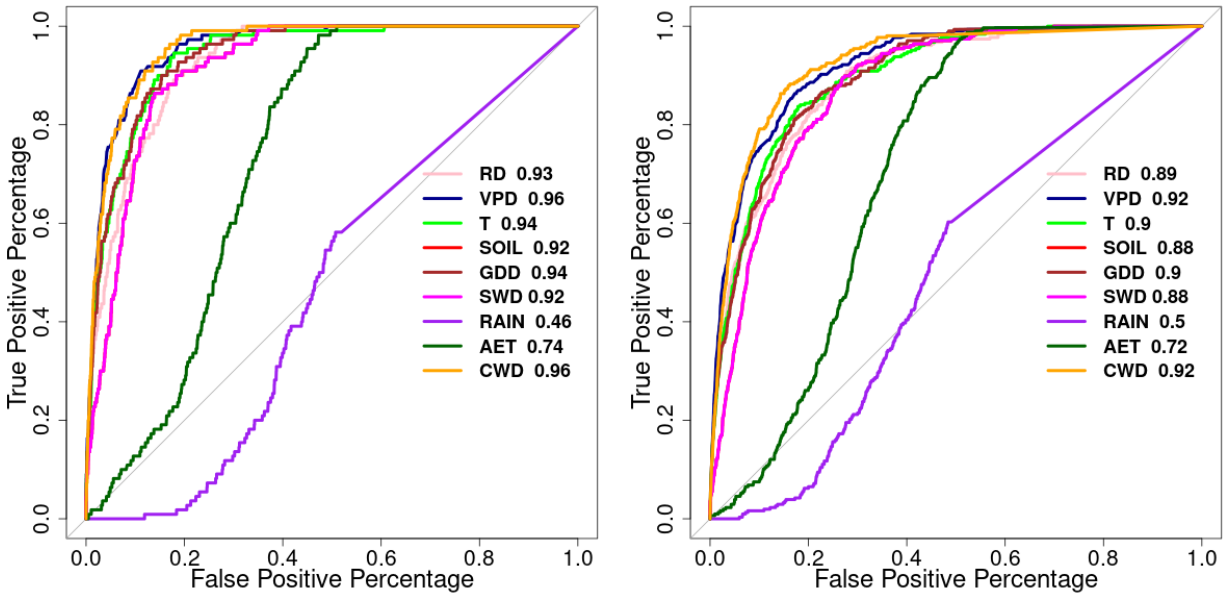

(a) Forest (b) Non-forest

Figure 6. ROC Curves for a) forest and b) non-forest cover in the Middle Rockies Ecoregions, 3-day rolling window.

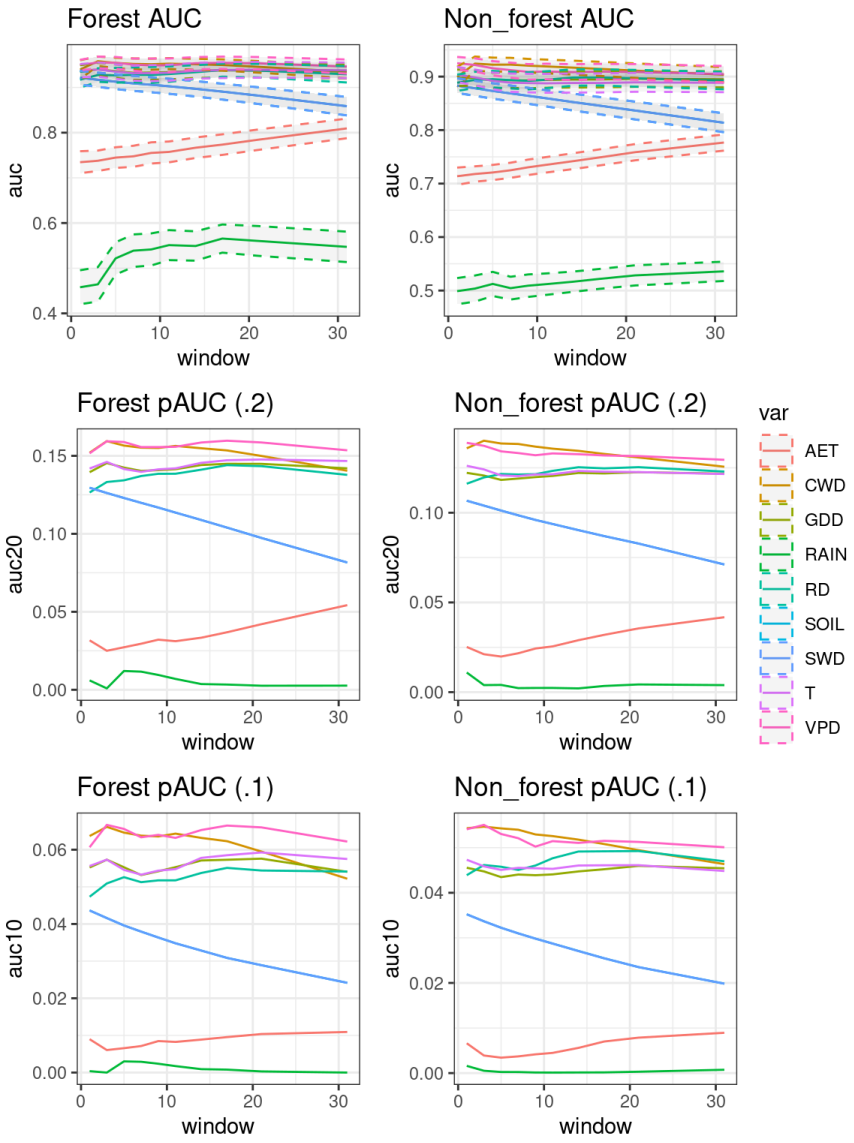

Figure 7. AUC, $pAUC_{0.2}$, and $pAUC_{0.1}$ values for different window widths used for calculations of rolling sums and means of variables in forest or non-forest cover types. Higher AUC values indicate better overall classification performance while higher pAUC values indicate better classification performance under drier conditions. Percentiles of 3-day rolling sums of CWD and VPD were selected as the best classifiers of ignition because these combinations maximize classification performance under driest conditions (pAUC) while overall classification performance (AUC) appears unaffected by rolling window width for these variables. 95% Confidence Intervals are shown for overall AUC values (dashed lines). Confidence Intervals for pAUC values were not calculated due to computational constraints because they require a lengthy bootstrapping process.

Comparison with other indices of fire danger

The percentile of 3-day rolling sum of CWD for the Valley Complex (Coyote) fire showed strong positive correlation with ERC (corr = 0.8), weak positive correlation with BI (corr = 0.6), and strong negative correlations with FM100 (corr = -0.7) and FM1000 (corr = -0.7) from 1979-01-01 to 2021-12-31 (Figure 8). The timing of ignition of the fire coincided with the peak maximum rolling sum of CWD and minimum FM100 for the year, and occurred slightly before the peak maximum BI, maximum ERC, and minimum FM1000 (Figure 9). On the day of ignition, the centroid pixel of the MTBS fire polygon for the Valley Complex fire had a percentile of 3-day rolling sum of CWD of 0.8, which corresponds to the percentile of CWD at or below which 69% of historical fires in the ecoregion burned (Figure 10a).

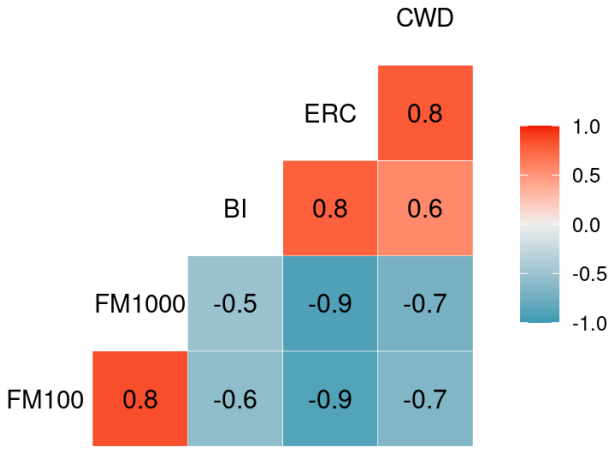

Figure 8. Pairwise Pearson correlations between the percentile of 3-day rolling sum of CWD and NFDRS indices for the Valley Complex (Coyote) fire.

Wildfire ignition danger rating

Wildfire ignition danger rating is determined by selecting a level of dryness that corresponds to a proportion of historical fires that burned at or below that level of dryness. The polynomial function estimating the empirical cumulative distribution function (eCDF) of percentile 3-day rolling sum of CWD for historical wildfires on forest cover types is (Figure

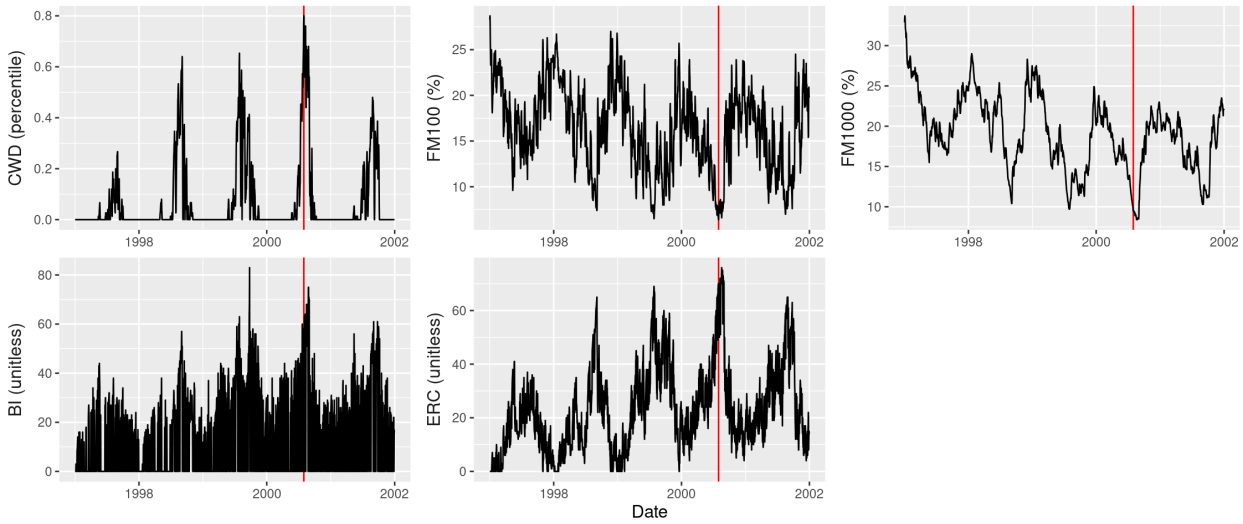

Figure 9. Daily time series of percentile of 3-day rolling sum of CWD and NFDRS indices for the Valley Complex (Coyote) wildfire. Red vertical line shows day of ignition (2000-07-31).

10a; $R^2 = 0.994$):

$$y = \exp(-4.1839624 + 5.5952288x + 0.2504363x^2 - 1.6207789x^3)$$

and for non-forest cover types is (Figure 10b; $R^2 = 0.985$):

$$y = \exp(-3.7077154 + 7.0748217x - 4.7397976x^2 + 1.4771369x^3)$$

Where x is a percentile of 3-day rolling sum of CWD and y is the historical proportion of wildfires that burned at or below that percentile of dryness.

We were interested in identifying wildfire refugia for whitebark pine using this model, so we identified a low level of fire danger to develop projections of wildfire danger using the forest cover type model. For our projections of wildfire ignition danger on forest cover, we selected the 35^{th} percentile of 3-day rolling sum of CWD, which corresponds to the level of

dryness at or below which 10% of historical fires on forest cover types ignited (Figure 10a).

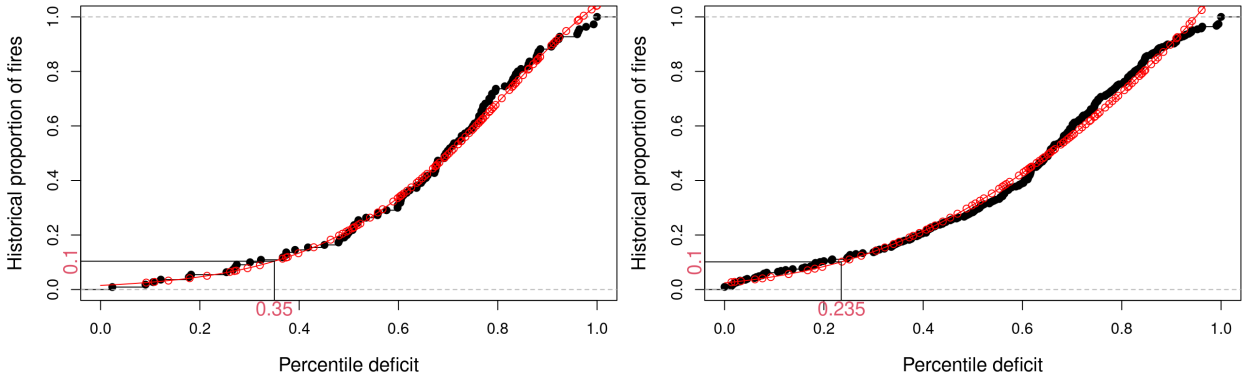

(a) Forest (b) Non-forest

Figure 10. Empirical cumulative distribution function (eCDF) of cumulative wildfire ignition counts versus 3-day rolling sum of CWD for a) forest and b) non-forest cover in the Middle Rockies ecoregion shown in black with regression function estimating the cumulative distribution function (CDF) overlaid in red (Forest $R^2 = 0.994$; Non-forest $R^2 = 0.985$). The process to determine wildfire ignition danger is illustrated. A proportion of historical wildfire ignitions (y-axis) is selected based on risk tolerance for management objectives; 0.1 of historical wildfire ignitions is used here. The 0.35 percentile of 3-day rolling sum of CWD corresponds to 0.1 of historical wildfire ignitions for forest cover types, while for non-forest cover types the percentile of dryness that corresponds to this level of danger is 0.235. When the percentile of a 3-day rolling sum of CWD exceeds 0.35 at a forested or 0.235 for non-forested location, it is considered at danger for wildfire ignition. Projections in Figure 11 average the sum of days above this threshold for each year in the periods projected.

Projections of wildfire ignition danger

Ensemble averages (Table 2) of long-term projections of fire ignition danger in forests in the Greater Yellowstone Ecosystem (GYE) within the Middle Rockies ecoregion made using this method show increased fire danger across the region by the end of the century under both RCP4.5 and RCP8.5 emissions scenarios, with larger increases in danger projected under the higher emissions RCP8.5 scenario (Figure 11). The projected increases in fire danger across the GYE are not equal across the region. For example, a forested location that could reach an average of 6 (RCP4.5) to 10 (RCP8.5) days above the fire danger threshold of 10% by the near-term (2023–2040) could increase to an average of 23 (RCP4.5) to 61 (RCP8.5) days

above the threshold by end-century (2081–2099). A different location could see larger absolute increases from 21–24 to 46–70 days for the same time periods and scenarios, respectively.

Discussion

Climatic classifiers of wildfire ignition

Climatic Water Deficit (CWD) and Vapor Pressure Deficit (VPD), metrics of atmospheric dryness, were consistently the strongest classifiers of wildfire ignition for large fires (at least 405 ha) in both forest and non-forest cover types across the Middle Rockies ecoregion, performing better than other climatic measures tested (Actual evapotranspiration (AET), soil water deficit (SWD), growing degree days (GDD), rain (RAIN), relative dryness (RD), soil moisture (SOIL), and temperature (T)). These results align with findings from the Southern Rockies ecoregion where CWD and VPD were the strongest classifiers of wildfire ignitions, although only percentiles of 14-day rolling sums were tested in that ecoregion (Thoma et al., 2020).

The strong performance of CWD and VPD as classifiers of wildfire ignitions likely results from their direct link to the dryness experienced by wildland fuels. As measures related to evaporative demand and water availability, they directly influence fuel moisture content, a critical factor in ignition (Littell et al., 2016; Riley et al., 2013). These variables integrate climatic conditions with the pyro-ecophysiology of vegetation, which dictates how live and dead fuels dry and become available to burn (Jolly and Johnson, 2018). Notably, the ability of CWD and VPD to classify ignitions was generally higher in forest cover types compared to non-forest cover types for a given rolling window width, indicating stronger links with the pyro-ecophysiology of the forest vegetation present in the Middle Rockies ecoregion (Figure 6).

The distribution of percentile values for the tested indicators differed between days with and without wildfire ignitions, indicating differing associations with wildfire ignitions

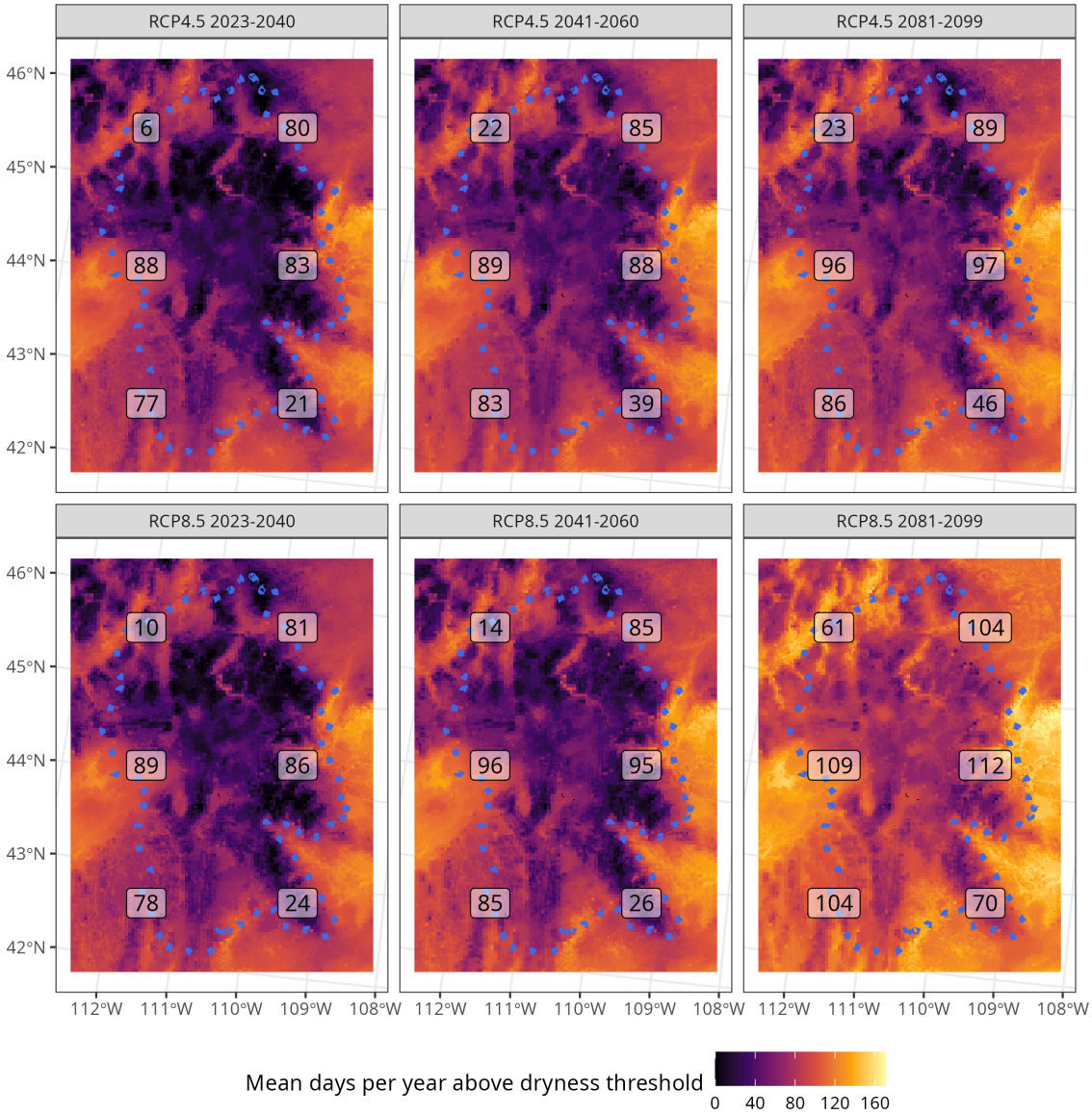

Figure 11. Ensemble projections of forest wildfire danger in the GYE (outlined with dotted blue line) using the model developed for forest cover. The GYE is selected as a subset of the Middle Rockies Ecoregion to showcase wildfire danger projections using this method. Mean days above wildfire danger threshold (0.35 percentile of dryness) for RCP4.5 and RCP8.5 ensemble conditions shown. GCMs used to make ensemble average conditions are listed in Table 2. The 0.35 percentile of dryness (3-day rolling sum of CWD) corresponds to a level of dryness at or below which approximately 10% of fires burned. Mean days per year above the fire danger threshold for periods 2023–2040, 2041–2060, and 2081–2099 are shown by the color ramp. Six points were assigned in a grid and values sampled for each interval shown, to show the changes in fire danger across time for the sampled locations.

(Figure 5). Wildfires appear to occur more often on days with high percentiles of CWD and days without ignition appear to be associated with low percentiles of CWD. VPD shows a similar pattern, although there is more overlap in the distribution of VPD percentiles between ignition and non-ignition days. It is notable that days with wildfire ignition almost always occurred with a percentile of 3-day rolling mean of VPD above zero, whereas wildfires occasionally occurred when the percentile of the 3-day rolling sum of CWD was zero. This suggests that VPD and CWD may capture slightly different aspects of dryness relevant to ignition, perhaps relating to different effects on different fuel types.

Conversely, measures of precipitation or plant water use—RAIN and AET—were consistently the lowest performing classifiers of ignition both overall (AUC) and under the driest conditions (pAUC) (Figures 6 & 7). AET is an estimate of water use by live plants, and its low performance as a classifier of ignition is likely because wildfire ignition, particularly of surface fires, is often controlled by the moisture content of dead fuels (Riley et al., 2013), which is not directly captured by a metric estimating live plant water use. While AET may influence fuel accumulation on longer time scales, it appears less relevant to the short-term conditions necessary for ignition. Similarly, RAIN, a direct measure of water input, performed poorly, especially in non-forest cover types and at shorter time windows. While rainfall is essential for increasing fuel moisture, its occurrence over the periods of time examined here may not be as direct an indicator of overall dryness as metrics like CWD or VPD, which reflect the balance between water demand and availability and thus the potential for fuels to dry out and remain dry. In addition, small rainfall events do not produce enough moisture to saturate soil and penetrate vegetation, and we did not classify RAIN into wetting or non-wetting events which have demonstrated links with wildfire behavior (Holden et al., 2018); inclusion of non-wetting rain days may confound the ability of RAIN to classify ignition events.

Soil moisture metrics—SOIL and SWD—had moderate performance as classifiers of

wildfire ignition (Figure 7). While soil moisture is often considered in fire danger indices (Krueger et al., 2022), our results suggest that for detecting wildfire ignition danger in the Middle Rockies, direct measures of atmospheric dryness or those reflecting integrated water balance may be more effective. The lower performance of soil moisture metrics could be related to the importance of dead fuels as ignition sources in this ecoregion as they are elsewhere in the western US (Riley et al., 2013). While living vegetation is connected hydraulically to soil water reserves through vascular tissue, these dead fuels are more decoupled from soil moisture dynamics. For example, large woody debris or a thick duff layer, insulated from the soil surface, might respond more directly to atmospheric dryness (VPD, RD) than to soil moisture (SOIL, SWD), while CWD integrates water demand and supply including soil reserves.

Energy metrics—T and GDD—also exhibited moderate classification performance, with similar AUC and pAUC values across tested rolling window widths as the soil moisture metrics (Figure 7). While they were better classifiers than precipitation or plant water use metrics, they were consistently outperformed by the leading measures of atmospheric dryness (CWD, VPD). These energy-based metrics can account for the drying effect of high temperatures, but do not take into account moisture availability or use by plants. Therefore, they can never fully explain the drying of dead fuels that is critical for wildfire ignition (Riley et al., 2013).

Optimal temporal scale for classifying wildfire ignition

To optimize the classification of wildfire ignitions in the Middle Rockies ecoregion, we recommend using the percentile of a 3-day rolling sum of either CWD or VPD. This window length yielded comparable overall AUC performance to longer windows for these variables but demonstrated superior performance under the driest conditions as measured by partial AUC values (Figure 7). Maximizing pAUC is critical for wildfire danger assessment, as misclassifying high-danger days (false negatives) where extremely dry days have potential for

extreme wildfire events can have severe consequences. The effect of rolling window width on predictive performance varied among climate indicators and between forest and non-forest cover types.

Atmospheric dryness (CWD, VPD, RD) indicators performed consistently across the rolling window widths examined. CWD and VPD are direct measures of accumulated drought stress or atmospheric dryness. It is possible that the fundamental signal indicating conditions "dry enough to burn" is captured effectively by these variables regardless of the specific accumulation period within the range we tested. However, the performance of CWD and VPD under the driest conditions (pAUC) decreased with increasing window length (Figure 7). This reinforces the finding from Riley et al. (2013) that climate metrics or fire danger indices averaged over windows of time longer than it takes fuels to dry results in weaker correlations with ignition. Additionally, classification performance (both AUC and pAUC) was higher in forest than in non-forest cover types for a given rolling window width (Figures 6 & 7). This might reflect differences in the drying rates of fine herbaceous fuels versus larger woody fuels present in forests, where fine fuels respond quickly to short-term atmospheric conditions while larger fuels require prolonged dryness (Viney, 1991). While overall predictive performance (AUC) of RD was similar to CWD and VPD, it had weaker performance than these variables under the driest conditions (pAUC) for a given rolling window width (Figure 7). VPD might better capture the true drying power of the atmosphere under extreme conditions than RD due to its incorporation of temperature effects on moisture holding capacity. CWD may better represent the accumulated dryness and water stress in both live and dead fuels resulting from extended dry periods than RD.

Soil moisture (SOIL, SWD) consistently decreased as the rolling window length increased (Figure 7). This is likely because instantaneous or short-term soil moisture measurements inherently integrate moisture conditions over longer periods, with soil moisture reserves acting as a capacitor as they accumulate water during wet periods and release it during dry

periods (Bisigato et al., 2013). Averaging these values over longer rolling windows instead of using instantaneous daily values effectively adds noise that reduces their predictive power for ignition events.

Precipitation and plant water use (AET, RAIN) indicators generally increased as the rolling window width increased (Figure 7), although RAIN's performance leveled off around a 10-day window in forest cover. AET is related to plant productivity and the magnitude/duration of favorable growing conditions (Stephenson, 1998) and is likely more relevant to fire danger on longer time scales by influencing fuel biomass accumulation. RAIN's increasing performance with window length in forests (but not non-forests) suggests that accumulated precipitation becomes more important for fuel moisture in woody fuels which have a higher saturation point and longer drying time than the fine fuels dominating non-forest areas (Viney, 1991).

Energy (T, GDD) indicators showed relatively constant predictive performance across all tested window widths. However, classification performance at any window width was lower than measures of atmospheric dryness.

Overall, classifier performance was consistently higher in forest cover types compared to non-forest cover types for a given indicator and rolling window width (Figure 6). This difference suggests that wildfire behavior in forests in the Middle Rockies is more likely moisture-limited, meaning sufficient fuel is present and dryness is the limiting factor controlling fire occurrence. In contrast, non-forest areas (e.g., grasslands and shrublands) are more likely fuel-limited, where conditions dry enough to burn are frequently present but fuel load is insufficient for ignition or formation of large wildfires (Littell et al., 2018; Meyn et al., 2007). This implies that our fire danger rating system may inherently provide more accurate predictions of ignition danger in forested environments within the Middle Rockies ecoregion.

Comparison with other fire danger indices

The ignition of the Valley Complex (Coyote) fire occurred near peak dryness as indicated by both our top-performing classifier, the percentile of 3-day rolling sum of CWD, and selected indices from the NFDRS (FM100, FM1000, BI, and ERC) (Figure 9). The correlations between our percentile of 3-day rolling sum of CWD metric and these NFDRS indices, ranging from 0.6 to 0.8, suggest that while they capture similar aspects of dryness related to fire danger, they also reflect distinct underlying processes. This divergence is expected because CWD integrates the simultaneous timing of energy and moisture, accounting for soil moisture reserves. In contrast, the NFDRS fuel moisture metrics (like FM10 and FM100) primarily model moisture availability in dead fuels. ERC models composite fuel moisture of dead and live fuels, while BI is an index related to potential burn severity and the effort needed to contain a fire in a particular fuel type.

The climate-based nature of this wildfire ignition danger rating system facilitates creating spatial projections of wildfire danger. Climatic Water Deficit (CWD) can be calculated from readily available point data from weather stations, gridded climate data, or obtained from precalculated datasets like the NPS Gridded Water Balance product (Tercek et al., 2023, 2021b). In contrast, the NFDRS (de Groot et al., 2015), commonly used by US land management agencies, requires complex inputs such as wind speed, cloudiness, and live fuel moisture, which are difficult to estimate long-term and make the NFDRS sensitive to poorly calibrated inputs. Our system, based on a single climatic input, automates calibration by normalizing our indicator of climate to local historical conditions at each pixel using a percentile transformation. This approach is functionally analogous to the NFDRS ignition component (IC), which assesses the likelihood of fine fuels igniting from a burning piece of wood (Jolly et al., 2024). Our system assesses fire danger by comparing the percentile of a 3-day rolling sum of CWD to the cumulative distribution of dryness at the time of historical fire ignitions. While recent NFDRS improvements have reduced the need for some

manual inputs (Jolly et al., 2024), producing estimates from gridded climate data remains computationally intensive (Farguell et al., 2025). A key difference is that our system provides an estimate of ignition potential only, unlike the NFDRS which also offers indices for spread, burning intensity, and energy release. However, our system's reliance on simple climate data makes long-term spatial projections of wildfire danger readily calculable. Like any fire model, ours should be evaluated in other ecoregions to identify potential patterns or differences in fire dynamics.

Long-term projections of wildfire ignition danger

Climate change is leading to longer and more intense fire seasons (Abatzoglou et al., 2021; Jolly et al., 2015; Littell et al., 2016), which in the Western U.S. has been linked to increases in CWD and VPD (Abatzoglou and Williams, 2016). Our results reinforce the finding that CWD and VPD are associated with danger of wildfire ignition. In the GYE, Westerling et al. (2011) found large increases in burned area and decreases in fire return interval across the ecoregion. Our projections of wildfire ignition danger in forests in the GYE support this claim, with projections showing increasing days at danger that could cause decreases in fire return intervals across the region by the end of the century due to projected increases in CWD, with larger increases in RCP8.5 than RCP4.5 ensemble projections.

Our projections of fire danger are conservative because they use a threshold of dryness corresponding to a relatively low level of fire danger - the 3-day rolling sum of CWD at or below which 10% of historical wildfires ignited. This threshold can be tuned based on the risk tolerance required for different management needs (consider managing for persistence versus managing for transition). For example, here we focus on identifying wildfire refugia for the slow-growing species whitebark pine, which requires conservative estimates of fire danger because we seek to identify locations that are unlikely to burn before the 50 years or longer the trees require to reach maturity. On the other hand, managers may want to

maximize opportunities to conduct beneficial burns. Here, accepting conditions at or below which 30–40% of historical ignitions occurred rather than 10% could highlight more days as potentially viable.

Wildfire refugia for whitebark pine

The end-of-century (2081-2099) RCP4.5 ensemble projections show likely persistence of low fire danger areas (potential planting locations that avoid wildfire-induced mortality) across high-elevations in the GYE in areas such as the Absaroka and Beartooth mountains, Wind River Range, Crazy Mountains, and Tetons (Figure 11). Increased CWD under the RCP8.5 ensemble projections shows virtually all areas in the GYE increasing in days at danger of wildfire ignition in the same time period. However, the large spread in projections of fire dangers between individual GCMs indicates the possible, but unlikely, persistence of wildfire refugia even under the RCP8.5 emissions scenario despite the unfavorable ensemble average RCP8.5 projections. The persistence of wildfire refugia that could be targeted for WBP planting therefore depends on patterns of future emissions. Based on our analysis, WBP plantings should target areas projected to exhibit low fire danger under the RCP4.5 emissions scenario. However, the ultimate long-term safety of planted trees from wildfire is as uncertain as the trajectory of future greenhouse gas emissions.

Limitations

There is potential for misclassification of vegetation cover types due to historical wildfires causing cover type conversion (Coop et al., 2020). In the short-term, fire driven cover change likely occurs in one direction, from forest to non-forest cover, due to aridification of the American West and the climate ratchet which controls the windows of time suitable for forest regeneration that is limited by establishment when seedlings are susceptible to seasonal drought (Jackson et al., 2009). This unidirectional shift likely results in misclassification of burned forests into the non-forest category. Unfortunately, this results in a fire danger rating

in non-forest areas under low-CWD conditions that is likely underestimating fire danger. Assuming every ignition we classified as non-forest was actually forest at time of ignition and experienced cover change, the maximum underestimation of fire danger would be around 10%, evident by visual inspection of the difference of proportion of historical wildfires occurring at a 50th percentile of CWD or less between forest and non-forest cover types, where the 50th percentile of forest ignitions corresponds to a historical wildfire proportion of approximately 0.2 and for non-forest approximately 0.3 (Figures 10a and 10b)

Our system does not differentiate between natural and artificially-ignited wildfires. Factors that increase accessibility to humans such as distance to roads increase the probability of human-caused wildfires (Jimenez-Ruano et al., 2022). There is even evidence that as a result of the COVID-19 pandemic, the 2020 wildfire season experienced increases in recreation-caused wildfires (Jorge et al., 2025). Jimenez-Ruano et al. (2022) split components of wildfire hazard into static and dynamic causes and developed spatial models of the static component of fire danger. Static factors are those that do not change or change only slowly such as terrain, fuel type, and human accessibility. The dynamic controls of wildfire ignition change more quickly and are factors such as weather, fuel condition, and ignition seasonality. Our model assesses fire danger primarily through dynamic factors, i.e., the effect of weather or climate through accumulated atmospheric dryness and its relationship to fuel condition. Jimenez-Ruano et al. (2022) suggest using their spatial models of the static component of fire danger as a foundation upon which dynamic data such as ours can be superimposed to improve predictions of wildfire danger.

The accuracy of our projections of wildfire danger into the future relies on the assumption that the forest and non-forest cover types present in the ecoregion will have the same relationship between the climate indicators and wildfire. However, our system is robust to spatial patterns of change of fuel abundance as long as sufficient fuel is available to burn, as it doesn't depend on fuel quantity. Our system is normalized across vegetation

types within forest and non-forest cover in the ecoregion, which means that projections of wildfire danger are likely to be robust as long as cover types shift within vegetation types currently observed within the ecoregion and that shifts to entirely new vegetation types are not observed. McKenzie and Littell (2017) challenged the view that hotter and drier conditions will universally result in increases in wildfire occurrence and severity due to non-stationarity in the relationship between water, energy, and wildfire. They found that the relationship between hot and dry conditions and wildfire is strong in mesic and arid forests and shrublands with substantial biomass, but weaker in the wetter or drier ends of a rainforest to desert gradient. They concluded that regional drought-fire dynamics are not likely to be stationary in future climate and that accurate predictions of wildfire dynamics need to consider vegetation changes as well as changes in the drought-fire dynamic due to climate change.

Conclusion

This study evaluates a wildfire ignition danger rating system for the Middle Rockies ecoregion based on accumulated measures of atmospheric dryness that are normalized to the local historical conditions. We identified percentile of 3-day rolling values of CWD or VPD as the climate indicators that best classify ignition events. We estimated the cumulative distribution function of wildfire ignition counts versus percentile of 3-day rolling sum of CWD to identify the proportion of fires that burned historically at different levels of dryness which can be used to assess wildfire ignition danger based on climatic conditions. We developed projections of wildfire danger in the Greater Yellowstone Ecosystem and found increasing wildfire danger across the region, with areas of lower fire danger persisting only under the lower-emissions RCP4.5 scenario. Our system of wildfire danger compares favorably to the widely used National Fire Danger Rating System in a comparison of our model versus NFDRS indices for a historical wildfire in the Middle Rockies ecoregion.

Acknowledgments

Computational efforts were performed on the Tempest High Performance Computing System, operated and supported by University Information Technology Research Cyberinfrastructure (RRID:SCR_026229) at Montana State University.

CLIMATIC INDICATORS OF WHITE PINE BLISTER RUST INFECTION IN WHITEBARK PINE

Contribution of Authors and Co-Authors

Manuscript in Chapter 3

Author: Stephen John Huysman

Contributions: Implemented the study design. Developed scripts used for analysis. Integrated newly received monitoring data to dataset. Drafted the manuscript.

Co-Author: David P. Thoma

Contributions: Conceived initial study design and consulted in direction of analysis. Reviewed manuscript drafts.

Co-Author: Elizabeth Jamison

Contributions: Conceived study design and developed initial scripts used for analysis. Assembled monitoring dataset.

Co-Author: Erin Shanahan

Contributions: Organized collection of monitoring data from data partners. Assisted with use and interpretation of monitoring data. Provided feedback on results and methodology.

Co-Author: Mike Tercek

Contributions: Reviewed results and consulted on methodology.

Co-Author: Danielle E. Marias Ulrich

Contributions: Reviewed results and consulted on methodology. Reviewed manuscript drafts.

Co-Author: Brian V. Smithers

Contributions: Reviewed results and consulted on methodology. Reviewed manuscript drafts.

Manuscript Information

Stephen J. Huysman, David P. Thoma, Elizabeth Jamison, Erin Shanahan, Mike Tercek, Danielle E. M. Ulrich, Brian V. Smithers

Status of Manuscript:
_X_ Prepared for submission to a peer-reviewed journal
____ Officially submitted to a peer-reviewed journal
____ Accepted by a peer-reviewed journal
____ Published in a peer-reviewed journal

Abstract

White pine blister rust (WPBR) is the primary driver of the range-wide decline of whitebark pine (WBP), a federally threatened species. As a keystone and foundational species of high-elevation ecosystems, WBP's decline has potentially widespread consequences for forest composition and ecological functions. An understanding of the climatic drivers of WPBR infection is necessary to manage impacts of the pathogen during ongoing climate change. We assembled a long-term dataset indicating WPBR presence or absence in WBP from monitoring programs across WBP's range in the contiguous United States. We identified a spatially explicit model that included August and September temperature and precipitation as the best climatic predictors of WPBR infection in WBP during the basidiospore transmission season, with larger trees more likely to be infected than smaller trees. At high levels of precipitation (around and above 100 mm total August and September precipitation), the relationship between mean August and September temperature and probability of WPBR infection is parabolic, with highest infection rates around 11 °C. This parabolic relationship inverts at lower totals of August and September precipitation (0 to around 100 mm) and minimum infection rates occur around 11 °C and maximum infection rates at low (around 7 °C) or high (around 13 °C) temperatures. Projections of WPBR disease hazard (defined as probability of WPBR infection) through the end of the century show wide variability in geography and magnitude of disease impacts depending on plausible changes in temperature and precipitation across WBP's range.

Introduction

Whitebark pine (WBP; *Pinus albicaulis* Engelm.) is a foundational and keystone species of high-elevation subalpine forests. It is considered a foundational species because it serves as a nurse tree that enables establishment of other subalpine plant species and it is considered a

keystone species because its seeds are a rich source of protein and fat utilized by animals such as birds, squirrels, and bears (Tomback et al., 2001). In recent years, it has experienced a precipitous decline caused by climate-driven disturbances (Goeking and Izlar, 2018) including wildfire and mountain pine beetle (*Dendroctonus ponderosae* Hopkins), which have both increased dramatically in recent decades (Bentz et al., 2011; Jolly et al., 2015). As of 2016, half of all standing WBP are dead (Goeking and Izlar, 2018). White pine blister rust (WPBR; *Cronartium ribicola* J.C.Fisch.) is a fungal pathogen native to Asia which affects all North American white pine species (*Pinus* subgenus *Strobus*) and has become the main driver of the range-wide decline of WBP (Dudney et al., 2020; Goeking and Izlar, 2018; Shanahan et al., 2016). Due to its widespread range-wide decline and its importance as a food source for wildlife, WBP was recently listed as threatened under the Endangered Species Act (Levin, 2022).

WPBR was introduced to both the east and west coasts of North America on imported nursery stock from Europe in the early 1900s and has caused widespread mortality in white pines across the North American continent (Geils et al., 2010; Ghelardini et al., 2017; Liebhold et al., 2012). The fungus has a 3-6 year life cycle with several life stages, each affecting different hosts and preferring specific environmental conditions for spore germination and growth of the organism. The basidiospore stage is responsible for transmission of WPBR to WBP from its alternate host species including *Ribes* and *Castilleja* spp. WPBR basidiospores are produced in late summer during August and September. Therefore, climatic conditions during this period are likely to describe the conditions that specifically drive the transmission of WPBR to WBP, or alternatively limit transmission when conditions are unsuitable due to the susceptibility of the spores to desiccation and solar radiation (Geils et al., 2010). WPBR basidiospores, being thin-walled and short-lived, are sensitive to dry conditions and are only able to infect new hosts within a few kilometers of dispersal (Geils et al., 2010; Kearns et al., 2014). Both WPBR sporulation and spore germination have also been shown to be inhibited

by high temperatures (Van Arsdel et al., 1956). The fungus infects host plants through open stomata. Therefore, conditions driving increased transpiration and stomatal opening, such as lower vapor pressure deficit (VPD), are likely to promote infection (Dudney et al., 2021).

Larger trees are more susceptible to WPBR infection because of greater leaf surface area increasing the likelihood of intercepting airborne spores. Tree diameter at breast height (DBH) has been found to be positively associated with infection probability in white pines (Campbell and Antos, 2000; Kearns and Jacobi, 2007; Shepherd et al., 2024; Thoma et al., 2019b). However, the disease is more likely to be lethal in smaller diameter trees, where the infection has less distance to travel from needles to the bole where it can girdle and kill trees (Burns et al., 2023; Geils et al., 2010).

Previous work has established links between climate, at different spatial and temporal scales, and WPBR infection in WBP and other white pines in different regions of North America. WPBR infection in white pines has been linked to regional weather in the western US (Kearns et al., 2014). In the Greater Yellowstone Ecosystem (GYE), average relative humidity and temperature across August and September were identified as the best predictors of WPBR infection in WBP, with larger trees more likely to be infected (Thoma et al., 2019b). Fine-scale microclimates have also been shown to drive infection. In Wisconsin in the Great Lakes region infection in white pines was related to distance to shore, solar radiation, humidity, and wind currents (Van Arsdel, 1961). Wet landscape positions driven by factors such as proximity to streams or other water sources and topographic factors such as slope or aspect that influence solar radiation have also been associated with increased disease prevalence (Kearns et al., 2014; Smith-Mckenna et al., 2013). Decreased vapor pressure deficit, by driving increased stomatal opening, has also been associated with infections in white pines, although the effect of changing climate conditions was found to be non-linear and related to other factors such as shifts in ranges in alternate hosts (Dudney et al., 2021). In the northern reaches of WBP's range in Canada, WPBR incidence was associated with

high spring precipitation, cool and wet summers, humid Septembers, and higher growing degree days, with increasing tree size also a significant driver of infection (Shepherd et al., 2024). To our knowledge, all studies to date have been local to regional in spatial extent, and no studies have examined the climatic drivers of WPBR in WBP across larger scales such as its range in the contiguous United States (CONUS).

Current WBP conservation efforts focus on planting naturally disease-resistant seedlings in restoration areas, particularly recently burned stands. Recently burned stands are thought to be the natural regeneration niche for WBP because its primary dispersal agent, Clark's nutcracker (*Nucifraga columbiana* Wilson, 1811), uses openings in burned patches for seed caches (Norment, 1991; Tomback et al., 1990). Wildfires also reduce competition for light and resources from other species which allows WBP a competitive advantage since it grows more slowly than subalpine fir (*Abies lasiocarpa* (Hook.) Nutt.) and lodgepole pine (*Pinus contorta* Douglas), its primary competitors.

Outplanted seedlings represent a significant investment of time and resources into the process of identifying disease-resistant trees, propagating seedlings from seeds collected from their cones, and outplanting seedlings in the field. Successful restoration therefore relies on seedling success and efficient use of these resources. While high levels of quantitative resistance have been identified in resistance trials of WBP seedlings propagated from disease-resistant trees, this resistance is not a complete immunity to WPBR infection and survival rates of planted seedlings in the field are expected to be moderate at best even for the most resistant seedling phenotypes identified (Sniezko et al., 2024). Identification of locations that minimize WPBR disease hazard, defined here as probability of WPBR infection, prior to planting is prudent to maximize seedling success and promote successful restoration.

Here, we used a new long-term monitoring dataset across WBP's range in CONUS in combination with gridded climate data to address the following key questions:

1. What are the broad-scale climatic drivers of WPBR infection, particularly during the

August and September basidiospore transmission phase?

2. How does tree size influence infection probability?

3. How might future climate change alter WPBR disease hazard in the CONUS?

To answer these, we summarized climate conditions during the transmission phase and used them, along with tree diameter, to develop a model predicting the probability of infection for individual trees. Projections of geographic disease hazard were then made using this model to the year 2100.

Methods

Study area

The study area includes monitoring data from most of WBP's range in the contiguous United States (Figure 12). A dataset was assembled from WPBR monitoring data collected in National Park Service (NPS), US Forest Service (USFS), and Bureau of Land Management (BLM) lands. Our interest in projecting WPBR hazard for future periods precluded using observations from the northern part of WBP's range in Canada because climate projections from the Multivariate Adaptive Constructed Analogs (MACA) data (Abatzoglou and Brown, 2012) do not extend above approximately 49°N latitude.

A total of 490 monitoring transects with observations containing WBP from 2004 to 2022 were analyzed from 9 national parks including Crater Lake NP (CRLA), Glacier NP (GLAC), Yellowstone NP and surrounding federal lands (GYE), King's Canyon (KICA), Lassen Volcanic Monument (LAVO), Mount Rainier NP (MORA), Northern Cascades NP and Lake Chelan NRA (NOCA_LACH), Sequoia NP (SEQU), and Yosemite NP (YOSE), as well as monitoring data contributed by BLM (BLM_ID) and US Forest Service (Sawtooth_NF) partners (Table 4). Monitoring efforts differ between land management units in factors such as number of species monitored (multiple conifers or just WBP), sample design (sample frame,

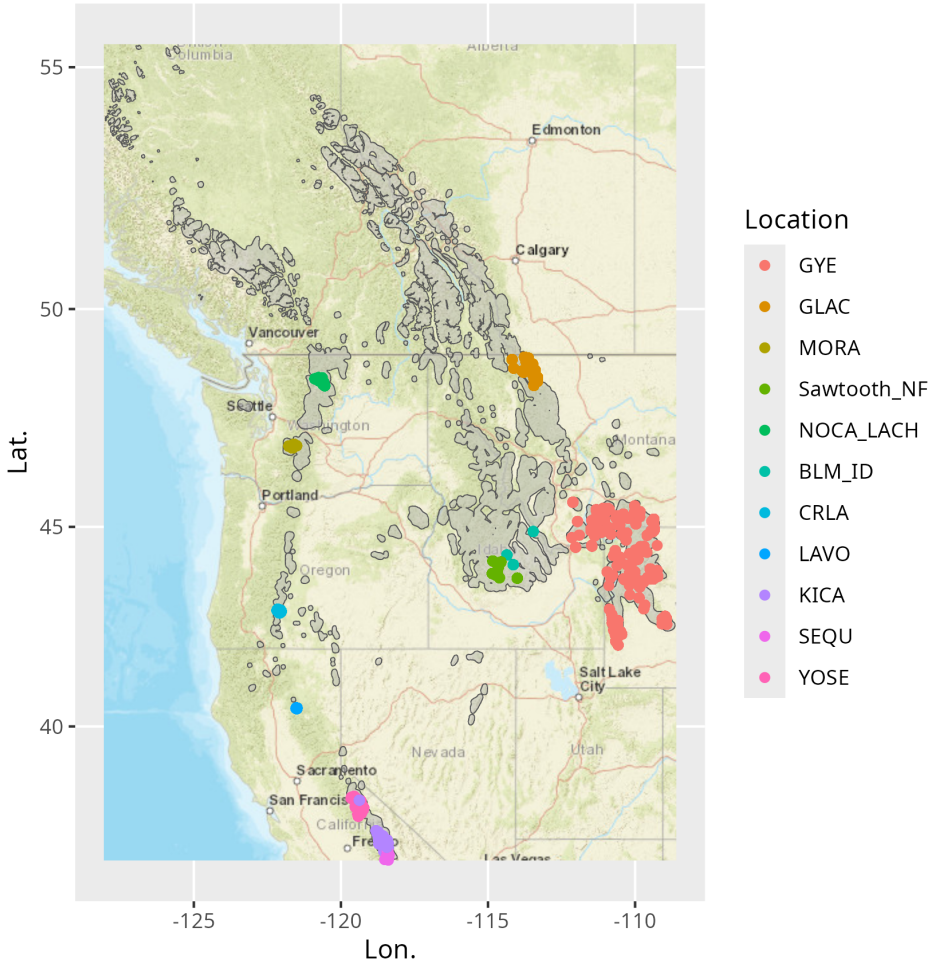

Figure 12. Map of study plots included in analysis. Existing WBP range from Keane et al. (2012) shown in grey.

use of transects or plots as sampling units, size of transects or plots), dates of implementation, amount of data collected (i.e., WPBR status, mountain pine beetle status), and availability of repeat observations or single visits. More detailed information about each monitoring program can be found in Greater Yellowstone Whitebark Pine Monitoring Working Group (2011) (GYE), Rochefort et al. (2010) (MORA, NOCA_LACH), McKinney et al. (2012) (CRLA, YOSE, SEQU, KICA, LAVO), Jenkins et al. (2020) (GLAC), Mancuso (2022) (Sawtooth_NF), and Rust and Gurvich (2018) (BLM_ID). An assessment of observation errors in the GYE monitoring program found a mean WPBR detection probability of 0.739

across observers (Shanahan et al., 2021); similar assessments are not available for the other monitoring units.

Our dataset combines observations from these monitoring programs that recorded tree-level data including: WPBR symptoms, DBH, tree status (live/dead), and year of data collection for WBP. WPBR symptoms include fruiting blister rust bodies (aecia), rodent chewing and gnawing, flagging of branches, blisters, cankers, and defoliation (Hoff, 1992; Six and Newcomb, 2005). To prepare the monitoring data for analysis, WPBR infection presence was recorded for each tree if clear signs or symptoms (e.g., cankers) were present or developed during repeat visits. For example, if cankers were recorded on any part of the tree, or if an uninfected tree was recorded as having cankers during a subsequent visit the tree was recorded as infected for purposes of this analysis. Because our interest is in climatic correlates of infection, and not survival, trees that were recorded as infected during any visit were placed in the infected category, even if during later visits trees did not show symptoms, because infected branches may have been removed from wind, snow, self-pruning, or animal damage. Observations where trees were recorded as dead or did not have DBH recorded were not included. These rules classified each live WBP tree with DBH data available as infected or uninfected during the 2004–2022 monitoring period.

Historical climate data

To characterize the climate relevant to WPBR infection at each transect, we obtained daily climate data for August and September to represent climatic conditions during the WPBR basidiospore transmission season from the gridMET 4 km gridded surface meteorological dataset (Abatzoglou, 2013). We included climate data from 2000 to 2022; this period starts four years prior to the first field observation (2004) to account for potential lags in the appearance of visible infection symptoms (Hoff, 1992). We calculated combined August and September mean daily temperature, mean daily relative humidity, total daily

Monitoring Area	Transects	Trees	asP (mm)	asT (°C)	asVPD (kPa)	asRH (%)	DBH (cm)	Inf. rate (%)
GYE	181	5502	90.27	10.51	0.88	46.33	15.80	45.80
GLAC	64	2125	119.66	10.51	0.75	54.55	15.55	75.06
MORA	31	862	104.58	10.54	0.60	62.41	16.34	46.71
Sawtooth_NF	12	665	60.25	11.52	0.99	43.09	16.25	11.57
NOCA_LACH	52	1478	89.55	10.83	0.76	50.35	13.34	54.89
BLM_ID	3	152	69.12	11.44	0.89	49.05	32.25	46.84
CRLA	30	1251	49.74	12.15	0.83	55.14	15.04	43.24
LAVO	30	833	41.15	12.00	1.05	42.79	13.95	51.82
KICA	41	5035	13.42	9.62	0.82	38.97	11.06	5.94
SEQU	11	386	6.08	10.46	1.00	34.08	20.40	1.51
YOSE	35	4003	24.28	11.15	0.96	36.67	8.39	3.82
Western U.S.	490	22292	60.74	10.98	0.87	46.68	16.22	35.2

Table 4. Summary of monitoring data. August and September climate averages were calculated for the period included in analysis (2000–2022). DBH (cm) is the average DBH of all trees in all transects in each monitoring area included in the analysis. Infection rate shows average rates of WPBR infection in WBP trees across all transects in each monitoring area. The Western U.S. row shows total number of transects and trees included in analysis as well as averages of asP, asT, asVPD, asRH, DBH, and infection rates across all monitoring areas.

precipitation, and mean daily vapor pressure deficit for each year in the 2000–2022 period. Finally, we averaged these annual combined August and September metrics across the entire 2000–2022 period to generate climate normals for each transect location: 2000–2022 August and September temperature (asT, $^{\circ}C$), relative humidity (asRH, $\%$), precipitation (asP, mm), and vapor pressure deficit (asVPD, kPa).

Correlation analysis

The probability of WPBR infection in individual trees (tree-level model) was estimated using Generalized Linear Mixed Models (GLMMs) using a logit link function. A series of tree-level models were fit with blister rust status (infected or not) as a response variable and predictors including log(DBH) (log-transformed DBH) and August and September climate variables as well as a spatial random field. Observations of tree diameter at breast height (DBH) were right-skewed (positive skewness), but approximately normally distributed after a log transformation was applied (Figure 14). Correlation between pairs of climate variables was calculated, and pairs of climate variables that exceeded a threshold correlation ($R \geq$

0.65) were excluded from the same model to limit multicollinearity but were included in separate models without other highly correlated variables.

Second-order terms were included for some variables such as temperature to allow for a hump-shaped effect where the climate is outside the range suitable for successful infection. Interactions between climate variables were included as previous work has identified significant interactions between variables such as asT and asRH (Thoma et al., 2019b). When second-order terms or interactions were included, all first-order terms were maintained, even when strength of evidence for the coefficients of these terms was weak in order to maintain interpretability of coefficients following the marginality principle in regression analysis (Nelder, 1977).

To account for spatial autocorrelation (SAC) in both monitoring and climate data, a spatial random field was included in models which explicitly models the spatial structure in the data including spatially varying but temporally consistent processes that are not included as fixed effects in the model. In the context of this study, these processes could include factors such as proximity to WPBR alternate hosts which were not included in the monitoring data. Ecological data observed across space are inherently autocorrelated, as observed in the patches and gradients that form naturally in the landscape. However, SAC presents issues for statistical testing because it violates assumptions of independence needed for many statistical procedures and inflates estimates of confidence in statistical testing, leading to spurious significance and underestimated uncertainty (Legendre, 1993).

Spatial random fields have been shown to improve model performance in Species Distribution Models which did not explicitly model spatial relationships in the data (Mielke et al., 2020). The spatial random field was estimated with a Stochastic Partial Differential Equation (SPDE) approach using a Matérn covariance function (Anderson et al., 2024). Parameters for the SPDE mesh were selected to approximately place mesh vertices equally distributed within clusters of points where data were collected, and mesh vertices were

increased until the estimates for the variance of the Matérn range were approximately minimized but no further to minimize the risk of overfitting (Anderson et al., 2024; Righetto et al., 2020), which resulted in a 2-dimensional SPDE mesh with a cutoff of 10km, inner and outer section max triangle lengths of 75 and 100 km, respectively, and inner and outer section border widths of 75 and 100 km, respectively (Figure 13). Observation coordinates were reprojected on a Lambert conformal conic projection to minimize distortion of distance to improve accuracy of the spatial random effect generated with the SPDE mesh (Anderson et al., 2024). Comparison of similar models fit with and without a spatial random field showed that the spatial random field effectively removed all visible evidence of SAC in diagnostic plots.

Our model estimating probability of WPBR infection can be written as follows:

$$
\begin{aligned}
y_s &\sim \text{Bernoulli}(\mu_s), \\
\mu_s &= \text{logit}^{-1}(\boldsymbol{X}_s^{\text{main}}\beta + \omega_s), \\
\omega &\sim \text{MVNormal}(\mathbf{0}, \boldsymbol{\Sigma}_\omega).
\end{aligned}
$$

where $\boldsymbol{X}_s^{\text{main}}$ represents a matrix of main effect covariates (intercept, first- and second-order terms for climate variables, variable interactions, and tree size), β represents a vector of estimated main effect coefficients, and ω_s represents the estimated spatial random field at a location s. ω is drawn from a multivariate random distribution with a covariance that is determined by the Matérn covariance function, which describes how spatial covariance decays with distance. The spatial random field represents the effect of latent spatial variables that are otherwise not accounted for in the model. In other words, this is spatially correlated noise arising from unmodeled processes such as proximity to WPBR alternate hosts (i.e., *Ribes* or *Castilleja* spp.), local soil characteristics, and other factors affecting disease transmission, such as proximity to streams or other water sources (Kearns et al., 2014).

Model predictive strength was evaluated with AICc (Table 5). The performance of the best-performing model was evaluated with an 8-fold cross-validated confusion matrix to quantify model performance (Figure 15).

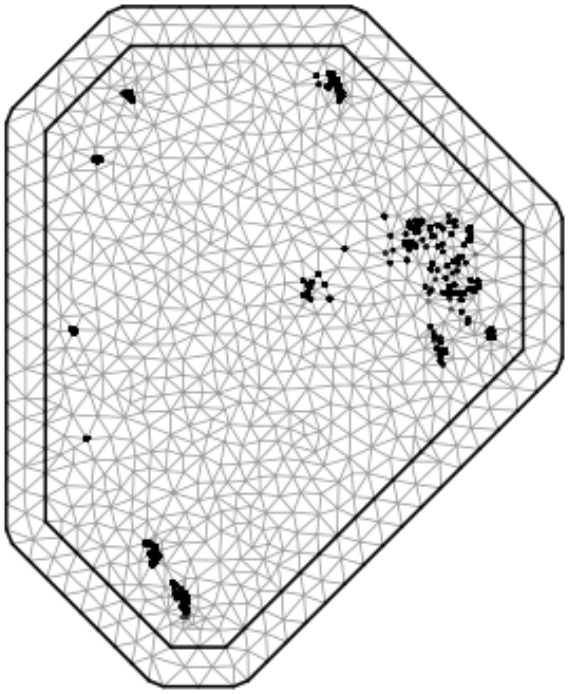

Figure 13. Stochastic partial differential equation (SPDE) mesh used to generate spatial random field in `sdmTMB`. Black points show locations of monitoring transects within the mesh. Connections between mesh knots are shown in grey. Inclusion of a spatial random field in GLMs can help minimize spatial autocorrelation (SAC).

Projections of white pine blister rust hazard

Projections of white pine blister rust hazard (probability of WPBR infection) were developed using the top model and future climate data from the 4 km Multivariate Adaptive Constructed Analogs (MACA) gridded climate data product (Abatzoglou and Brown, 2012). Average August and September daily temperature (asT) and relative humidity (asRH) were calculated from daily temperature and relative humidity minimum and maximum for 12 general circulation models (GCMs) and representative concentration pathways (RCPs; RCP4.5

Figure 14. Exploratory data analysis of variables used in modeling white pine blister rust (WPBR) infection in whitebark pine (WBP). The pairs plot displays scatter plots illustrating the relationships between different climate variables (2000-2022 August and September temperature [asT, $^{\circ}C$], precipitation [asP, mm], relative humidity [asRH, $\%$], and vapor pressure deficit [asVPD, kPa]) and tree diameter at breast height (log_dbh_cm, cm), along with histograms and boxplots showing the distribution of each variable and its distribution across trees with and without WPBR infection (br_status, *True* if tree showed signs of infection else *False*). Tree DBH (cm) was log-transformed (log_dbh_cm) to address its right-skewed distribution to meet assumptions of normality in linear models. The figure also presents Pearson correlation coefficients (R) between pairs of variables; pairs with a correlation $|R| \geq 0.65$ were exclude from being included in the same statistical models to mitigate multicollinearity. This exploratory analysis informed the selection of predictor variables for the WPBR infection models.

and RCP8.5) across twenty-two-year-long periods to match the length of the climate normals used to train the model: current (2007–2029), near-term (2030–2052), mid-term (2053–2075), and end-of-century conditions (2077–2099). The ensemble average asT and asRH for RCP4.5 and RCP8.5 scenarios were also calculated from the same 12 GCMs. The MACA dataset provides projections for 13 GCMs; however, the temperature minimum dataset from the CCSM4 GCM could not be accessed and this GCM was excluded from this analysis.

Probability of WPBR infection was estimated using the model selected in the above analysis ($\text{br\_status} \sim \text{asT}^2 \times \text{asP} + \log(\text{DBH}) + \omega_s$) for the four time periods for each GCM and ensemble averages for each RCP. Areas in the projections were masked with the "existing" WBP Distribution layer provided by the WPEF (Keane et al., 2012) to limit projections only to areas currently known to contain WBP in order to quantify changes in probability of infection within the current distribution of WBP. To quantify areal changes in disease hazard, projected probability of WPBR infection was classified into low-hazard rate ($\text{p(infection)} \leq 0.10$), medium-hazard rate ($0.25 \geq \text{p(infection)} > 0.10$), and high-hazard rate ($\text{p(infection)} > 0.25$) within existing WBP habitat. The percentage of area classified as each hazard rate class out of the range of WBP in the contiguous United States (total area 311,643.8 km^2) was calculated.

Computational environment

The analysis was conducted in `R` version 4.4.3 (R Core Team, 2024) using the packages `terra` (Hijmans, 2024) and `sf` (Pebesma, 2018) for spatial analysis, `tidyverse` (Wickham et al., 2019) for tabular data manipulation, and `ggplot2` (Wickham, 2016), `GGally` (Schloerke et al., 2024), `visreg` (Breheny and Burchett, 2017), and `tidyterra` (Hernangómez, 2023) for plotting. Logistic regression models with spatial random fields were fit using the `sdmTMB` package (Anderson et al., 2024). The `fmesher` package was used to create the Stochastic partial differential equation (SPDE) mesh used by `sdmTMB` (Lindgren, 2024). Models were

compared using the `model.sel` function from the `MuMIn` package(Bartoń, 2025). Model performance was assessed with confusion matrices made using the `cvms` package (Olsen and Zachariae, 2024). Spatial autocorrelation was assessed with semivariogram plots (Gotelli and Ellison, 2013).

Results

Climatic correlates of WPBR infection in WBP

WPBR infection rates across monitoring units varied from 1.51% of trees in SEQU to 75.06% of trees in GLAC (Table 4). A linear model relating average 2000–2022 August and September precipitation and temperature to infection rates in monitoring units (inf_rate $\sim$ asT^2 $\times$ asP) had an R^2 of 0.64, suggesting that up to 64% of the variation in infection rates between monitoring units could be explained by the interaction between asT and asP.

We found that probability of WPBR infection in individual trees was best estimated by a model including average 2000–2022 August and September temperature (first and second-order effects) and precipitation (first-order), as well as the interaction between temperature and precipitation, with a spatially varying random effect (Table 6). The model has a Matérn range (range at which points become spatially independent for the estimated spatial random field) of 65.09 km (Figure 13). The second-best-performing model included first and second-order effects of August and September Temperature and tree DBH, with a delta AICc of 78.63 (Table 5).

Cross-validation (based on the confusion matrix resulting from an 8-fold cross-validation of the top model) showed the top model had a predictive accuracy of 80.9%, a sensitivity of 63.3% (percent of infected trees that were correctly identified as infected), and a specificity of 88.2% (percent of uninfected trees that were correctly identified as uninfected) (Figure 15).

Increasing tree DBH was associated with higher risk of WPBR infection after accounting for the effect of asT, asP, and latent spatial variables (Figure 16) resulting in a higher

Model	**df**	**logLik**	**AICc**	**ΔAICc**
$\text{asT}^2 \times \text{asP} + \log \text{DBH}$	9	-8624.2	17266.4	0.0
$\text{asT}^2 \times \text{asRH} + \log \text{DBH}$	9	-8637.3	17292.7	26.3
$\text{asT} \times \text{asP} + \log \text{DBH}$	7	-8655.0	17323.9	57.6
$\text{asT} \times \text{asRH} + \log \text{DBH}$	7	-8664.5	17343.1	76.7
$\text{asT}^2 + \log \text{DBH}$	6	-8666.5	17345.0	78.6
$\text{asT} + \text{asP} + \log \text{DBH}$	6	-8667.1	17346.2	79.8
$\text{asVPD}^2 + \log \text{DBH}$	6	-8667.5	17346.9	80.6
$\text{asP} + \log \text{DBH}$	5	-8670.3	17350.6	84.2
$\text{asT} + \log \text{DBH}$	5	-8670.7	17351.4	85.0
$\text{asT} + \text{asRH} + \log \text{DBH}$	6	-8670.5	17353.0	86.6
$\text{asVPD} + \log \text{DBH}$	5	-8674.2	17358.3	92.0
$\log \text{DBH}$	4	-8679.6	17367.2	100.9
$\text{asRH} + \log \text{DBH}$	5	-8678.7	17367.5	101.1
$\text{asRH}^2 + \log \text{DBH}$	6	-8677.9	17367.9	101.5

Table 5. Model selection table. The response variable for all models is blister rust status (1 for infected, 0 for not) and all models included a spatial random field (ω_s). Models with second order terms also include first-order terms for the same variables following the hierarchical principle. The top-performing model as evaluated by AICc is $\text{br\_status} \sim \text{asT}^2 \times \text{asP} + \log(\text{DBH}) + \omega_s$.

Term	**Coefficient estimate**	**Coefficient SE**
Intercept	-2.63	0.52
$\log \text{DBH}$	0.64	0.02
asT	-48.74	15.08
asT^2	83.61	11.02
asP	0.00	0.00
asT x asP	0.96	0.19
asT^2 x asP	-0.97	0.15

Table 6. Estimated coefficients and standard errors for selected model ($\text{br\_status} \sim \text{asT}^2 \times \text{asP} + \log(\text{DBH}) + \omega_s$).

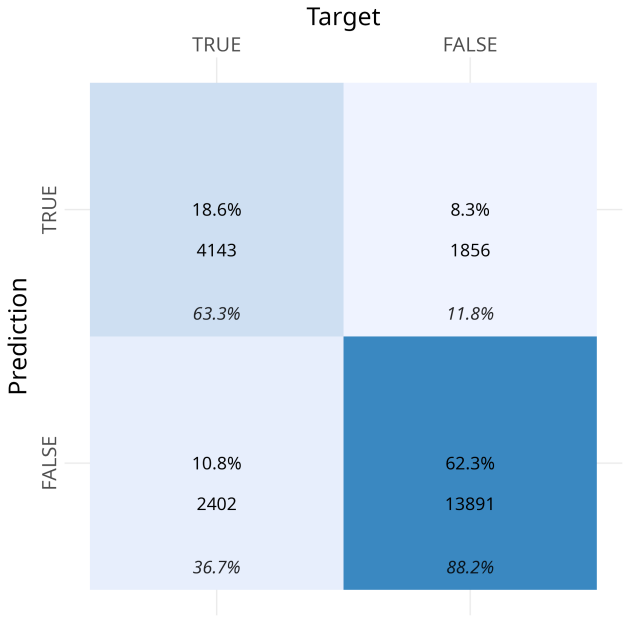

Figure 15. 8-fold cross-validated confusion matrix for the selected model ($\text{br\_status} \sim \text{asT}^2 \times \text{asP} + \log(\text{DBH}) + \omega_s$). Percentages and numbers in center of boxes are the percent and absolute numbers, respectively, of all observations classified in that quadrant. Percentages at bottom of boxes are column-wise classification rates showing prediction accuracy within target classes, i.e., the percentage of infected trees that were correctly classified as infected (True positives) or incorrectly classified as uninfected (False negatives).

probability of infection for mature trees (Figure 17b) compared to seedlings (Figure 17a) for any combination of asT and asP. The effect of asT varies at different levels of asP, and vice versa (Figure 17). At lower levels of precipitation (0 mm precipitation during August and September), asT has a U-shaped relationship with probability of WPBR infection, with lowest probability of infection observed around 11°C. The effect of asT on probability of infection is parabolic as precipitation in August and September increases, leveling out around 100 mm asP and then becoming parabolic at higher levels of asP with highest infection rates observed around 11°C. asP has an estimated coefficient of 0 (Table 6). Therefore, asP itself has no direct linear effect on probability of infection besides through its interaction with asT (Est. coef. 0.96) and asT^2 (Est. coef. -0.97) (Table 6). Thus, as temperature changes, the change in probability of WPBR infection for a given tree size and location will depend on

asP (Figure 17).

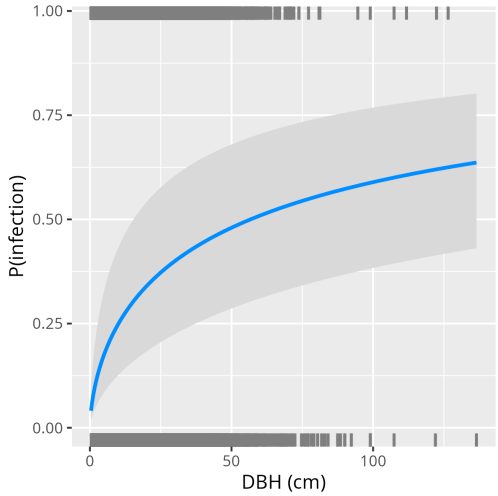

Figure 16. Effect of tree-size predictor DBH (cm) on probability of infection holding other fixed effects at their median values (asT: 10.67 °C, asP: 50.41 mm) and after accounting for latent spatial variables.

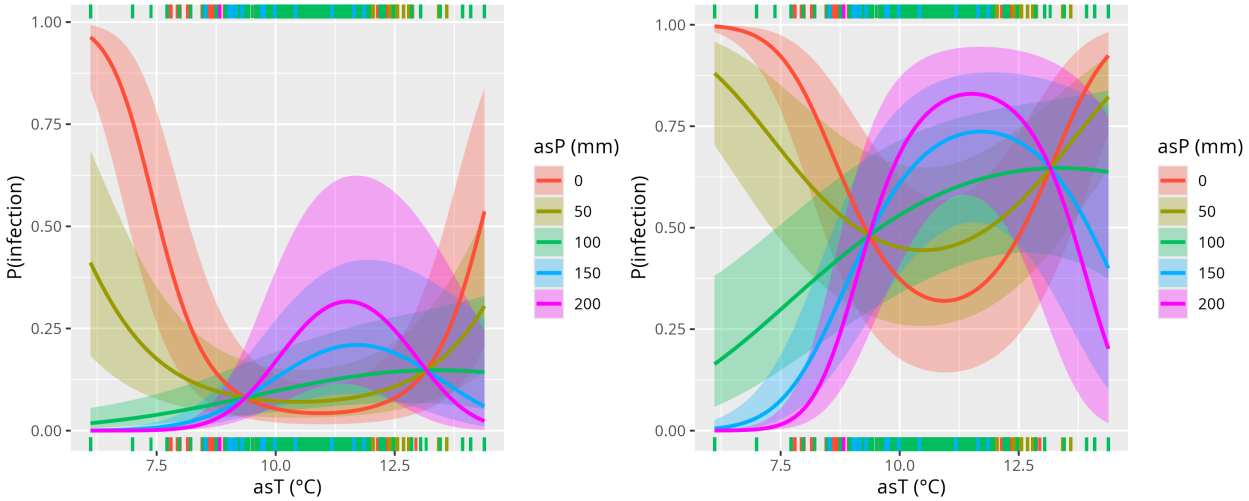

(a) Seedlings (1 cm DBH)

(b) Mature trees (40 cm DBH)

Figure 17. Effect of interaction between asT and asP on probability of infection for a) seedlings (1 cm DBH) and b) mature trees (40 cm DB), after accounting for other spatially varying processes. asP is visualized as the effect of asT at different levels of asP.

Mean August and September temperature for 2000-2022 did not vary much between monitoring areas, but there was considerable variability in August and September precipitation

with a range of 6.08 to 119.66 mm (Table 4). SEQU in particular experiences very dry summers, with almost no precipitation occurring during August and September in most years (Figure 18), which could be associated with the low infection rates in the monitoring area (mean infection rate 1.51%) as mean temperatures in the region (10.46 °C) are near the temperature that minimum infection rates are predicted at low levels of asP (Figure 17).

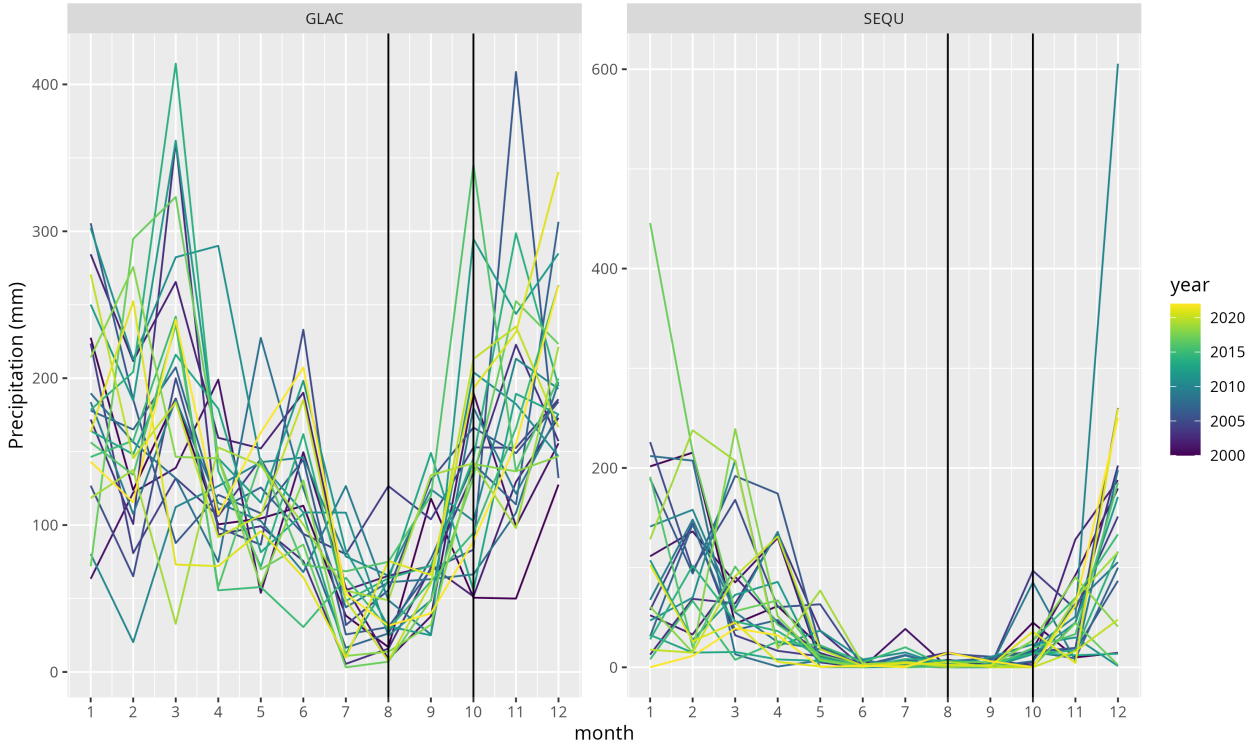

Figure 18. Monthly sum of precipitation (mm) for GLAC and SEQU across all years in study. These locations were chosen as examples of a wet region with high infection rates (GLAC) and a dry region with low infection rates (SEQU) (Table 4). Vertical lines are placed to highlight the August and September period that is understood to be the WPBR basidiospore transmission season.

Projections of WPBR disease hazard in WBP

Projections of WPBR hazard for WBP seedlings (1 cm DBH) generally show an increase in the area classified as high-hazard over time, while the area classified as medium-hazard decreases; however, projections vary significantly depending on the combination of GCM and

RCP (Figure 19a). Projections for mature trees (40 cm DBH) generally show a decrease in the area classified as high-hazard and an increase in area classified as low- and medium-hazard, but again with significant variability between projections (Figure 19b).

Geographic patterns of modeled probability of WPBR infection under RCP4.5 and RCP8.5 end-of-century ensemble projections vary between seedlings (Figures 20a & 20b) and mature trees (Figures 20c & 20d). A general increase in probability of infection is modeled across WBP's range for seedlings, with lower projected probability of infection in both scenarios for areas such as the Western Cascade range, Sierra Nevada, GLAC, and high-elevation regions of Idaho and the GYE. For mature trees, much smaller proportions of the landscape are projected to remain low disease hazard compared to seedlings, with smaller areas in the same regions that show low disease hazard for seedlings also showing low disease hazard for mature trees under both RCP4.5 and RCP8.5 ensemble projections.

Discussion

Bioclimatic controls of WPBR infection in WBP

We found that probability of WPBR infection in individual WBP trees across CONUS was best estimated by a model including average 2000–2022 August and September temperature (first and second-order effects) and precipitation (first-order) and their interactions, tree size (log(DBH)), and a spatially varying random effect (Table 6). These variables represent the climatic conditions during the basidiospore transmission season which is the period of time that WPBR is able to transmit from an alternate host to WBP.

Consistent with previous work in the GYE (Thoma et al., 2019b) and Canada (Shepherd et al., 2024), larger diameter trees are predicted to be more likely infected than smaller trees, which is consistent with the hypothesis that greater leaf area in larger trees presents more opportunities for basidiospore entry through stomata (Figure 16). (Shepherd et al., 2024) also specifically modeled seedling infection, finding that for WBP it was explained by canopy

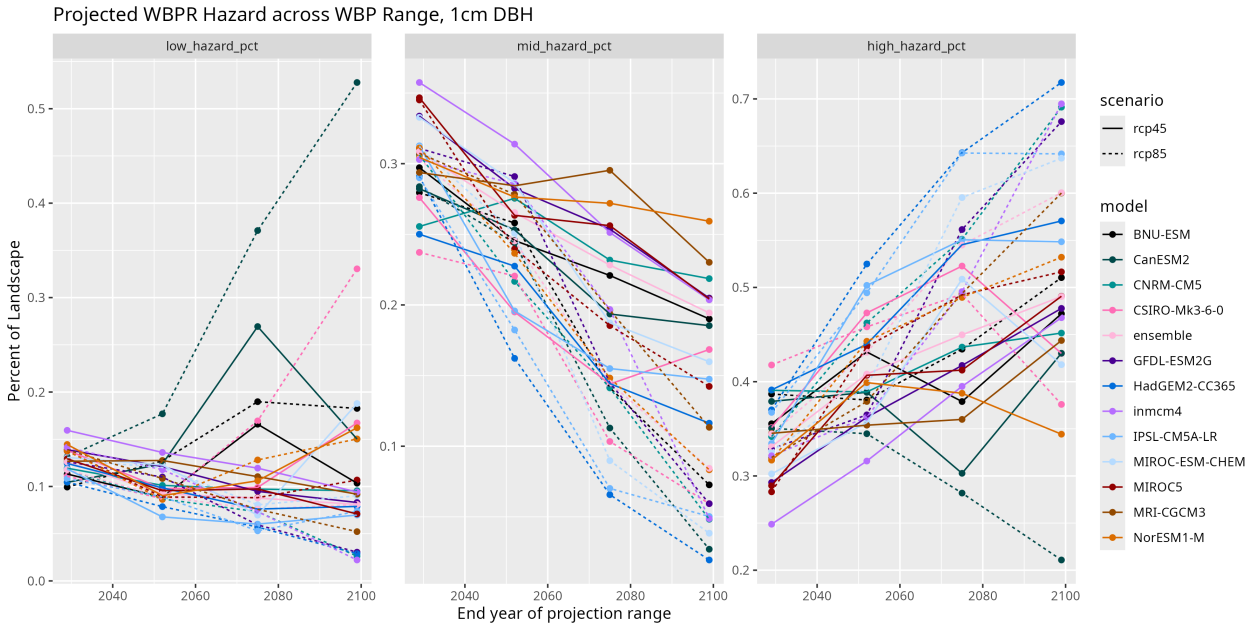

(a) Seedlings (1 cm DBH)

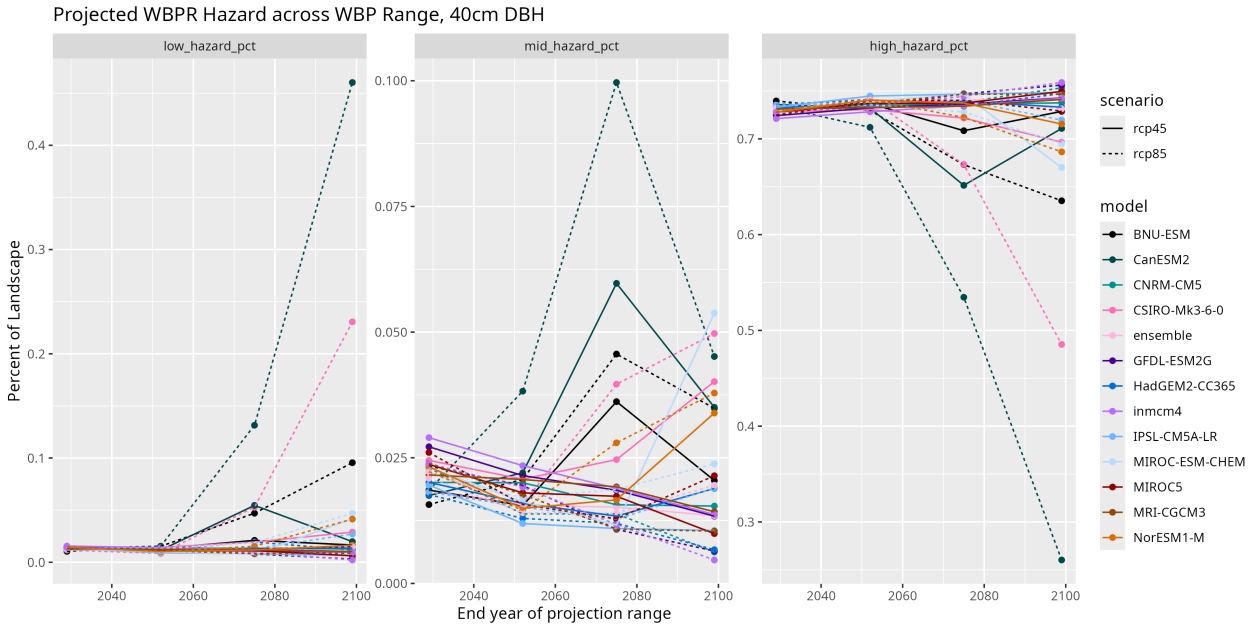

(b) Mature Trees (40 cm DBH)

Figure 19. Changes in projected area classified as low (p(infection) $\leq$ 0.1), medium (0.1 $<$ p(infection) $\leq$ 0.25), and high (p(infection) $>$ 0.25) WPBR hazard classes under each GCM and Pathway studied for a) seedlings (1 cm DBH) and b) mature trees (40 cm DBH). Percents of landscapes are calculated using from the total area of WBP range in the Contiguous United States in the WPEF "Existing" distribution data (311,643.8 km^2)

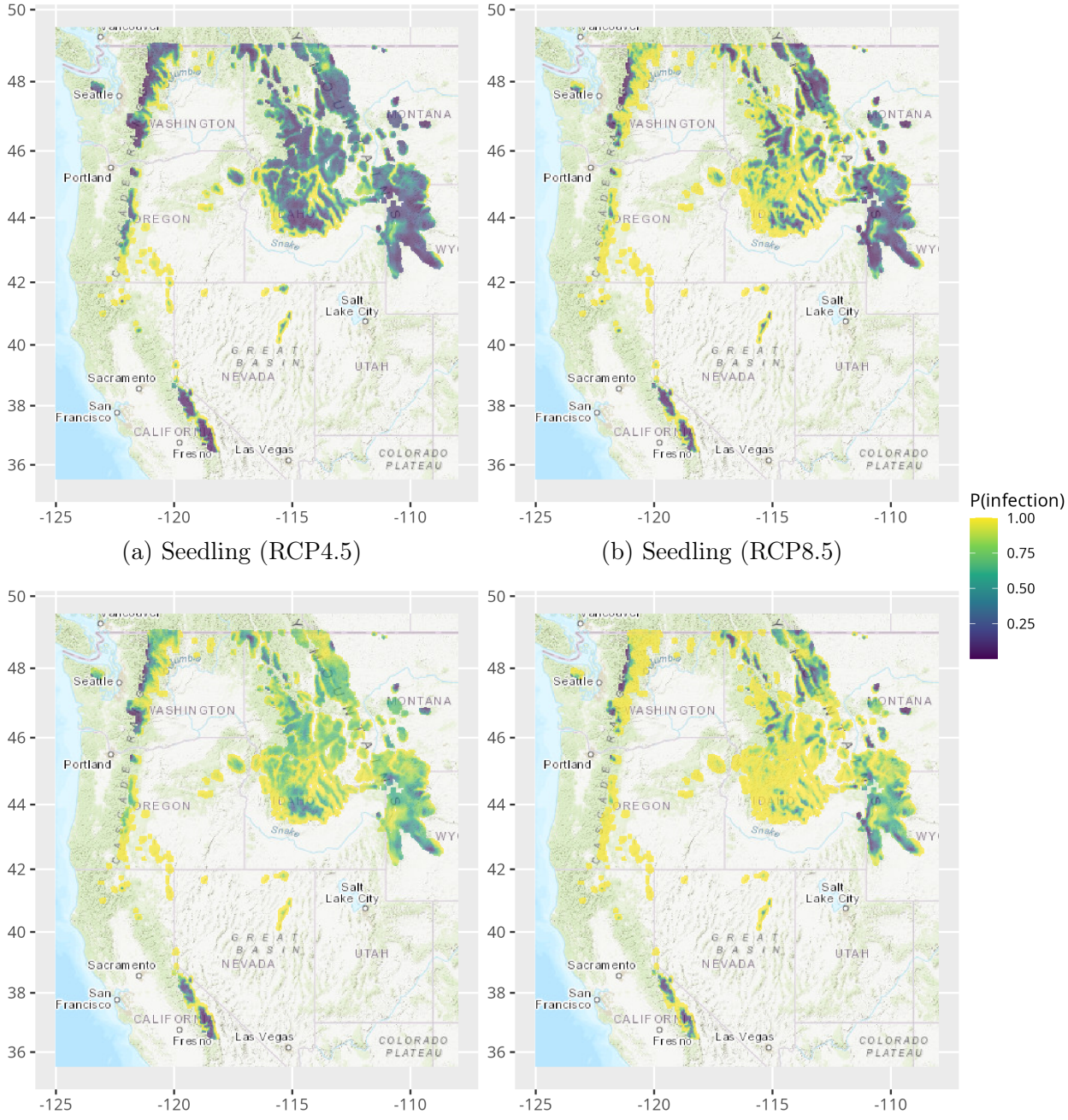

(a) Seedling (RCP4.5)

(b) Seedling (RCP8.5)

(c) Mature tree (RCP4.5)

(d) Mature tree (RCP8.5)

Figure 20. End-of-century probability of WPBR infection projected under the 12 GCM ensemble conditions for a,b) seedlings (1 cm DCH) and c,d) mature trees (40 cm DBH) for RCP4.5 and RCP8.5 emissions scenarios. Predictions include all fixed and random effects. Projections are limited to the existing WBP range from Keane et al. (2012).

kill, growing degree days, elevation, heat load, latitude, spring precipitation, and spring solar radiation. We applied our model to seedlings by adjusting DBH but do not derive seedling-specific climatic drivers beyond the general model.

The effect of temperature on August and September temperature was found to vary at different levels of August and September precipitation, and vice versa, similar to the interaction between August and September temperature and relative humidity in the GYE found by Thoma et al. (2019b). At higher levels of precipitation (approximately or greater than 100 mm asP), maximum infection rates are predicted around 11 °C average August and September temperature. Conversely, at lower levels of precipitation (0 to around 100 mm asP), this relationship inverts and minimum infection rates are predicted around 11 °C average August and September temperature and highest infection rates at low (around 7 °C) or high (around 13 °C) temperatures. This relationship that is predicted at lower precipitation levels should be interpreted with caution due to the limited number of observations at these combined low temperature and precipitation values. Additionally, as WPBR infection is fundamentally dependent on adequate moisture for basidiospore survival, germination, and entry into needles through open stomata, this finding of very high probability of infection under conditions of low precipitation at temperature extremes is biologically implausible as insufficient moisture would inhibit these critical steps. (Thoma et al., 2019b) included only a first-order effect for temperature, but likewise found that maximum infection probability in the GYE was predicted around August and September average temperatures of 11 °C, after accounting for August and September average relative humidity, tree size, and transect-to-transect variability. The inclusion of a second-order term for temperature in our model improved model performance because it allows for infection probabilities to drop beyond the peak temperature where conditions become either too hot or too cold for optimal infection (Figure 5).

It is widely understood that infection rates vary regionally. For example, infection

rates in GLAC were much higher than SEQU over 2000–2022 (Table 4). We hypothesized that infection rates are related to the climate conditions that are more conducive to WPBR transmission, as evidenced by the linear model at the monitoring unit level relating infection rates to the interaction between asT^2 and asP which has an R^2 of 0.64. This suggests that up to 64% of the variation in WPBR infection rates at the monitoring unit level is explained by interactions between asP and asT. We hypothesized that climate would also explain individual tree infection probability because the accumulation of individual tree infections results in differences in infection rates at the monitoring unit level. We chose not to model transect-level infection rates (if any tree in a transect is infected the whole transect is classified as infected) because Thoma et al. (2019b) and Shepherd et al. (2024) showed a strong dependence of infection of individual trees on tree DBH, which required analyzing the monitoring at the level of individual trees. This dependence of tree size as a predictor of WPBR infection results in divergent model predictions for different tree sizes, with much lower probability of infections predicted for seedlings (1 cm DBH) than mature trees (40 cm DBH) for any combination of August and September temperature and precipitation (Figures 16 & 17) resulting in very different projections of end-of-century disease hazard for seedlings and mature trees (Figure 20). The tree size-dependent effect on infection hazard has significant implications for managers.

Our findings build on previous regional studies of the effect of climate on WPBR infection. In the GYE, the interactions of August and September relative humidity and temperature were found to be the strongest predictors of WPBR infection in WBP, with similar infection optimums occurring around average August and September temperatures of 11°C (Thoma et al., 2019b). RH could predict infection rates by explaining the "wetness" that drives basidiospore production or germination due to control on stomatal closure, leading to lower infection rates when RH was low. At the broader spatial scale examined here, we found that August and September precipitation better explained this "wetness" than RH, as was

found in the GYE, after accounting for August and September temperature, tree size, and other spatially varying processes. Other studies in the Sierra Nevada and Rocky Mountains identified twenty-year averages of VPD (Dudney et al., 2021) or four-year averages of August and September maximum VPD (Burns et al., 2023) to be key predictors of WPBR infection in WBP and other white pines. VPD, precipitation, and relative humidity are interconnected measures of atmospheric moisture or dryness important for WPBR infection. In the northern reaches of WBP's range in Canada, which was excluded from this analysis for reasons noted above, WPBR infection was associated with high spring precipitation, cool/wet summers, and high September relative humidity (Shepherd et al., 2024). (Shepherd et al., 2024) also found that low solar radiation was associated with higher infection rates, which was hypothesized to be a result of low leaf temperatures with higher solar radiation creating temperatures unsuitable for WPBR infection, consistent with our finding that high temperatures, at least at high precipitation, reduce modeled infection probability. While higher summer temperatures may limit probability of infection, it is also associated with higher WPBR-related mortality in WBP in mountain ranges in California (Young et al., 2023).

Conditions of high atmospheric moisture, whether indicated by high RH, low VPD, or high precipitation, prevent basidiospore desiccation and promote open stomata in WBP needles, facilitating infection (Dudney et al., 2021; Thoma et al., 2019b). Our finding that increased August and September precipitation is correlated with higher infection probability (Figure 17) supports this. While rainfall could physically wash spores from needles, potentially reducing infection (Kearns et al., 2014), our broad-scale analysis identified August and September precipitation as the strongest moisture-related predictor. This contrasts with finer-scale studies where annual VPD or August and September RH were better-performing predictors of infection (Dudney et al., 2021; Thoma et al., 2019b). Such scale-dependent differences in predictor importance might reflect varying infection processes or genetic resistance across populations, factors potentially captured entirely or in part by the spatial

random effect in our model.

Projections of future disease hazard and uncertainty in projections

Projected disease hazard is generally higher across WBP's range for mature trees than for seedlings, with smaller locations in those same regions that are low disease hazard for seedlings also projected to remain lower disease hazard for mature trees (Figure 20). In general, areas that recently had low rates of infection, such as the Sierra Nevada in California (Table 4), are projected to maintain low rates of infection for all sizes of trees in higher elevations, with increases in probability of infection at lower elevations. On the contrary, the Crown of the Continent ecosystem containing Glacier National Park, which has among the highest recent infection rates, is projected to show low probabilities of infection under some climate projections. Lower rates of infection for all size classes of tree in this region are notably projected under the higher-emissions RCP8.5 scenario than the lower-emissions RCP4.5.

Given planting objectives that seek to establish trees that will survive to cone-bearing age around the end of the century, those areas with lower disease hazard for mature trees (dark blue areas in Figures 20c & 20d) should be selected for seedlings outplanted today. However, we note that given the uncertainty both in the effect of climate on modeled probability of WPBR infection (Figure 17) as well as in the projected ranges of temperature and precipitation that result in divergence in disease hazard classes made using this model to predict probability of WPBR infection using different GCMs and RCPs (Figure 19), that recommendations for specific areas to plant today using this model can be made only with low certainty.

Another source of uncertainty comes from the spatial random field included in the model that is time-invariant in modeled projections (Figure 13). This component of the model accounts for spatially-varying biotic and abiotic factors affecting WPBR disease incidence

that are not otherwise accounted for by climate terms and DBH. This includes factors such as proximity to alternate hosts of WPBR that are significant drivers of WPBR infection and can interact with climate to produce non-linear shifts in disease prevalence (Dudney et al., 2021; Geils et al., 2010). The model assumes that these spatially-varying factors are time-invariant, but it is likely that at least some of these factors incorporated as a spatial random effect in the model such as distribution of WPBR alternate hosts are likely to change in the future. Projections made with this model could be improved by incorporating monitoring data for some of these spatially-varying factors as well as incorporating longitudinal data to allow modeling how these factors vary through time as well as through space.

Monitoring data are lacking from some parts of WBP's range (Figure 12), such as portions of the Cascade Range, much of Idaho, and the Northern Rockies outside of GLAC, which limits accuracy of the SPDE mesh in those areas, and therefore accurate estimation of the spatial random effect and overall model accuracy. The model will perform most accurately in areas with many sampling points well distributed in the region, such as the GYE and Sierra Nevada (Figure 12), and least accurately in areas in which sufficient sample points are lacking for accurate interpolation of the SPDE mesh or areas in which climate varies significantly from the training data and extrapolation of the model is required.

Study strengths and limitations

This study represents a significant advancement by providing the first comprehensive analysis of climatic drivers influencing WPBR infection in WBP across the species range in CONUS. We synthesized extensive, long-term monitoring data from diverse federal and state agency partners producing a novel dataset that enabled the largest-scale study of climatic drivers of WPBR infection in WBP to date. The application of spatial generalized linear mixed models using `sdmTMB` enabled incorporation of climatic interactions while explicitly accounting for spatial autocorrelation through a spatial random field. Spatial autocorrelation

is a critical consideration often overlooked in large-scale ecological analyses that introduces potential bias in coefficient estimates and inference (Legendre, 1993). This work provides a robust foundation for understanding range-wide WPBR dynamics and generating spatially explicit projections of disease hazard relevant to the conservation of the threatened WBP.

Despite these strengths, limitations in our monitoring and climate data as well as modeling approach warrant consideration. The monitoring data used to train our model are not longitudinal (although repeat measures are available for some monitoring units); therefore, we cannot know the exact timing of infection in monitored trees. This restricts our ability to relate infection to climate normals (climate data averaged over relatively long time frames). The consequence is loss of information that would allow us to tie optimal climate conditions for infection to wave years of infection when most infections likely occurred. It also forces infections to be associated with climate conditions that aren't conducive to infection. For example, in SEQU, precipitation during August and September is low most years, averaging 6.08 mm of precipitation (Table 4). However, despite low summer precipitation most years, infections could have primarily occurred during "wave years" when there was sufficient moisture for transmission (Figure 18). For example, during El Niño years, there is considerably more summer monsoonal activity in the Sierra Nevada which could create conditions more conducive to spread of WPBR (Goddard and Gershunov, 2020).

The mean detection probability of WPBR infection was found to be 0.739 across observers in the GYE (Shanahan et al., 2021), which leads to lower estimated prevalence of WPBR when not considered in the modeling framework. While this error can be accounted for with model-based approaches where data on observation error are available, this is not possible across WBP's range because similar estimates of observer bias are not available for monitoring units outside the GYE.

The climate data used for this analysis are relatively coarse (4 km) compared to biological scales and perform poorly in mountainous areas, where the elevation used by gridMET can

vary significantly from actual elevations occurring within the grid cell. Temperature and precipitation are estimated by these gridded climate datasets with lapse rates (Tercek et al., 2021a), resulting in error in estimates of these variables in stand locations that can be at a significantly different elevation than the grid cell mean elevation. For instance, consider a tree located somewhere in a 4 km climate grid cell in which it is 1000 m lower in elevation than the mean elevation of the grid cell. If the lapse rate is 6 °C/km (here km is vertical relief), the estimated average temperature at the tree associated with the mean grid cell average temperature could be biased low by 6 °C (1000 m × 6 °C / 1000 m). If the tree were another location in the 4 km grid cell at a higher elevation, the bias could be similar in the opposite direction. The consequence of this is that uncertainty in the tree-level temperature and precipitation adds error that cannot be modeled, even by the spatial random field used in our models.

This work reveals the need in ecological studies involving climate for gridded climate data with the properties of the gridMET and MACA datasets (i.e., data products that allow for the comparison of historical and projected modeled climate data without bias correction that are available at biologically relevant scales) but that also provide larger spatial coverage than what is offered by those datasets. The gridMET and MACA datasets are only available for CONUS with north boundaries around 49° N and south following the US border reaching a minimum around 26° N. These spatial limits are based on political boundaries and limit use of these products when using these climate data to study species with distributions that cross either the north or south borders of the US, such as WBP which has a distribution through the western US and Canada that reaches as far north as 55° N in west-central British Columbia. In the case of our study, this is a range of 6 degrees of latitude that represent more of the climate diversity inhabited by WBP where WPBR monitoring data was available but which could not be used to train our models. Gridded climate datasets that cover the entirety of North America such as the 1 km Daymet dataset (Thornton et al., 2014) exist,

however these datasets are historical only and comparisons with projected climate data such as MACA require bias correction that requires advanced statistical knowledge and substantial computational effort. The WorldClim 2.1 (Fick and Hijmans, 2017) dataset provides a unified data product with historical and projected climate data that are comparable without bias correction at a monthly timestep and 30 arc-second resolution (approximately 1 km grid spacing at the equator) which is an adequate spatiotemporal resolution for our project and cover the entirety of the range of WBP, but the product does not provide projections for water vapor pressure that can be used to calculate climate variables such as RH (Thoma et al., 2019b) and VPD (Dudney et al., 2021) which have established links to WPBR infection in WBP. Selecting climate data for ecological studies remains a complicated process that ultimately requires tradeoffs in at least one quality, such as spatiotemporal resolution, spatial extent, or availability of relevant climate variables.

Our models use a spatial random field that robustly accounts for spatial autocorrelation and unmeasured latent spatial variables. However, it represents an additional source of uncertainty due to the model's sensitivity to the parameters used to create the SPDE mesh which is used to estimate the spatial random field (Figure 13). Formal procedures to specify an optimal mesh are still being developed; however, it is clear that the mesh has a large impact on both model fitting and inference (Righetto et al., 2020). Cross-validation could be used to tune mesh parameters to optimize model variance and bias, while avoiding overfitting.

We conducted our model selection process with dual goals of achieving explanatory power of the causal mechanisms of blister rust infection in WBP as well as predictive power to project blister rust hazard across the landscape into the future. We made choices such as limiting multicollinearity, which improved explanatory power of the model but also potentially hindered its predictive performance (Graham, 2003). Model explanatory power and predictive performance represent tradeoffs in model performance and require different choices during model creation (Shmueli, 2010). It is possible that models with less explanatory power such

as random forests or other machine learning approaches could improve predictive performance under future climate scenarios, at the expense of explanatory power.

Implications for WBP conservation and management

This first large-scale analysis of climatic drivers of WPBR infection in WBP provides a foundation to plan conservation and management of the threatened WBP. Our CONUS-wide maps of projected disease hazard can inform restoration by identifying potentially lower-risk planting sites or prioritizing areas for conserving existing resistant trees. When considering management objectives for different tree sizes it is important to consider the increasing risk of infection as tree DBH increases, a factor accounted for in our model of probability of WPBR infection. However, recommendations of specific areas for management actions using this model can only be made with low certainty. This is due to the significant uncertainty in both our modeled influence of climate and tree size on WPBR infection probability (Figures 16 & 17) and the projected trajectories of disease hazard, which become increasingly uncertain further into the future (Figure 19). This uncertainty necessitates adaptive management strategies and possibly diversifying planting locations.

The model performance assessed by the confusion matrix shows better performance predicting absence of disease than presence (Figure 15). If this model is used to identify refugia from WPBR, this is fortuitous because the model can be used to accurately identify areas that would have lower disease pressure for management objectives like planting. This is important because outplanted seedlings are resistant but not necessarily immune to WPBR (Sniezko et al., 2024).

Conclusions

We found that mean temperature and total precipitation during August and September were the best indicators of WPBR infection in WBP after accounting for tree DBH and

other spatially varying processes across its range in the contiguous United States. We could only model the effect of climate on blister rust infection with a large amount of uncertainty given the available data. Most projections of WPBR disease hazard show increasing risk of infection by the end of the century, with a large degree of variability between projections, especially for projections made at later time periods.

This is the first study of the climatic drivers of WPBR infection in WBP across its range in the contiguous United States. As WBP is both a foundational and keystone species of high-elevation forests, its decline has widespread consequences for forest composition and ecological functions. Because WPBR is a primary agent in the precipitous decline of WBP, conservation of WBP will require consideration of WPBR disease hazard. Our maps of projected probability of WPBR infection in WBP are a foundational tool for land managers interested in conservation of this important tree species. Our maps of projected probability of WPBR infection can be used to identify areas of low disease hazard where WBP seedlings can be outplanted or resources should be allocated to conserve existing stands.

Acknowledgments

This work could not have been performed without the generous contribution of long-term five-needle pine monitoring data from NPS, USFS, and BLM partners.

- Rob Daley: NPS I&M Greater Yellowstone Network
- Erin Shanahan: NPS I&M Greater Yellowstone Network
- Debarah Taylor: USFS Sawtooth National Forest
- Michael Mancuso: USFS Sawtooth National Forest
- John Boetsch: NPS I&M North Coast and Cascades Network
- Dawn LaFleur: NPS Glacier National Park
- Devin Stucki: NPS I&M Upper Columbia Basin Network

- Hannah Alverson: BLM Idaho
- Carl Jorgensen: Forest Health Protection, Boise Field Office
- Chrissy McTavish: Plant Pathologist USFS R4 FHP
- Monica Vermillion: RS/GIS data specialist USFS R4 FHP
- Laura Jones: NPS Grand Teton National Park
- Erin Borgman: NPS I&M Rocky Mountain Network
- Beth Fallon: I&M North Coast and Cascades Network
- Sylvia Hultain: NPS I&M Sierra Nevada Network
- Jonny Nesmith: NPS I&M Sierra Nevada Network
- Sean Smith: NPS I&M Klamath Network
- Lauren Youngblood: NPS I&M Klamath Network
- Alice Chung McCubry: NPS I&M Klamath Network
- Sharon Hood: USFS Fire lab in Missoula

We would also like to thank partners in Canada who shared WPBR monitoring data with us, although we were unable to include the data in the present analysis due to lack of coverage in the climate datasets we used. We hope to be able to accomplish a truly rangewide analysis in the future with their help.

- Michael Murray
- Robert Sissions

We thank the members of the Fall 2024 STAT510 Statistical Consulting course at Montana State University, who provided a valuable review of and feedback on our statistical methodology.

- Ian Laga
- Kingsley Abunyewa

- Maddie Alderman
- Ben DeVries
- Ebenezer Mensah
- Nana Ama Oye Allotey
- Natasha Gesker
- Joseph Niakoh
- Therese Azevedo
- Lakviru Perera
- Bernard Ntiamoah
- Roland Owusu

Computational efforts were performed on the Tempest High Performance Computing System, operated and supported by University Information Technology Research Cyberinfrastructure at Montana State University.

IDENTIFYING OPTIMAL PLANTING MICROSITES FOR WHITEBARK PINE USING A HIGH-RESOLUTION WATER BALANCE MODEL

Contribution of Authors and Co-Authors

Manuscript in Chapter 4

Author: Stephen John Huysman

Contributions: Conceived and implemented the study design. Developed scripts used for analysis. Drafted the manuscript.

Co-Author: David P. Thoma

Contributions: Provided conceptual guidance for the water balance model and interpretation of results. Reviewed manuscript drafts.

Co-Author: Mike Tercek

Contributions: Provided original scripts for the water balance model and assisted with modifications made for this study. Reviewed early manuscripts.

Co-Author: Danielle E. Marias Ulrich

Contributions: Reviewed manuscript drafts.

Co-Author: Brian V. Smithers

Contributions: Provided review of methodology. Reviewed manuscript drafts.

Manuscript Information

Stephen J. Huysman, David P. Thoma, Mike Tercek, Danielle E. M. Ulrich, Brian V. Smithers

Status of Manuscript:
_X_ Prepared for submission to a peer-reviewed journal
____ Officially submitted to a peer-reviewed journal
____ Accepted by a peer-reviewed journal
____ Published in a peer-reviewed journal

Abstract

Successful planting of long-lived tree species can benefit from consideration of the future climate conditions at the individual tree scale (microclimates). Current gridded climate data products available at resolutions ranging from 800 m to 4 km provide climate data that can be used to screen large areas for climate suitability. However, the spatial scale of these products is not well-suited to identifying microclimates that may provide a benefit to planted seedlings. A high-resolution 1 m water balance model (downscaled from coarser resolution gridded climate data) is developed to examine high-resolution variability in microclimates. This model of microclimate modifies a regional climate grid cell of temperature and precipitation using slope, aspect, and soil properties to estimate actual evapotranspiration and climatic water deficit. Fine-scale patterns in these variables can improve the ability to identify planting sites that have lower drought stress and more plant-available water that increases likelihood of establishment. Burroughs Creek in Shoshone National Forest, WY USA, which was identified for whitebark pine planting in 2024, is used as a case study to illustrate these fine-scale patterns. At macroclimate scales, projections show the site transitioning to a climate that is likely to be unfavorable for whitebark pine. Although projections of climate change at the end of the century reveal potential for extreme drought stress across the entire area, topoedaphic features that could potentially shelter planted tree seedlings from high drought stress are identified as microrefugia based on the modeled water balance at microclimate scales, which may be overlooked with coarser methods. Microrefugial sites included steep north aspects and locations with higher water holding capacity, both of which promote higher soil moisture during the summer dry season.

Introduction

Whitebark pine (WBP; *Pinus albicaulis* Engelm.) is a foundational and keystone species of high-elevation ecosystems. It is considered foundational because it is an early pioneer species of these ecosystems where it serves as a nurse tree, promoting establishment of other sympatric species. It is also a keystone species because it is a critical food source for wildlife due to its seeds which are a rich source of protein and fat (Tomback et al., 2001). In recent years, it has undergone a precipitous decline, with over half of standing WBP trees dead as of 2016 (Goeking and Izlar, 2018). This decline is driven by climate-driven disturbances including wildfire, mountain-pine beetle (*Dendroctonus ponderosae* Hopkins, 1902), and white pine blister rust (WPBR; *Cronartium ribicola* J.C.Fisch.). WPBR is a non-native pathogen and other than genetic resistance in some WBP individuals, there are no known natural defenses against it (Sniezko and Liu, 2023). The pathogen has become the primary existential threat against WBP because it attacks trees before individuals reach reproductive age as well as reducing the reproductive capacity of older trees through topping, which is the killing of upper, cone-producing portions of the tree. For these reasons, a core component of WBP restoration strategies involves the planting of WPBR-resistant seedlings (Tomback et al., 2022), which are costly to produce due the need for identifying disease resistant trees, propagating seedlings from seeds collected from their cones, and outplanting seedlings in the field. Ensuring the survival of outplanted seedlings is paramount to a successful restoration program.

Site selection for planting long-lived trees, such as WBP which has a lifespan of 400 to 1,000 years (Tomback et al., 2001), based on current and projected climate presents challenges for land managers. Successful planting of such species requires selecting sites that are not only conducive for seedling establishment at the time of planting, but also suitable into the future at least until the trees reach reproductive age, which can take upwards of 50 years

(Tomback et al., 2001).

The work presented here addresses two important scales relevant to successful outplanting: regional macroclimate (≥ 1 km^2) and local microclimate (< 1 km^2). Current prescriptions recognize the need for favorable macroclimatic conditions for planting, for example the prescription of a maximum 1.0 °C mean annual temperature currently recommended for WBP planting in the U.S. Rocky Mountains which accounts for potential future warming in upper-elevation zones (Bower and Aitken, 2008; McCaughey et al., 2009). In most cases, this temperature guideline is probably adequate because water is generally not a limiting factor in cold environments (Zscheischler et al., 2014), however, water can be seasonally limiting in dry years and dry areas of the landscape even where cold temperatures are not limiting. Moreover, it is well established that plants require simultaneous availability of heat, water, sunlight, and nutrients for growth and establishment, which is not accounted for by temperature alone (Stephenson, 1998). Whitebark pine grows best with full sun exposure and is growth-restricted when shaded by competition with sympatric trees such as subalpine fir (*Abies lasiocarpa* (Hook.) Nutt.) (Tomback et al., 2001). For this reason, planters often target recently burned WBP stands where competition from other species is reduced. Whitebark pine grow in shallow and rocky soils in a wide variety of geologic parent materials including limestone, granite, and schist where other tree species cannot survive - however, once established, WBP is a "survivor" that can persist even in otherwise unfavorable conditions (Tomback et al., 2001). Seedlings are more sensitive to drought than mature trees due to their shallow, poorly developed root systems (Johnson et al., 2011). Therefore, it is important to select outplanting sites that reduce drought stress for successful establishment.

Both spatial and temporal aspects of water availability for establishment and growth need to be considered when selected regional and tree-level outplanting sites. The more favorable locations with more plant-available water and lower drought stress are microclimates that have been referred to as climate microrefugia and have been proposed as targets for

management of climatically sensitive species because they can allow species to persist even when regional macroclimates are unfavorable (Dobrowski, 2011; Morelli et al., 2016). At fine scales, site characteristics influenced by slope, aspect, and soil properties can create microclimates that modify regional macroclimate making some local climates more suitable for establishment and growth and avoidance of climatic extremes resulting in stress or mortality. The opposite is also true where site characteristics can modify regional climate in the opposite direction making some microsites less favorable for survival.

Establishment windows for seedlings are narrow and episodic in high-elevation environments. Plant establishment occurs during years of favorable climate but increased aridity or extreme summer drought prevent recruitment and establishment of younger cohorts. This concept has been termed the "climate ratchet" and provides a temporal framework to understand how climate change can gradually and irreversibly constrain establishment that eventually results in population collapse (Jackson et al., 2009). The concept of the climate ratchet highlights the importance of identifying and protecting climatic microrefugia for outplanting and conservation of climatically sensitive species. Without the buffering from unfavorable regional climates provided by microrefugia, seedlings may fail to reach maturity if summer drought stress exceeds physiological thresholds during early life stages. These microrefugia can prevent species extirpation and maintain sources for subsequent regional colonization and expansion if macroclimate conditions become favorable again.

The climatic water balance can be used to identify optimal planting microclimates because it accounts for the simultaneous availability of water and energy as well as the influence of terrain and soils on climate in a way that directly reflects the biophysical environment experienced by plants (Stephenson, 1998). This research focuses on two measures from the climatic water balance: Actual Evapotranspiration (AET), which represents the length and magnitude of growing conditions favorable to plants, and Climatic Water Deficit (CWD), which is a measure of drought stress representing plant water needs unmet by available water.

As indicators of plant water use (AET) and plant water need (CWD), these two variables are more robust predictors of vegetation distributions than other climate variables such as temperature or precipitation and are well correlated with vegetation distributions across local to continental spatial scales (Dilts et al., 2015; Stephenson, 1998, 1990). AET is directly correlated with growth rates in WBP seedlings and selecting planting sites with high AET can promote establishment (Laufenberg et al., 2020). Although no evidence of mortality caused by CWD has been observed in WBP, it is likely that high summer CWD could be detrimental to WBP establishment.

The climatic water balance has been used to model environmental variability within relatively coarse climate grid cells and to model tree and shrub distributions in the Western U.S. The water balance model downscales and transforms grid cell-scale temperature and precipitation data to biologically relevant scales and variables such as AET and CWD (Lutz et al., 2010). This downscaling within a grid cell is accomplished by incorporating site characteristics available at scales finer than the grid cell resolution into a water balance model, therefore transforming temperature and precipitation into variables that are more proximal to the plant experience. For example, the water balance model accounts for within grid cell variation in soil properties that affect soil water holding capacity and slope and aspect which modulate solar radiation to increase or decrease evapotranspiration rates. Water balance variables are more proximal to the climate experienced by plants because they account for the simultaneous availability of water and energy. For example, plants cannot use rainfall directly; it is only accessible as soil moisture. However, water stored as soil moisture is not available to plants year-round. Soil moisture can only be used by plants when sufficient energy is available to drive transpiration. For these reasons, the downscaling accomplished via water balance results in a model of plant-relevant climate that more accurately represents the plant experience and explains why water balance variables generally provide more explanatory power for plant distributions than temperature and precipitation or other climate variables

(Lutz et al., 2010; Stephenson, 1998, 1990)

Fine-scale terrain features can create climatic microrefugia, which are landscape features that are decoupled from regional climates and have allowed populations of species to persist through unfavorable climate regimes in the past (Dobrowski, 2011). For example, during cold periods, species limited by minimum temperatures could find refuge on south-facing slopes where stronger solar insolation increases air temperature and affects snow/ice pack duration. Alternatively, during warm periods survival of cold-adapted species is promoted in convergent locations where cold air pooling occurs or more northerly aspects where there is weaker solar insolation. The fine-scale terrain features needed to create these refugia may only be apparent at fine spatial scales (1-10 m), and may be masked by coarser terrain models. For example, a water balance model using the 30 m SRTM DEM showed aridification across a landscape under projected climatic conditions, however, when a 3 m LiDAR DEM was used, fine-scale features that reduced CWD were revealed that could enable the persistence of mesic plant species (Dyer, 2019).

Regional evaluation of the current and future geography of the recommended maximum mean annual temperature of 1.0 °C is possible using available gridded climate data, which are available at daily time steps and spatial resolutions between 800 m to 4 km. However, these spatial and temporal scales present issues when used to select sites for tree planting based on climatic suitability. Scale has been described as the "central problem in ecology" (Levin, 1992), and failure to account for spatial scale may be a source of apparent discord between ecological studies that are actually in agreement (Hernández, 2020). The relatively coarse spatial scale of gridded climate data products exceeds the physical scale of individual organisms and can result in a mismatch between the scale of climate predictors and biological responses (Moudrý et al., 2023). Different resolutions of climate data can result in different model predictions about species responses to climate, with finer resolutions associated with lower prediction error (Gillingham et al., 2012).

In this study, we developed a high-resolution 1 m water balance model to examine the influence of fine-scale variation in soils and topography on climate with the intent to identify microrefugia for outplanting WPBR-resistant seedlings. Burroughs Creek in the Shoshone National Forest, WY USA (Figure 21) was selected as a case study to demonstrate this methodology. Two planting units, RL1 and WB2, were identified for planting and direct seeding of whitebark pine in 2024 for reforestation after the Burroughs wildfire of August 30, 2013 (Monitoring Trends in Burn Severity Fire ID `wy4368810966320130830`).

Given the planting prescription of 71–121 seedlings per hectare (Tomback et al., 2022) to achieve the cone densities needed to attract Clark's nutcracker (*Nucifraga columbiana* Wilson, 1811), the primary dispersal agent of WBP, planters at Burroughs Creek would need to plant a total of 1,697–2,892 seedlings in planting unit RL1 and 3,245–5,530 in unit WB2 to achieve this density. This is an approximate cost of $17,600.00 for the 8,422 seedling plugs needed to achieve the higher limit of this planting density at $2.09 per seedling estimated by the National Whitebark Pine Restoration Plan in 2021 (National Whitebark Pine Restoration Plan, 2021). Planters can more efficiently use this costly resource by focusing planting on landscape features that provide favorable growing conditions. This work helps to address the question: where should these seedlings be planted to optimize survival and establishment?

Methods

Macroclimate of Burroughs Creek

Planting suitability of Burroughs Creek for WBP was evaluated at a macroclimate (1 km) scale to compare the location to other regions where WBP grows and to assess whether it meets guidelines such as a the maximum mean annual temperature of 1.0°C (Bower and Aitken, 2008; McCaughey et al., 2009).

Historical (2000–2019) and ensemble end-of-century (2070–2099) RCP4.5 and RCP8.5 averages of annual AET and CWD were retrieved from the NPS 1 km Gridded Water Balance

Model (Tercek et al., 2023, 2021b) for WBP monitoring points located in the contiguous United States (CONUS) from the White Pine Blister Rust monitoring dataset (Chapter 3). WBP monitoring data located in Canada were excluded because they are not covered by the 1 km NPS Gridded Water Balance Model. The data were used to plot the current and projected climate of Burroughs Creek and other known locations of whitebark pine in a two-dimensional climate space characterized by the relationship between AET and CWD.

Mean annual temperature for Burroughs Creek was retrieved from the Multivariate Adaptive Constructed Analogs (MACA) dataset (Abatzoglou and Brown, 2012) to compare historical and future conditions at the site with the 1.0 °C maximum mean annual temperature planting guideline (Bower and Aitken, 2008; McCaughey et al., 2009). Because Burroughs Creek overlaps the intersection of four 4 km MACA grid cells, a point was chosen (43.7061975°N, 109.6778133°W) from the MACA grid cell that is closest to the mean elevation of the location (2814 m; Table 9). The gridMET/MACA grid cell has an elevation of 2,813.28 m which is similar to the average of approximately 2,814 m for both planting units (Table 9). Therefore, while temperature lapse rates would cause temperature to vary within the grid cell at different elevations as described in the lapse rate corrections below, this point should accurately represent temperature on average at the site.

Sensitivity analysis

A sensitivity analysis was used to examine drivers of modeled microclimate variability caused by each individual topoedaphic modifier of macroclimate at the site. A daily climate time series from the planting unit centroid for 1980 to 2020 from the Daymet gridded climate product (Thornton et al., 2014) and ranges of slopes, aspects, and soil WHC at the proposed planting site were used as input to the water balance model. The mean slope (14.8°), aspect (175°) and soil WHC (44 mm) for the WB2 planting unit (Table 9) were used to determine baseline AET (mm) and CWD (mm) for comparison against influence of other values of slope,

aspect, and WHC site modifiers in the simulation. While holding other variables constant, the range of slopes observed at the site from 0° to 47°, aspects from 0° to 360°, and soil WHC from 30 to 80 mm were entered into the water balance model and average annual sums of AET and CWD recorded.

High-resolution water balance model

A 1 meter raster (gridded) Thornthwaite-style water balance model (Thornthwaite, 1948) was developed at a daily time step for the area within the bounding box surrounding the two planting units selected for Burroughs Creek (Units RL1 and WB2, Figure 21). Topographic and elevation data were obtained from the 1 meter LiDAR digital elevation model (DEM) provided by the USGS 3DEP (U.S. Geological Survey, 2020). Slope and aspect were calculated from the LiDAR DEM using tools provided in QGIS (QGIS Development Team, 2024).

The daily water balance at a 1 m resolution was modeled using the source code used to generate the NPS 1 km Gridded Water Balance product for the coterminous United States (Tercek et al., 2021b), modified to use 1 m DEM data as input with lapse rate corrections described below. PET was estimated using the Oudin method (Oudin et al., 2010) and was adjusted for variable heat loading based on 1 m resolution slope, aspect, and latitude as well as day of year (Equation 3 from McCune and Keon, 2002). Annual sums of AET and CWD were calculated for the historical dataset as well as for each GCM/RCP combination. Ensemble averages for annual sums of AET and Deficit were created.

Soil water holding capacity (WHC) was estimated for the top 25 cm of the soil profile using the "available water storage from 0–25cm" (`aws025wta`) data from SSURGO (Soil Survey Staff, 2024). This soil depth was selected to represent the rooting depth of outplanted WBP plugs. The SSURGO soil surveys were mapped at 1:24,000 and provided as polygons which were converted to a 1 m raster in QGIS using the 1 m LiDAR DEM raster as a spatial

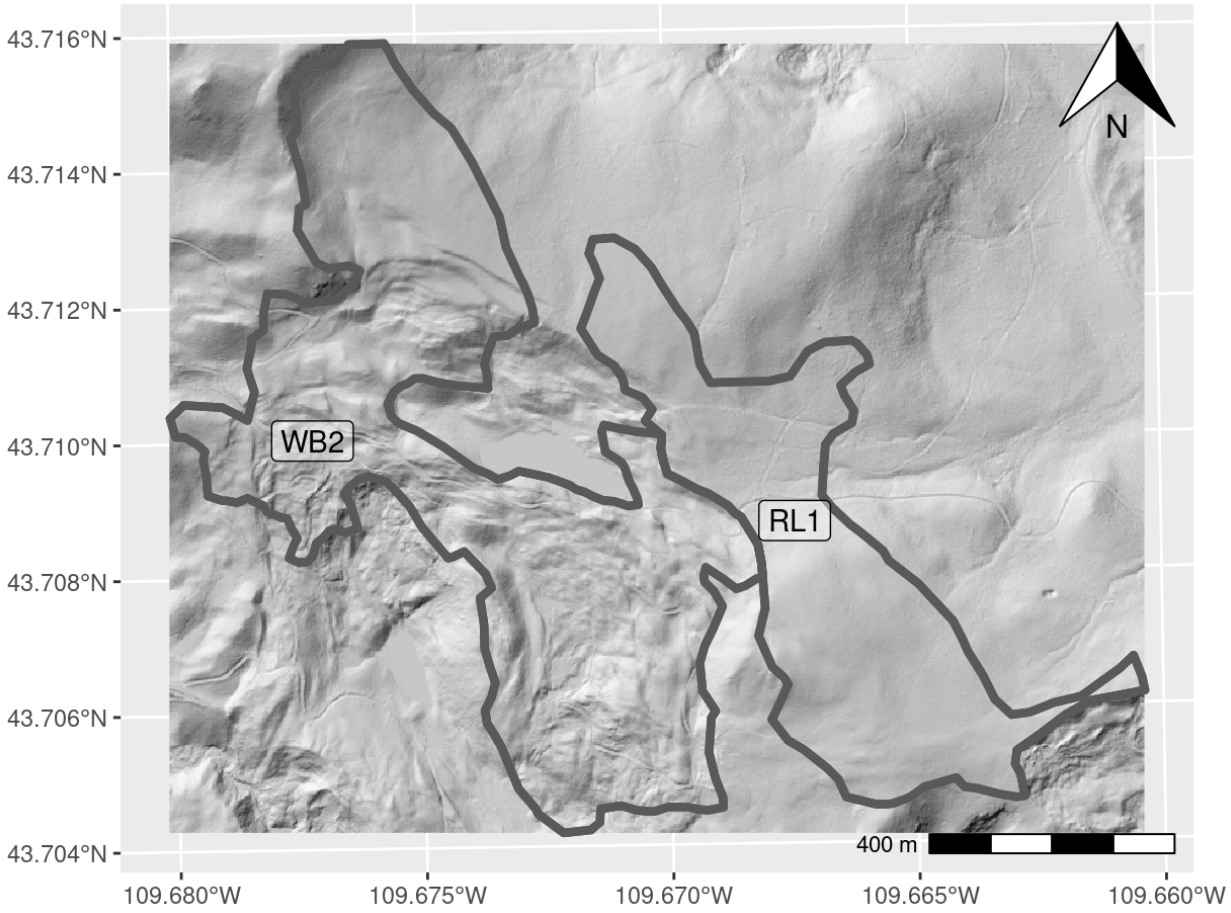

Figure 21. Burroughs Creek hillshade from 1 m USGS LiDAR data, which uses slope and aspect to simulate shadows to enhance visualization of topography, with outlines of the two WBP planting units selected for planting in 2024. A sun angle of 45° and direction of 0° were used to generate the hillshade.

reference where each 1 m cell sampled values from the `aws025wta` data.

Historical daily climate data (maximum temperature, minimum temperature, precipitation) from 1979 to 2022 were obtained from the Gridded Surface Meteorological dataset (gridMET) at a 4 km resolution (Abatzoglou, 2013). Projected climate data for the same variables were obtained from MACA at the same timestep and spatial resolution (Abatzoglou and Brown, 2012). The MACA dataset was downscaled using gridMET, so time series between 1979 and 2099 can be treated as continuous with no breaks between past and future and with no need for bias correction (Tercek et al., 2023).

Burroughs Creek is smaller than the 4 km gridMET climate grid cells and overlaps the intersection of four climate grid cells. To remove spatial discontinuities in the modeled water balance for the site, the climate grid cell with an elevation closest to the mean elevation for the site was selected and climate data from this grid cell was applied across the site. The same point located in a gridMET/MACA grid cell with an elevation of 2,813.28 m that was used to retrieve MACA mean annual temperature data for the macroclimate analysis above was used to represent the entire site (43.7061975°N, 109.6778133°W).

Gridded climate products such as gridMET and MACA assign an elevation to each grid cell, which can vary considerably from the actual elevation of any point within the cell, with commensurate influence on the accuracy of the temperature estimates for any point within that grid cell due to lapse in temperature with elevation (Tercek et al., 2021a). Spatially variable temperatures were determined within the 4 km grid cell using lapse rates estimated using temperature datalogger measurements of Mt. Washburn in Yellowstone National Park (Tercek et al., 2021a), located approximately 135 km from Burroughs Creek. The north and south monthly high and low lapse rates were averaged from Tercek et al. (2021a) to estimate a lapse rate that could be applied to aspects from 0° to 360° (Table 7). Daily temperature data for each 1 m LiDAR DEM pixel was adjusted using these monthly lapse rates based on the difference between the 1 m LiDAR elevation and the elevation used by the 4 km gridMET and MACA datasets, using the following equation:

$$T_{1m} = T_{4km} + L_s * (E_{1m} - E_{4km})$$

Where T_{1m} (°C) is the temperature adjusted for estimated lapse rate for a 1 m LiDAR DEM pixel, T_{4km} is gridMET/MACA temperature (°C) at 4 km resolution, L_s is the monthly lapse rate (°C * km^{-1}) from table 7, E_{1m} is the elevation of the 1 m LiDAR DEM pixel, and

Month	N	S	Mean
Jan.	-5.98	-5.91	-5.945
Feb.	-6.49	-7.89	-7.19
Mar.	-7.33	-10.52	-8.925
Apr.	-9.28	-11.29	-10.285
May	-9.03	-10.78	-9.905
Jun.	-8.28	-10.02	-9.15
Jul.	-7.82	-9.65	-8.735
Aug.	-7.32	-8.40	-7.86
Sep.	-7.71	-8.99	-8.35
Oct.	-8.47	-9.20	-8.835
Nov.	-6.67	-7.97	-7.32
Dec.	-6.24	-6.33	-6.285

(a) Monthly high temperature lapse rates

Month	N	S	Mean
Jan.	-1.62	-0.92	-1.27
Feb.	-2.03	-2.46	-2.245
Mar.	-2.78	-2.65	-2.715
Apr.	-4.08	-4.52	-4.3
May	-3.50	-3.23	-3.3365
Jun.	-1.67	-0.70	-1.185
Jul.	-0.34	-0.32	-0.33
Aug.	-0.68	0.41	-0.135
Sep.	-0.63	-0.37	-0.5
Oct.	-2.42	-3.31	-2.865
Nov.	-2.62	-2.95	-2.785
Dec.	-2.68	-2.51	-2.595

(b) Monthly low temperature lapse rates

Table 7. Monthly a) high and b) low temperature lapse rates applied to 1 m grid cells within the 4 km climate grid cell. Units for lapse rates are °C * km^{-1}. Lapse rates from Tercek et al. (2021a) for north and south aspects were averaged to approximate a spatially continuous lapse rate that could be applied to aspects from 0° to 360°. Monthly lapse rates were applied to daily high and low temperatures based on month and 1 m elevation bias (difference between elevation in 4 km gridMET cell and USGS 1 m LiDAR data).

Future	GCM/RCP	Note
Warm/Wet	MRI-CGCM3 RCP8.5	
Hot/Wet	CanESM2 RCP8.5	Best-case AET scenario (highest)
Warm/Dry	MRI-CGCM3 RCP4.5	Worst-case AET scenario (lowest), best-case CWD scenario (lowest)
Hot/Dry	HadGEM2-CC365 RCP8.5	Worst-case CWD scenario (highest)

Table 8. Future climate scenarios used to model projected water balance in Burroughs Creek. GCM/RCP combinations were chosen to bracket extremes of hot/warm and wet/dry regions in Fig. 22 above. Projections representing the "best" case (i.e., high AET and low CWD) and "worst" case scenarios (i.e., low AET and high CWD) for tree planting are noted.

E_{4km} is the elevation of the 4 km gridMET/MACA grid cell.

To illustrate this process, given a 1 m LiDAR DEM pixel with an elevation of 2500 m within a 4 km gridMET climate cell with an assigned elevation of 2000 m (elevation bias 0.5 km) and an estimated lapse rate for daily high temperatures in January of -5.945 °C * km^{-1}, all daily high temperatures for January for this pixel would be lowered by 2.9725 °C (-5.945 °C * km^{-1} * 0.5 km = -2.9725 °C correction factor).

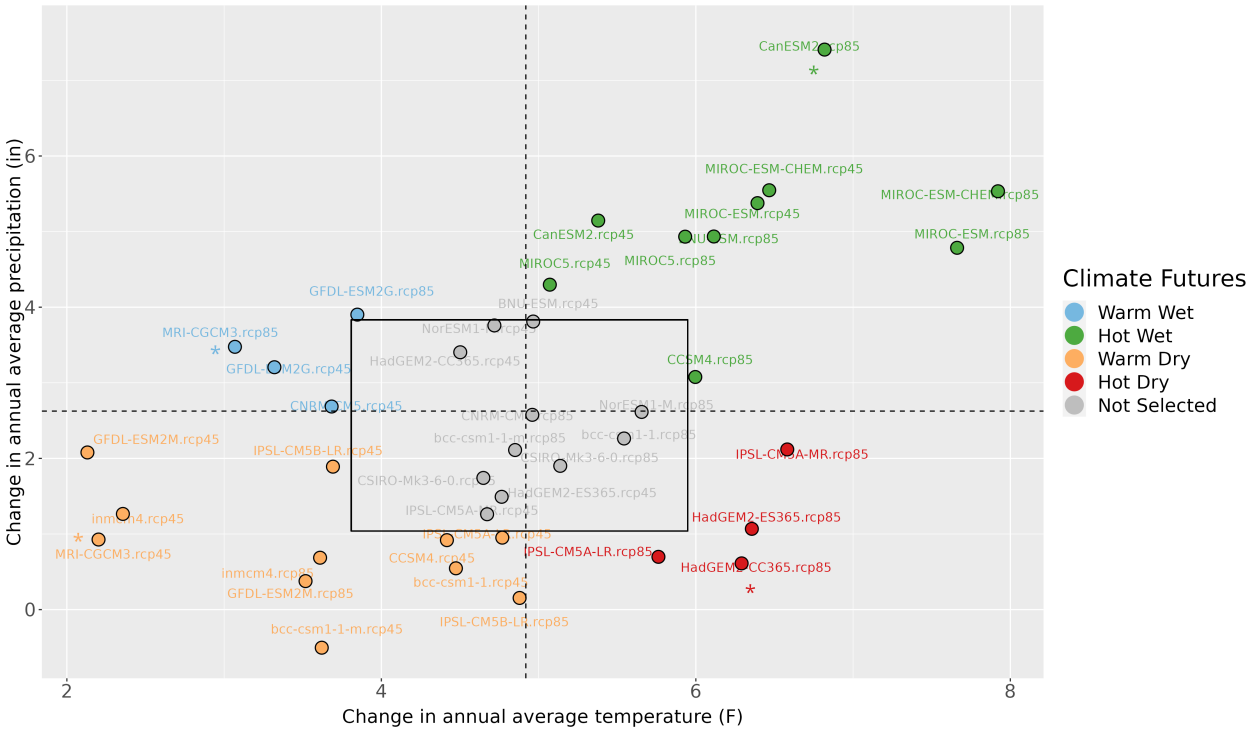

Figure 22. Change in Yellowstone National Park average temperature and precipitation by 2050 by General Circulation Model (GCM) and Representative Concentration Pathway (RCP) run. The GCM/RCP combinations that are most extreme in temperature and precipitation change from each quadrant (Lawrence et al., 2021) were selected for this study (Table 8). Selected GCM/RCP combinations are marked with an asterisk (*). While Burroughs Creek is not located within Yellowstone National Park, it is assumed to have a similar climate to the park due to their proximity (approximate distance from Mt. Washburn, YNP is 135 km) and co-location within the Greater Yellowstone Ecosystem. Figure from Mike Tercek, personal communication, 12 June 2024.

For comparisons with projected conditions, current climatic conditions are represented by average annual sum of AET and CWD for the period from 2002 to 2022. In addition, 1988 is included as an historical year of extreme drought, when record low summer rainfall resulted in widespread wildfire through the Greater Yellowstone Ecoregion (Christensen et al., 1989). Four projected GCM/RCP combinations were selected to bracket the range of plausible future climates based on 'Warm/Wet', 'Warm/Dry', 'Hot/Wet', and 'Hot/Dry' scenarios determined by extremes in projected changes in annual temperature and precipitation in the region (Figure 22, Lawrence et al. (2021)). From these four scenarios, the scenarios that resulted in

the highest or lowest projected mean annual sums of AET and CWD were selected as "best" and "worst" case scenarios (Table 8). However, because these best- and worst-case scenarios were originally selected based on extremes of changes in temperature and precipitation, it is possible that they do not represent the most extreme AET and CWD out of all GCM/RCP combinations available in the MACA dataset (Figure 22). AET and CWD were not calculated for all GCM/RCP combinations due to computational resource constraints. Higher AET is assumed to promote plant growth, while higher CWD is assumed to be detrimental to plant growth through increased drought stress. Climate projections for annual sums of AET and CWD are averaged across the years 2075–2099 to represent "end-of-century" conditions for each of the four selected scenarios. Given the slow rate of development of WBP trees and time needed to reach reproductive maturity, this is approximately when trees planted today would begin producing cones.

Low interannual moisture variability is a feature of potential microrefugia (Morelli et al., 2016). These features could maximize tree longevity because adult trees can survive periods of unfavorable conditions if they are adapted to them but extreme swings in climatic conditions cause mortality in poorly adapted trees (Neumann et al., 2017). Interannual variability in projections of AET and CWD is quantified by the standard deviation (SD) across the whole period included in the MACA projections (2006–2099).

Results

Macroclimate of Burroughs Creek

Historical AET and CWD (2000–2019) of Burroughs Creek at the broad spatial scales provided by the 1 km NPS Gridded Water Balance Dataset are situated within the historical climate space of other known whitebark pine locations in the GYE and across the specie's range in the contiguous United States (Figure 23). Projections at the macroclimate scale show Burroughs Creek transitioning to the edge or outside historical climate conditions of

WBP in the GYE. However, the 1 km water balance projections show a transition under RCP4.5 conditions of the site to the edge of the climate space of the GYE or under RCP8.5 conditions to outside the current climate space of the species.

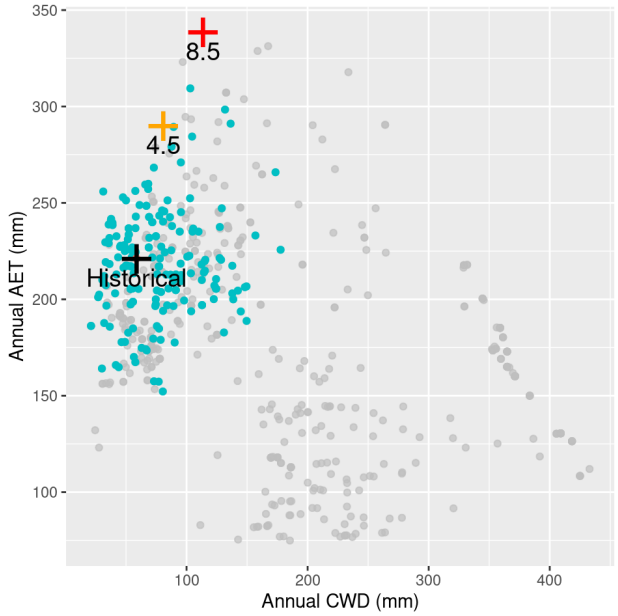

Figure 23. Macroclimate space of whitebark pine at 1 km scale. Whitebark pine observations in CONUS from the white pine blister rust monitoring dataset (Chapter 3) were used to create a bioclimatic niche of the species from historical (2000–2019) average annual AET and CWD from the NPS 1 km gridded water balance model (Tercek et al., 2023, 2021b). Historical 2000–2019 average annual AET and CWD for points located in the Greater Yellowstone Ecosystem are highlighted in blue and all other WBP locations in the monitoring dataset across CONUS are grey. Cross symbols indicate Burroughs Creek historical 2000–2019 (black) and projected end-of-century (2070–2099) ensemble averages for RCP4.5 (orange) and RCP8.5 (red) from the NPS Gridded Water Balance Model.

The 2024 mean annual temperature of Burroughs Creek is 2.5 °C under RCP4.5 average and 2.7 °C under RCP8.5 average conditions, exceeding the 1.0 °C maximum mean annual temperature planting guideline (Bower and Aitken, 2008; McCaughey et al., 2009), and projections show continued increases in temperature under both RCP4.5 and RCP8.5 ensemble averages (Figure 24). However, confidence intervals for 2024 overlap the 1 °C guideline.

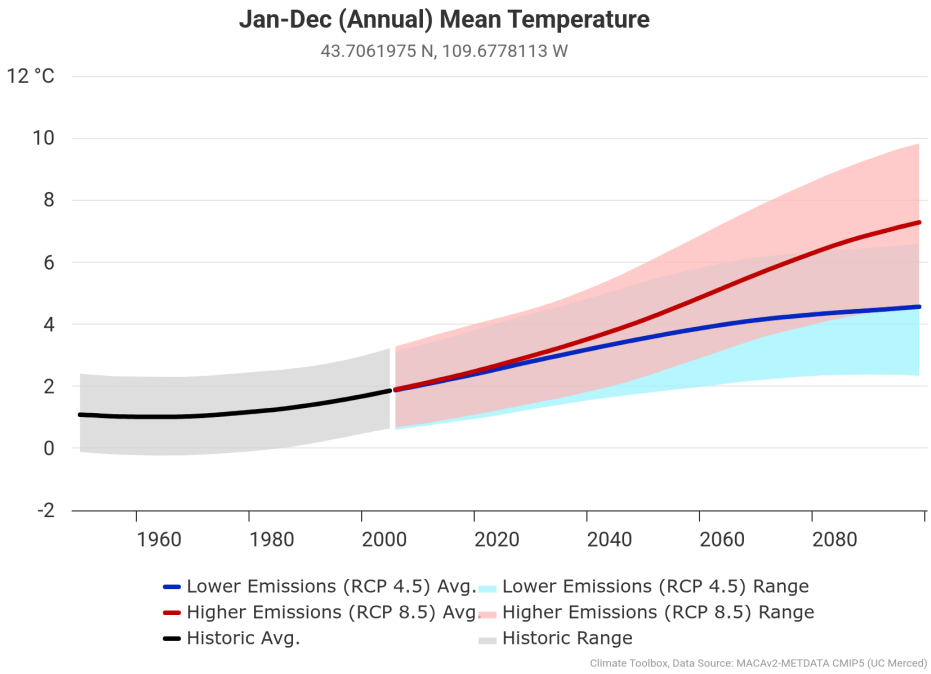

Figure 24. Mean annual temperature for Burroughs Creek under historic and ensemble average of projected RCP4.5 and RCP8.5 scenarios from the MACA dataset. A current maximum mean annual temperature of 1.0 °C is recommended for planting of WBP in the U.S. Rocky Mountains by Bower and Aitken (2008); McCaughey et al. (2009). Temperature values are not adjusted for elevation bias in the 4km grid cell using the equation described in the methods section.
Hegewisch, K.C., Abatzoglou, J.T., 'Future Time Series' web tool. Climate Toolbox (https://climatetoolbox.org/) accessed on 5 Apr 2025.

Topoedaphic characteristics

Considerable variability in topography between the planting units is revealed by the high-resolution LiDAR DEM (Table 9). Planting unit WB2 shows more intra-unit variability in topography, as well as higher extremes in slope and a more southern aspect, overall than planting unit RL1. Planting unit RL1 is less variable in topography than unit WB2, with lower maximum slope and a general south-southeast aspect throughout. These differences in topography are represented in the heat load layer developed from the 1m LiDAR data, with WB2 presenting more variability in heat load within the planting unit than unit RL1 (Figure 25).

Unit	Area (ha)	Mean elev. [min, max] (m)	Mean slope [min, max] (°)	Mean aspect (°)	Mean soil WHC [min, max] (mm)
RL1	23.9	2814 [2786, 2850]	7.8 [.03, 40]	132	36 [30, 42]
WB2	45.7	2814 [2724, 2946]	14.8 [0.02, 47]	175	44 [35, 79]

Table 9. Topoedaphic statistics of the two planting units selected for WBP outplanting in 2024 located in Burroughs Creek summarized from 1 m LiDAR DEM and SSURGO soil survey data. Both planting units have aspects ranging from 0° to 360°.

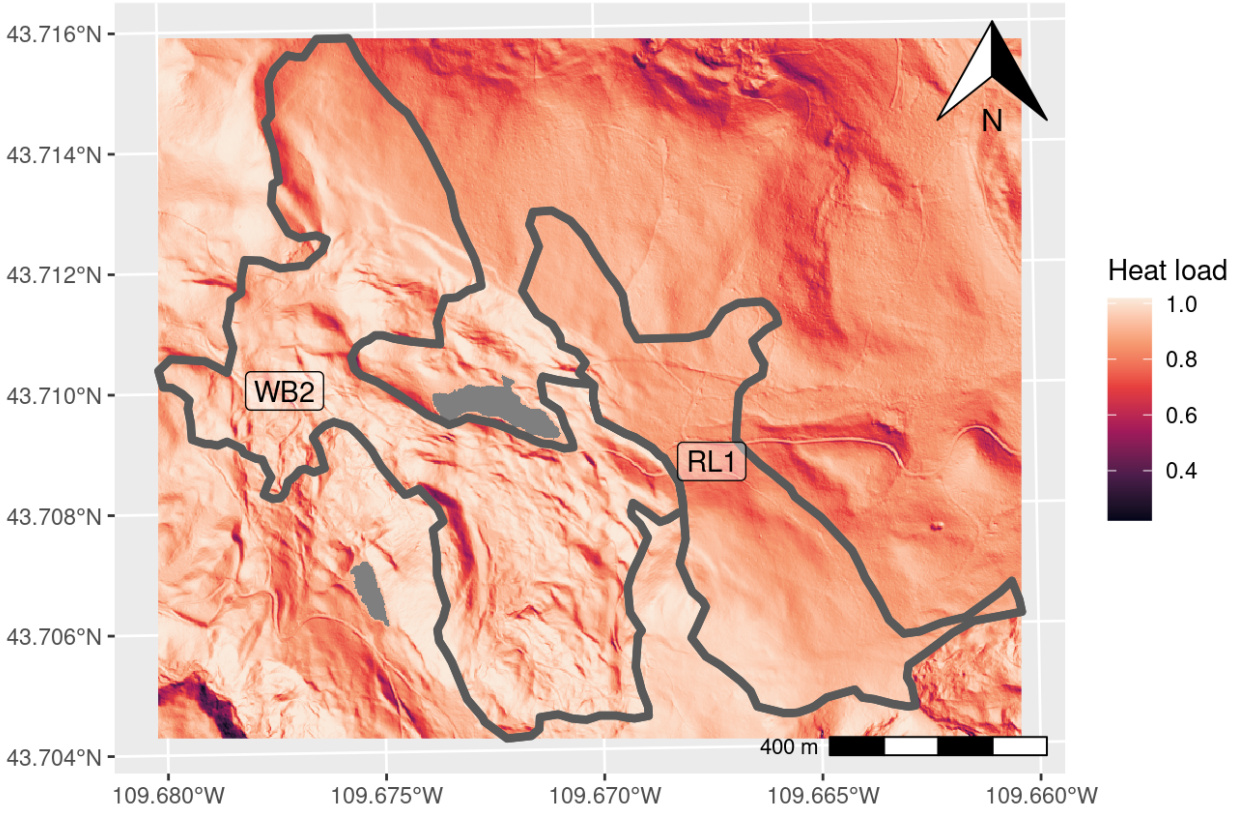

Figure 25. Heat load layer developed with topography derived from 1m LiDAR data for Burroughs Creek. The heat load is an estimate of maximum potential annual direct incident solar radiation based on slope, aspect, and latitude (Equation 3 from McCune and Keon, 2002). The heat load is a unitless multiplier of PET following Appendix S1 in Lutz et al. (2010). PET is estimated by the Oudin method (Oudin et al., 2010) which accounts for air temperature, latitude, and day of year. The site contains two small lakes (grey).

Soil WHC also varies between the two planting units. Unit RL1 is dominated by lower WHC Worock-Storm family soils, while soil WHC through WB2 is generally higher with Garlet-Presa family soils dominating the site as well as higher WHC Cryaquepts, Cryaquolls, and Cryofluvents soils present in drainages (Figure 26, Soil Survey Staff (2024)).

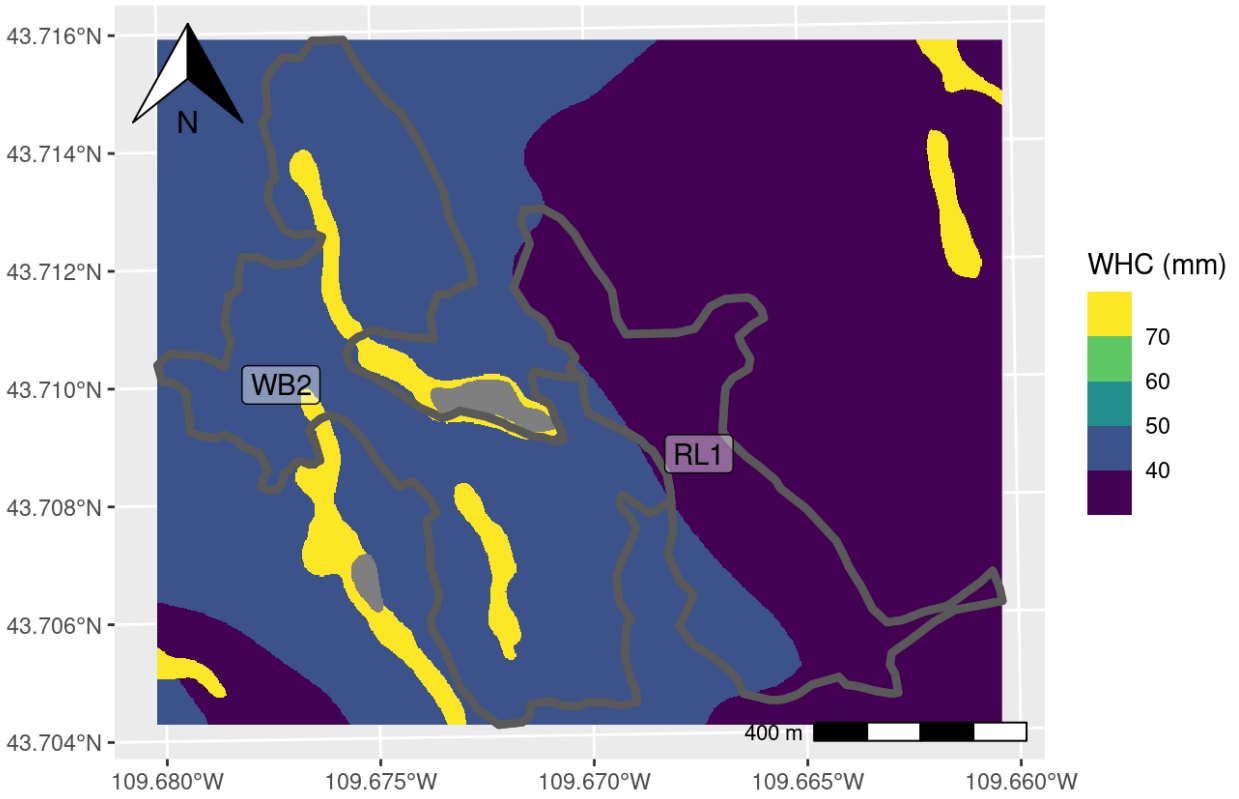

Figure 26. Soil water holding capacity (WHC) (25cm depth) for Burroughs Creek. The site contains two small lakes (grey) where soil data are unavailable.

Sensitivity analysis

The sensitivity analysis of the water balance model using the range of topoedaphic characteristics observed in planting unit WB2 (Table 9) showed wide variability in average annual sums of AET and CWD due to site characteristics (Figure 27).

Within unit WB2, AET varied by 36 mm (min: 163 mm, max: 199 mm) when soil WHC varied between 30 and 80 mm. Slope and aspect played less significant roles that caused variation in AET of 8 mm when slope was varied between 0° and 47° (min: 168 mm, max: 176 mm) and 23 mm when aspect was varied between 0° and 360° (min: 156 mm, max: 179 mm).

CWD varied by 54 mm (min: 91 mm, max: 145 mm) when aspect varied between 0° and 360°.

Slope and soil WHC played less significant roles that caused variation in CWD of 20 mm when slope was varied between 0° and 47° (min: 116 mm, max: 136 mm) and 36 mm when soil WHC was varied between 30 and 80 mm (min: 113 mm, max: 149 mm).

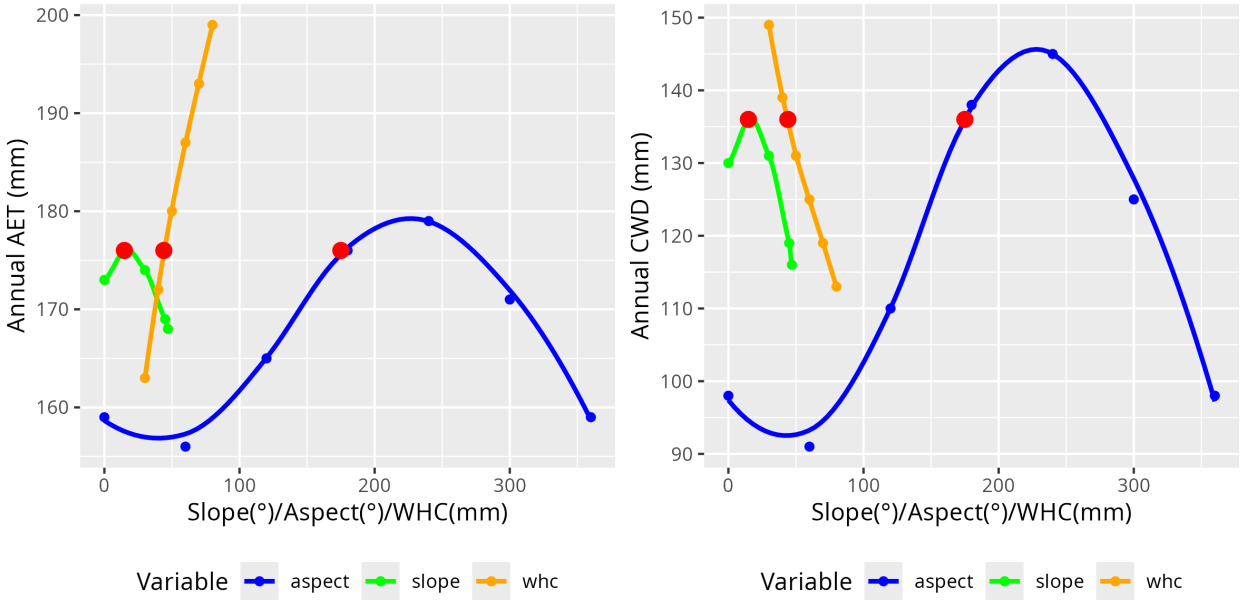

(a) AET

(b) CWD

Figure 27. Water balance model sensitivity analysis showing average annual sum of a) AET and b) CWD for Burroughs Creek using a single 1 km Daymet gridcell daily time series from 1980–2020. AET and CWD at the mean slope (14.8°), aspect (175°) and soil WHC (44 mm) for the WB2 planting unit (Table 9) are shown with red dots. Slope, aspect, and WHC were each varied across the full range of these values in WB2 while holding all other variables constant at the WB2 planting unit means. A smoothed line was fit to points using a LOESS function. Absolute values of AET and CWD calculated using Daymet climate data in these figures should not be directly compared with AET and CWD calculated using the gridMET or MACA climate data products elsewhere in the analysis without bias correction.

Historical 1 meter water balance

Greater extremes of modeled historical AET and CWD are found in the WB2 unit (Figures 28 & 29). Higher AET areas of Burroughs Creek are modeled along the higher WHC soils present in the drainages and lakeside in WB2 where the locations with highest AET and lowest CWD are found. North-facing aspects on hillsides in WB2 have lower modeled

historical AET, but are also sheltered from the high extremes of CWD modeled elsewhere in the planting unit.

Conditions modeled in 1988 are extreme relative to the 2002–2022 historical conditions. Low precipitation in 1988 resulted in minimal modeled average annual AET throughout both planting units, except where high WHC soils are found (Figure 28). The maximum modeled annual CWD for 1988 is around 250 mm, compared with a maximum average annual CWD around 160 mm for 2002–2022, indicating a high magnitude of drought stress during 1988 (Figure 30b). However, the model shows that north to northeast aspects were sheltered from extremes of CWD in 1988, with low CWD modeled in these locations similar to the 2002–2022 normals (Figure 29).

Annual AET and CWD during 2013 when the Burroughs wildfire occurred were similar to the average annual AET and CWD from 2002–2022 (Table 10; Figure 30).

Projected 1 meter water balance

Projections of AET and CWD in the Burroughs Creek units at the end of the century (2075–2099) vary considerably (Figures 28, 29, & 30). Drought stress is projected to increase across the units under all projections, with average annual CWD in the hot/dry future far exceeding CWD modeled during the 1988 drought. AET is likewise projected to increase across the site under all projections, however climate projections showing large increases in AET such as the hot/wet future also project increases in CWD. North to northeast aspects are projected to remain sheltered from high CWD values, even in the worst-case highest CWD hot/dry future, as they were during the 1988 drought (Figure 29).

All climate projections show an increase in AET and CWD from the 2002–2022 baseline, and Warm/Wet, Hot/Wet projections approaching the CWD experienced during the 1988 drought year and the Hot/Dry projection far exceeding it (Table 10).

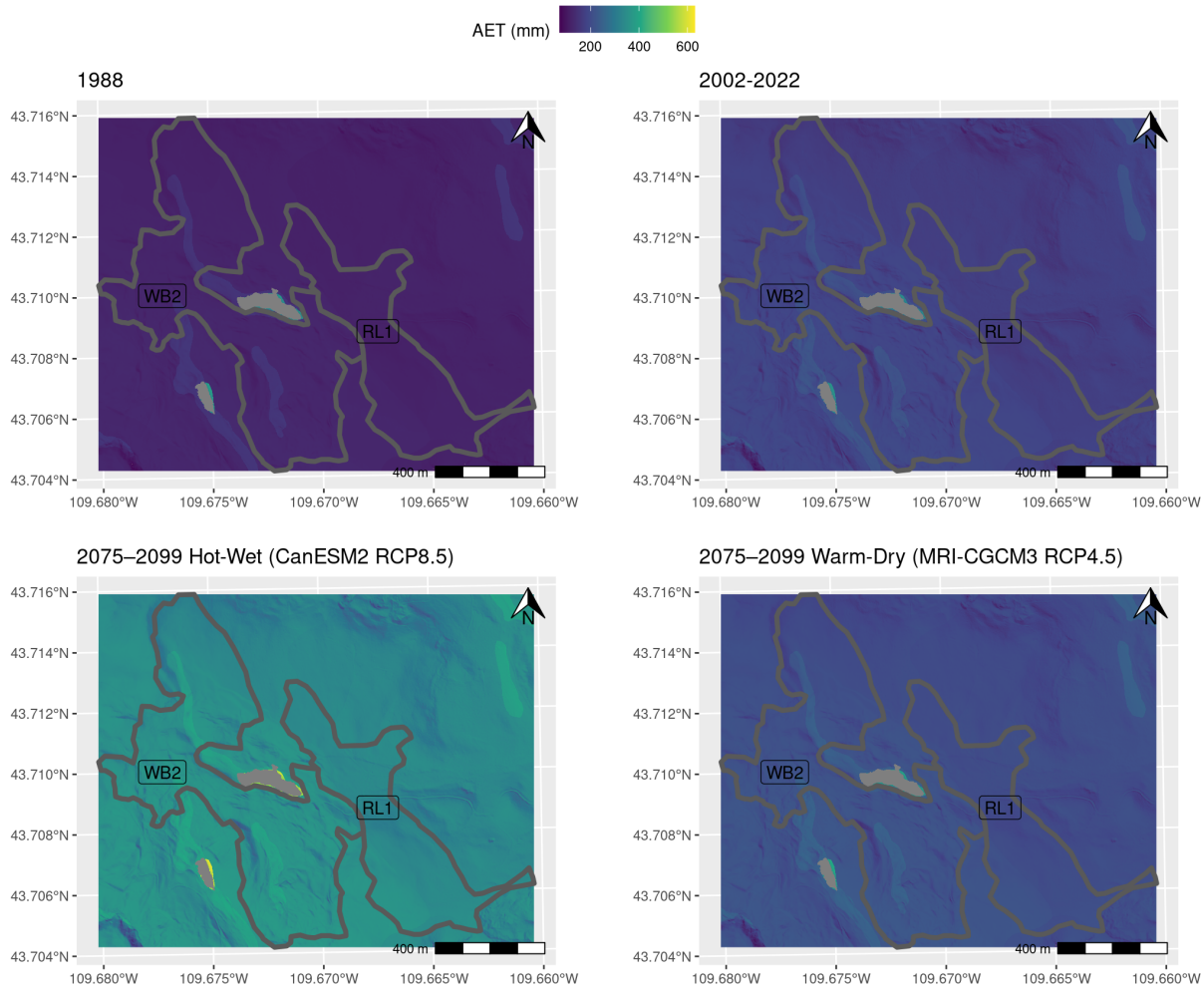

Figure 28. 1 meter historical and projected average annual AET for Burroughs Creek. Historical 1988 annual AET, historical 2002–2022 average annual AET, projected 2075–2099 hot/wet average annual AET, and projected 2075–2099 warm/dry average annual AET are displayed. Color ramps are shown on the same scale to enable direct comparison between scenarios.

Year(s)	**GCM/RCP**	**Mean AET (mm)**	**Mean CWD (mm)**
1988 (Drought Year)		123	198
2013 (Fire Year)		169	127
2002–2022		179	123
Warm Wet 2075–2099	MRI-CGCM3 RCP8.5	238	164
Hot Wet 2075–2099	CanESM2 RCP8.5	340	177
Warm Dry 2075–2099	MRI-CGCM3 RCP4.5	207	138
Hot Dry 2075–2099	HadGEM2-CC365 RCP8.5	236	294

Table 10. Summary of climate conditions for historical and projected water balance.

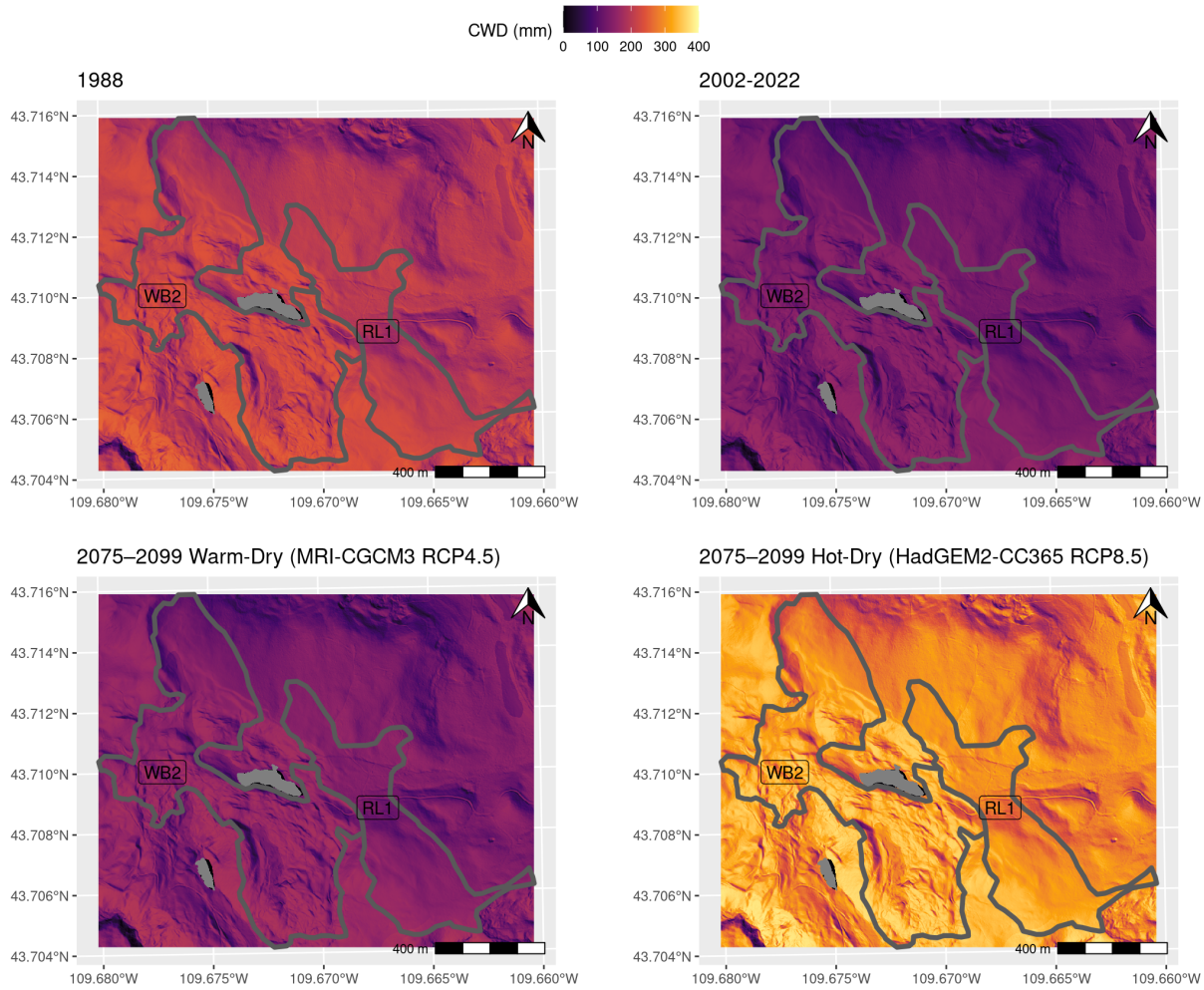

Figure 29. 1 meter historical and projected average annual CWD for Burroughs Creek. Historical 1988 annual CWD, historical 2002–2022 average annual CWD, projected 2075–2099 warm/dry average annual CWD, and projected 2075–2099 hot/dry average annual CWD are displayed. Color ramps are shown on the same scale to enable direct comparison between scenarios.

Interannual variability in climate projections

Interannual variability (SD) in projections of AET and CWD from 2006 to 2099 vary between GCM/RCP combinations (Figures 31 & 32). Hot/wet has the highest and warm/dry has the lowest maximum SD in projected annual AET. Hot/dry has the highest and warm/dry has the lowest maximum SD in projected annual CWD. There is considerable overlap in

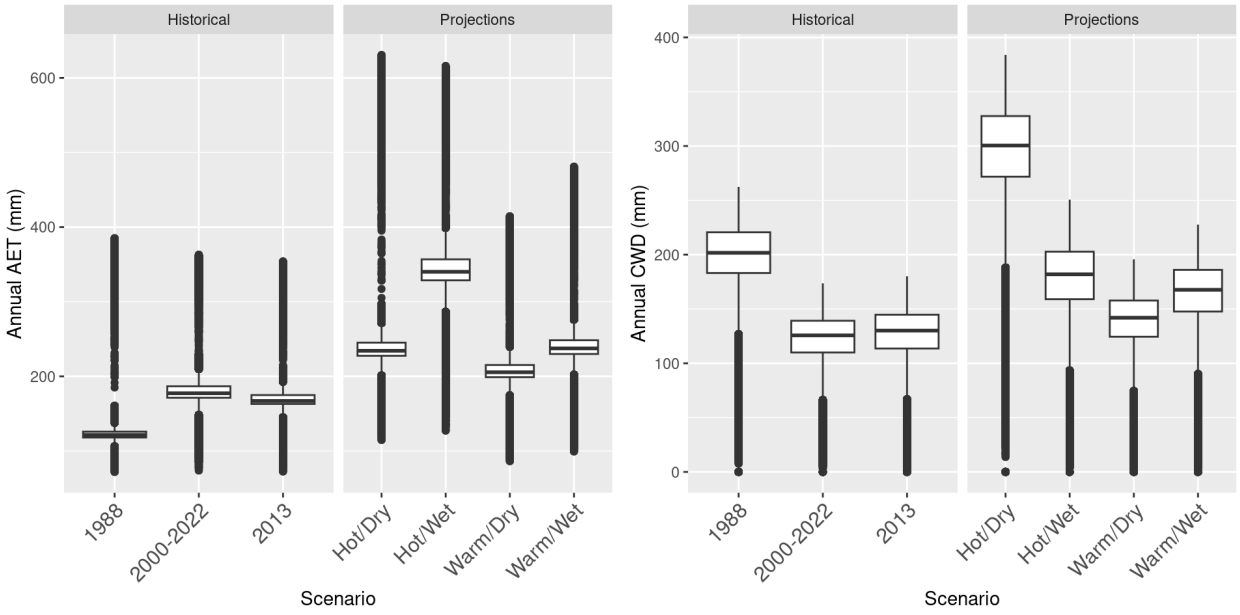

(a) AET (b) CWD

Figure 30. Historical and projected average annual a) AET (mm) and b) CWD (mm) for Burroughs Creek. Historical modeled AET and CWD are shown for the 1988 drought year, 2013 fire year, and 2002–2022 period. All pixels in the Burroughs Creek bounding box are included in box plot distributions, including pixels outside of the WB2 and RL1 planting units.

areas that have low-SD in both annual AET and CWD, with the same north-eastern slopes minimizing interannual variability in both variables.

Discussion

General considerations for WBP planting site selection

Here, fine-scale patterns in AET and CWD are mapped to help identify microrefugia for outplanting whitebark pine seedlings that will enhance likelihood of establishment and persistence as refugia long enough for planted seedlings to reach reproductive maturity. Outplanting WPBR-resistant seedlings is a core component of WBP restoration strategies due to the threat the pathogen poses (Tomback et al., 2022). The expense of planting WPBR-resistant seedlings justifies careful consideration of planting sites and microsite climates to

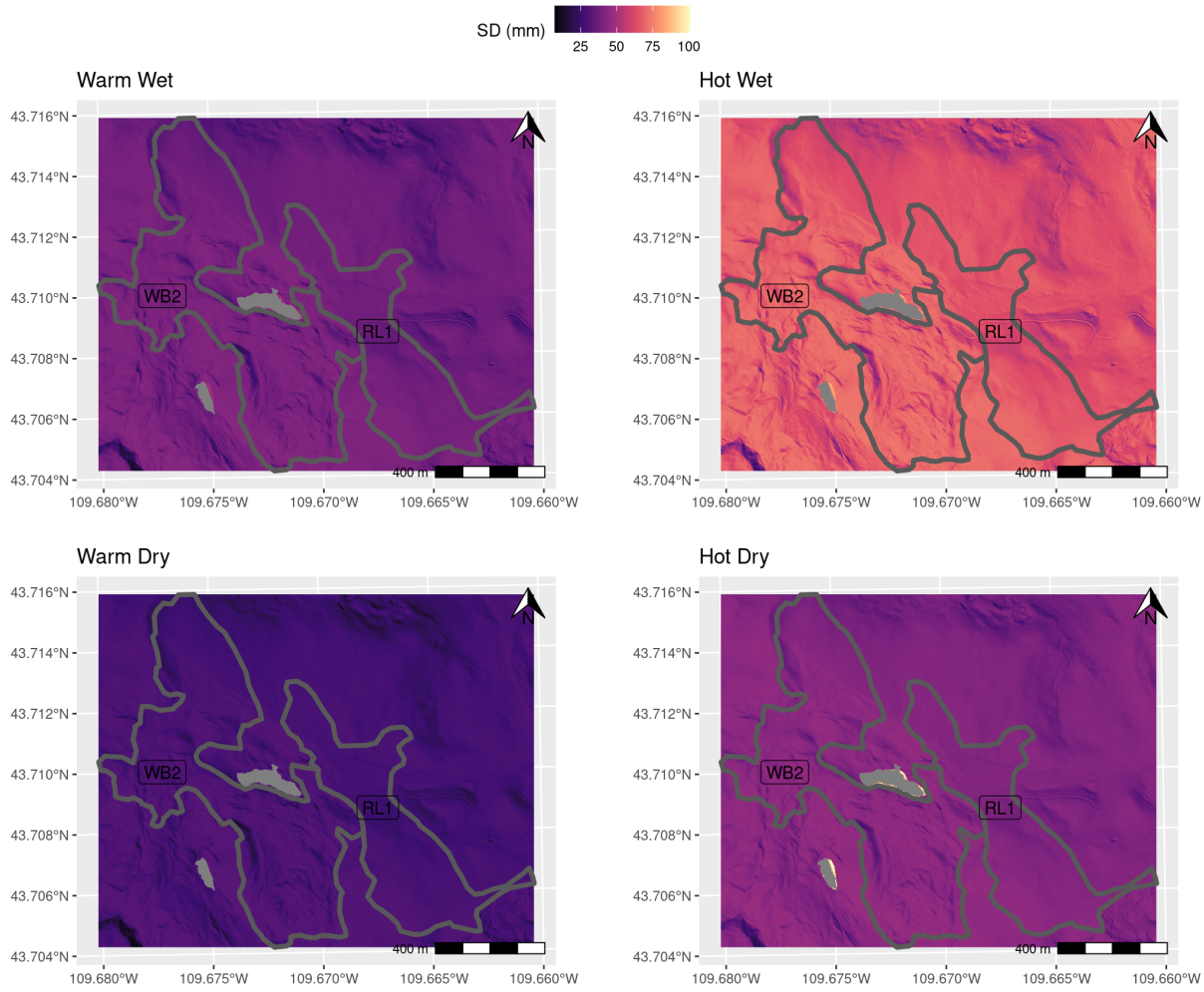

Figure 31. Interannual variability (standard deviation) in projected annual AET (2006–2099). These maps show the year-to-year consistency of projected AET. Lower standard deviation indicates more stable growing conditions across years, which may favor the establishment and longevity of long-lived species like whitebark pine by reducing exposure to variable resource availability.

maximize return on investment. Climate uniquely affects each life stage of whitebark pine development from germination to reproductive success. Seedlings of tree species are generally less tolerant of drought stress than mature trees (Johnson et al., 2011), and WBP seedlings in particular are less tolerant of warm-dry conditions than mature trees (Hansen et al., 2021). Increased AET is directly correlated with faster growth and establishment of WBP seedlings (Laufenberg et al., 2020). Climate-driven disturbance agents such as wildfire (Riley et al.,

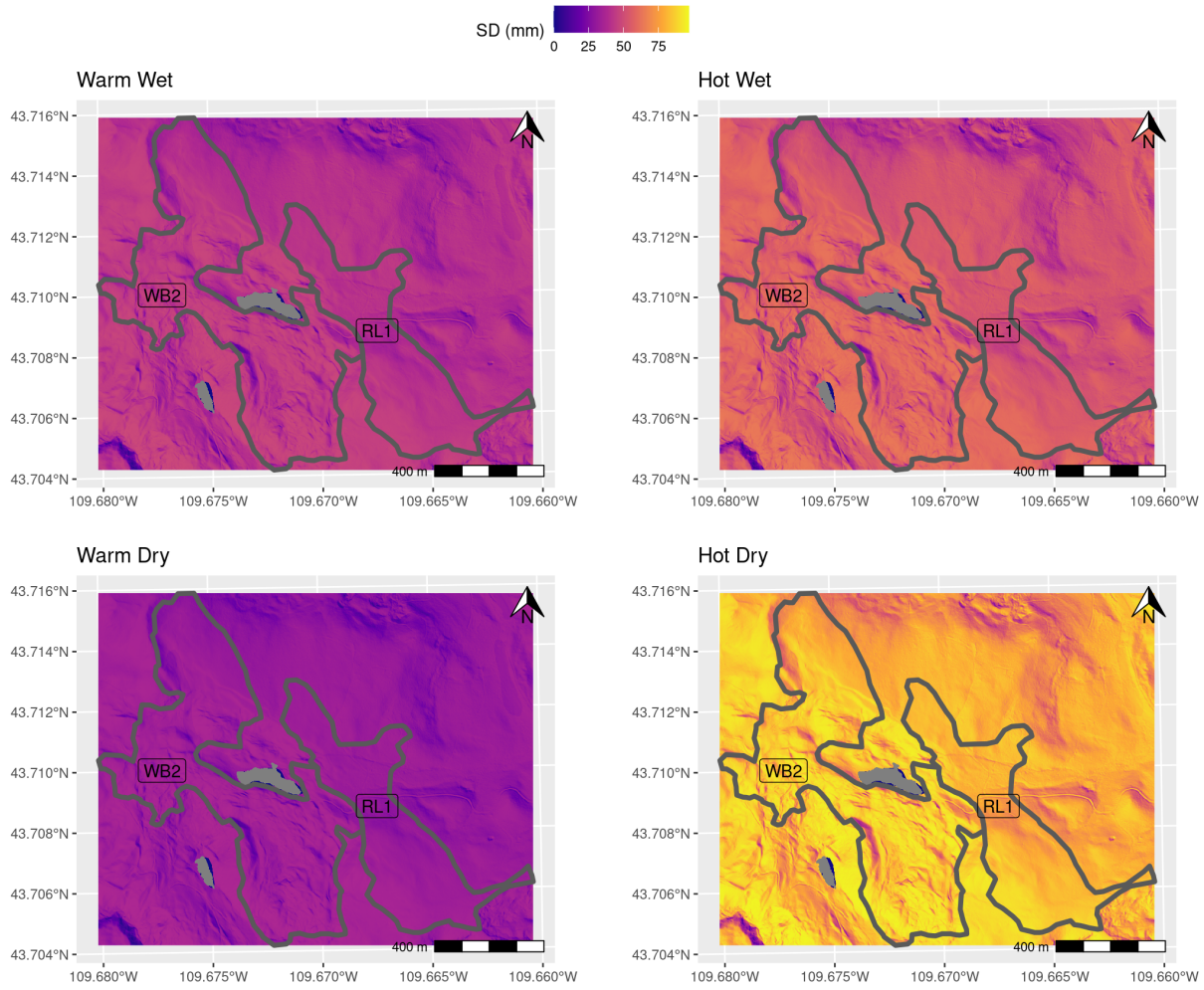

Figure 32. Interannual variability (standard deviation) in projected annual CWD (2006–2099). These maps show the year-to-year consistency of projected CWD. Lower standard deviation indicates more stable drought stress conditions across years, which is a characteristic of potential climate microrefugia that can buffer sensitive species like whitebark pine from climatic extremes and potentially increase longevity.

2013), mountain pine beetle (Buotte et al., 2016), and WPBR (Thoma et al., 2019b) affect tree growth and survival at all life stages.

Tree planting sites are typically selected based on historical climatic conditions, without explicit consideration of climate projections. For example, the 1.0 °C planting prescription for whitebark pine in the Northern Rockies is intended to account for potential climate warming in upper elevations (Bower and Aitken, 2008) but does not account for differential warming

between regions of the Northern Rockies or between microclimates. Selecting planting sites based on historical climate conditions may be counter productive if the climate conditions have moved or will move outside the historic range of conditions that supported whitebark pine stands in the past (Rammer et al., 2021). For example, south facing sites selected based on recent fires in whitebark pine stands may not be suited to establishment due to warming combined exacerbating effects of high heat load on south aspects that dries soil faster than on other aspects.

This study uses coarse-scale 4 km gridded climate data available in remote areas and leverages the capability of water balance modeling to estimate sub-grid variability of climate in a way that is important to plants (Lutz et al., 2010). The modification of regional climate is achieved by accounting for physical processes that affect abundance and duration of water available for plants. Soil properties determine the quantity of water that can be stored and made available to plants. Given equal precipitation, plants growing in soils with lower soil water holding capacity would experience a drier environment than those growing in higher WHC soils, as the lower WHC soils would more quickly deplete storage of plant-available water between precipitation events and have less capacity to recharge during precipitation events before excess water runs off. Slope and aspect affect the duration of water availability for a given amount of soil water storage by modifying heat load that models the effect of solar radiation on sloping surfaces described by McCune and Keon (2002). At a given latitude, southwest aspects receive higher heat loading and experience more evapotranspiration than northwest exposures. Steeper slopes accentuate the heat load effect lessening load on north aspects and increasing load on southwest facing aspects. The climatic water balance integrates the effects of variable soil water storage, slope, and aspect to develop estimates of water availability and drought stress that are more proximal to the wetness or dryness experienced by plants than temperature or precipitation alone (Stephenson, 1998).

Microsite controls on water availability and drought

The sensitivity analysis revealed that at Burroughs Creek, soil WHC is the strongest control on AET while aspect is the strongest control on CWD (Figure 27). Deeper soils are associated with higher AET, which is directly correlated with growth rates in WBP (Laufenberg et al., 2020). North to northeast aspects minimize CWD and therefore also reduce drought stress in plants. These sensitivity findings will vary in other locations because different ranges of slope and soil WHC may be present and will interact with different regional climate inputs to affect water balance estimates.

Modeled CWD during the 1988 drought year is more spatially variable than modeled AET during the same year (Figures 28 & 29). Record low precipitation during 1988 (Christensen et al., 1989) likely limited AET while CWD has no upper limit and can increase indefinitely with temperature. Because CWD is not limited by precipitation in the model during this year, it is more spatially variable than AET due to topographic features, especially aspect (Figure 27b). Therefore, if avoidance of drought stress during years with low precipitation is a consideration for planters, it may be more important to consider CWD when selecting planting sites as it is more spatially variable than AET in those years.

The fine-scale patterns of water availability and the results of the sensitivity analysis identify specific features on the Burroughs Creek landscape as ideal planting environments. Water availability is critical for seedling establishment and will support continued growth that increases the likelihood of seedlings reaching reproductive maturity. Plant-available water for a given amount of precipitation is most strongly controlled by soil WHC which is highest in planting unit WB2 where Cryaquepts, Cryaquolls, and Cryofluvents soils occur (Figure 26). Conversely, CWD is most strongly controlled by aspect thus planting seedlings on northeast facing slopes will reduce drought stress with further reductions on those slopes where soil WHC is highest in Cryaquepts, Cryaquolls, and Cryofluvents or Garlet-Presa family soils. These conditions which maximize water availability and minimize drought stress

are primarily found along northeast slopes in positions along the lower parts of the drainages present in unit WB2. These patterns are spatially and temporally consistent. The spatial pattern is controlled by topoedaphic features that are unlikely to change over time barring severe erosion of soil that alters water holding capacity. The patterns are also temporally consistent in a relative way. That is, due to the topoedaphic controls on water availability and drought the spatial patterns of higher water supply or lower drought stress hold through time for any temperature or precipitation regime (Figures 28, & 29).

Strengths

The strength of this approach lies in its ability to detect relative differences in wetness and dryness across a landscape in a way that directly reflects the growing environment of plants. These relative patterns in the water balance across the landscape come with a higher degree of certainty than absolute estimates of AET and CWD. The model can help identify microclimates in locations where ideal combinations of soil and topography exist relative to other positions on the landscape. These locations may be difficult to identify visually, even for trained and experienced observers. For example, two hillslopes may have similar slope and aspect but different soil water holding capacities that lead to drier conditions on one than the other. In addition, planters may be skillful at identifying suitable planting sites based on current climatic conditions, but the methodology can quantify the potential change in a landscape position under plausible future climates relative to current conditions. The model reveals the potential for extreme drought stress in some landscape positions based on future climates, relative to current and past climatic conditions at the site (Figure 30b). Therefore, planting site selection based on current conditions alone is unlikely to result in plantings that avoid this stress in the future.

Limitations

This work examines the variability of microclimates within relatively coarse climate grid cells due to sub-grid cell topograhic and edaphic features. These methods likely present a more accurate representation of climate at fine scales relevant to tree planting compared with unmodified use of gridded climate data products. However, several caveats and limitations exist with the use of these methods. These limitations reveal the potential for future work to enhance the accuracy and precision of these methods that could improve map products for tree planting site selection.

Climate data from a single gridMET/MACA grid cell were used to represent the entire Burroughs Creek site. These products are designed to show broad-scale patterns at regional scales that hold across large groups of pixels (Abatzoglou, 2013). Uncertainty increases when these climate data products are applied to sub-grid cell scale locations such as point-scale data or the relatively small area examined here.

Temperature and precipitation data are not available at high resolutions in this study system and all available gridded climate data products have uncertainty in areas of complex topography such as mountains regions (Behnke et al., 2016). The model and its climate inputs do not consider some sub-grid cell phenomena affecting air temperature such as temperature inversions and cold air drainage. Precipitation also varies at sub-grid cell scales due to topographic effects such as orographic precipitation (Lin et al., 2001). Snow accumulation and melt were modeled at the scale of the entire site, and not downscaled based on topography. In reality, snow accumulation and melt is affected by factors such as slope, aspect, as well as horizontal movement through snow drift (Dingman, 2015). Future analyses could incorporate the high-resolution topographic data used here to improve accuracy of snow melt and accumulation dynamics at fine scales.

Holden et al. (2011) presented a methodology to downscale gridded temperature measurements using networks of low-cost temperature dataloggers. This is a low-cost method

that could be applied to areas targeted for planting to develop local corrections for gridded climate datasets could improve temperature estimates in light of sub-grid cell phenomena such as temperature lapse rates and effects such as temperature inversions and cold-air drainage. This would improve estimates of spatial variation in temperature in the model but absolute accuracy in estimates of the water balance is not necessary as noted above. While this method has been applied as a modification of historical climate data, the stationarity of the downscaling method should be considered when applied to projected climate data. This method could also be applied using precipitation gauge network to improve modeling spatial patterns of precipitation inputs by developing estimates of precipitation lapse rates similar to the temperature lapse rate adjustments applied here.

Soil survey data provided by the SSURGO database is intended to be used at scales of 1:24,000. There is likely considerable variation in the soil characteristics observed at the fine spatial scales that is not captured in these surveys. Soils are treated as areas with discrete rather than continuous WHC between 1 m pixels. However, there is likely to be considerable gradation between and heterogeneity within soil types. *In situ*, trees can also access features like subsurface flows and water in bedrock (McCormick et al., 2021), which are not accounted for in this model. Planting decisions made using this data should consider observed soil characteristics in the field in conjunction with data presented here. The sensitivity analysis can serve as an indicator of the effect of changing soil WHC on modeled AET and CWD (Figure 27).

While the climate and topoedaphic inputs to the model are imperfect, in ways described above, even perfect climate data may not allow for absolute determination of measures such as AET and CWD. PET is estimated here using the physiology of a reference agricultural grass species (Zotarelli et al., 2024), which is an unrealistic vegetation type in subalpine environments. PET calculated based on the physiology of whitebark pine, if such data were available, would change model output. In addition, whitebark pine would likely be growing

among other plant species, all of which have different water demands and would all contribute to spatial patterns of water use. Absolute drought tolerances of whitebark pine are also not known, so even perfect climate inputs would not allow us to identify suitable microclimates for this species with absolute certainty. A strength of this approach is the ability to assess relative suitability of a location for planting suitability in the context of plausible future climates. However, given these limitations and the fact that the future climate inputs are also imperfect and need to be interpreted in that context, relative assessments of spatial patterns of water use and availability may be the highest degree of certainty that is achievable with current available data and modeling techniques.

The relative nature of the water balance model used here can make direct comparisons with existing research difficult. For example, Laufenberg et al. (2020) reported a threshold of 250 mm of annual AET above which whitebark pine growth accelerates, recommending that whitebark pine planting projects target locations that exceed this value. However, their work was based on the Daymet gridded climate dataset, instead of gridMET which was used here, and therefore climate values provided in this product cannot be compared directly to that threshold without bias-adjustment as well as accounting for the non-linear nature of calculations in the water balance model. The general trend of increasing AET leading to more rapid plant growth reported in Laufenberg et al. (2020) can be assumed to apply here even though the specific recommended AET threshold may not.

In addition to considering the fine-scale patterns in the climatic water balance which the model identifies, planters should consider current planting prescriptions for whitebark pine which recommend avoiding competition with understory or overstory trees such as lodgepole pine and subalpine fir, swales or frost pockets, high snow loads, snags, and targeting areas that provide shade and wind protection and adequate growing space (McCaughey et al., 2009; Scott and McCaughey, 2006).

Planting recommendations for Burroughs Creek

We propose that WBP planting at Burroughs Creek should recognize the likelihood that the macroclimate at this location may be unfavorable to WBP by 2099 when trees planted today would reach reproductive age (Figure 23). The site also currently slightly exceeds the maximum mean annual temperature of 1.0 °C recommended by Bower and Aitken (2008) for WBP planting in the U.S. Rocky Mountains that accounts for potential warming in upper-elevation zones and projections show continued increases in mean annual temperature, assessed here with temperature from the MACA dataset (Figure 24). If trees will be planted there despite the unfavorable projected climate, successful planting will require consideration of the fine-scale favorable microclimates that the model can identify. The sensitivity analysis reveals the potential for wide variability in microclimates created by topoedaphic features which could modify unfavorable macroclimates, making them potentially more suitable for WBP planting (Figure 27).

Depending on management objectives, optimal site characteristics may vary and these results can be interpreted in different ways. For example, when planting in a marginal site like Burroughs Creek, if management goals are to:

1. Maximize survival rates of seedlings — planters should choose planting locations that maximize AET to achieve higher seedling growth rates and minimize CWD to reduce drought stress. Increased AET is associated with faster growth rates of WBP seedlings, with a sharp increase around 350 mm annual AET (Laufenberg et al., 2020). Although direct comparisons with this work cannot be made without bias correction between the different climate datasets used, in general higher AET can be assumed to correlate with faster seedling growth and establishment. While there are no known direct downsides to high AET, indirect negative impacts could occur if higher AET levels are associated with factors such as climatic conditions conducive to white pine blister rust infection.

An algorithm could be developed to highlight the union of high AET and low CWD based on maps produced by the model. The CWD threshold may vary based on the risk tolerance of a manager. Pixels that are identified as ideal based on these conditions could then have their suitability tracked through time based on projected climatic conditions.

2. Grow trees to cone-bearing age as quickly as possible — choose planting locations that maximize AET over the duration needed for trees to reach reproductive age, approximately 25–50 years. This objective is similar to the first, however, this objective would place a higher priority on AET to achieve optimal growth rates, possibly at the expense of some increased drought stress and subsequent seedling mortality if high AET landscape positions are also associated with higher CWD. Locations with maximal AET satisfy this planting criterion (Figure 28).

3. Maximize longevity of adult trees — select planting locations that minimize interannual variability in stressors. It is thought that trees can survive unfavorable conditions if they are adapted to them, and extreme swings in climatic conditions cause mortality in trees that are not adapted to those extremes (Neumann et al., 2017). Locations with low interannual variability in CWD would satisfy this planting criterion (Figure 32).

Regardless of specific planting objectives, extreme CWD is likely to threaten tree survival on the site in the future through drought stress and wildfire potential. In 1988, a year in which severe drought led to widespread wildfire through the greater region, the Burroughs Creek site (defined by the bounding box surrounding the two planting units, e.g., Figure 21) experienced an average annual CWD of 198 mm (Table 10), with some locations experiencing higher or lower deficit depending on the effects of topoedaphic features (Figure 29). A wildfire occurred at Burroughs creek in 2013; however, annual AET and CWD in 2013 were not notably different from the 2002–2022 average annual AET and CWD (Table 10; Figures

30a & 30b). As demonstrated in the wildfire ignition danger rating system for the Greater Yellowstone Ecosystem (Chapter 2), wildfire ignitions in this ecoregion are best predicted by a short window (three day rolling sum) of CWD and it is likely that the annual average CWD calculated here smooths out short-term peaks in CWD that resulted in the 2013 wildfire. All of the projections of CWD exceed the 2002–2022 historical baseline average CWD of 123 mm across the site, with Warm/Wet and Hot/Wet futures approaching the 1988 drought year CWD and the worst case Hot/Dry scenario far exceeding it with an average CWD of 294 mm (Table 10).

Planters can utilize topoedaphic features to plant in locations that buffer from extreme CWD (Figure 29), which will reduce tree stress and promote survival of planted seedlings. High CWD is characteristic of summers of the region when soil moisture and precipitation are generally low, which may stress small trees with shallow or poorly developed root systems (Johnson et al., 2011). The persistence of these lower deficit locales through time within a matrix of relatively high deficit may be evidence of microrefugia (Dobrowski, 2011; Morelli et al., 2016). Microrefugia may allow climatically sensitive species to persist in future climate regimes that are regionally unfavorable. These microrefugia would be valuable for the purposes of planting long-lived tree species such as whitebark pine.

Unit WB2 has large areas of soils with higher WHC present at the bottom of drainages in the unit (Figure 26). The relatively higher soil WHC present in these soils has the effect of increasing AET and decreasing CWD where they are present. However, these soils currently support riparian plant communities (Soil Survey Staff, 2024), and are not likely to be locations that whitebark seedlings could be competitive.

Conclusion

While the environmental sensitivities for the life-stage of WBP establishment are not quantitatively known, drought during establishment is not conducive for survival. For this

reason, even a relative mapping of potential for drought stress can be a useful guide for regional and microsite selection for planting. Given that current WBP planting sites are selected based on where WBP currently grows or was killed by fire, this model can be used to select sites within those locations that are equally or less drought prone compared to historical conditions. The sensitivity analysis reveals that at Burroughs Creek, AET is affected most by soil WHC and CWD is affected most by aspect. This microsite model can be used to identify planting locations with maximal AET to maximize seedling growth rates and establishment, minimal CWD to minimize drought stress, or minimize interannual variability in AET or CWD to select sites with stable microclimates to maximize planted seedling longevity.

Acknowledgments

Computational efforts were performed on the Tempest High Performance Computing System, operated and supported by University Information Technology Research Cyberinfrastructure (RRID:SCR_026229) at Montana State University.

We appreciate the assistance of Nancy Bockino, who gave us the opportunity to assist with the whitebark planting project at Burroughs Creek, as well as Tanner Shuler and Celina Montes from the Shoshone National Forest, Washakie Ranger District who visited the site with us and provided valuable feedback on our methodology.

CONCLUSION

Whitebark pine and climate change

Whitebark pine plays a critical role in subalpine environments of North America and its successful conservation has far-reaching benefits for other organisms and downstream ecosystems. These benefits are a result of its widespread distribution and the important ecological services it provides, such as creating a critical source of food for animals, facilitating establishment of other plant species, and stabilizing soils. The recent listing of the species as threatened under the Endangered Species Act recognizes the broad consequences of its ongoing decline (Levin, 2022). The threats whitebark pine faces are widespread. Climate is a strong secondary influence on its decline, which is primarily caused by threats such as white pine blister rust, mountain pine beetle, and wildfire. Successful conservation of whitebark pine presents many challenges for land managers, in part due to the difficulties of understanding and predicting impacts of a changing climate on whitebark pine across multiple, biologically relevant scales to inform effective management. The research presented here aims to solve these challenges by developing and applying climate-based models and tools addressing specific gaps in our knowledge of climate impacts to whitebark pine.

Summary of key findings

Wildfire refugia in the Greater Yellowstone Ecosystem

Chapter 2 presented a wildfire ignition danger rating system for the Middle Rockies ecoregion based on percentiles of 3-day rolling sums of climatic water deficit (CWD) or vapor pressure deficit (VPD), measures of dryness reflecting drought stress in plants and atmospheric dryness, respectively. The percentile function captures the spatial and temporal context of the dryness metrics at each location, facilitating direct comparison of dryness

between locations. Wildfire danger is then determined by comparing current local conditions to the distribution of conditions under which historical wildfire ignitions occurred, thus providing the means to determine if conditions on a given day are dry enough to ignite.

Projections of wildfire danger for forests in the GYE made using this method show increases in annual number of days with high fire danger from the near-future to the end of century across the ecoregion. These increases are minimized under the lower-emissions RCP4.5 climate projections, with persistence of some lower-risk areas at high elevations across the ecosystem. However, under the "business as usual" RCP8.5 projections, virtually no areas with lower fire that could serve as wildfire refugia for whitebark pine remain.

Climatic drivers of white pine blister rust infection

Chapter 3 presented a spatially explicit model of probability of white pine blister rust infection in whitebark pine that was developed using a novel dataset assembled from long-term white pine blister rust monitoring data from land management agencies across the Western U.S. The best performing model predicts the probability of white pine blister rust infection with August and September mean temperature, total precipitation, and their interaction, as well as tree size (DBH). The model also includes quadratic terms for temperature, allowing for a parabolic/U-shaped effect of temperature, which allows for an optimal temperature where temperature is neither too high nor too low to limit infection. At higher levels of precipitation ($\geq$ 100 mm precipitation during August and September), the highest rates of infection are found around 11 °C mean temperature during August and September. However, at lower levels of precipitation, the parabolic relationship of temperature inverts and minimal infection rates are predicted at 11 °C with highest rates at low and high temperatures—a relationship that should be interpreted with caution due to the low number of observations with combined August and September temperature and precipitation values at these levels. Projections of white pine blister rust disease hazard made across whitebark pine's range in

the Western US to 2099 show shifts in geographic patterns of disease hazard, with significant variability across regions and emissions scenarios. The region with the lowest rates of infection in recent history—the Sierra Nevada in California—is projected to maintain low rates of infection for all tree sizes at higher elevations with increases in probability of infection at lower elevations. On the contrary, the Crown of the Continent ecosystem containing Glacier National Park, which has among the highest recent infection rates, is projected to show low probabilities of infection under some climate projections. Lower rates of infection for all tree sizes in this region are notably projected under the higher-emissions RCP8.5 scenario than the lower-emissions RCP4.5.

Planting microsite selection using a high-resolution water balance model

Chapter 4 presented a case study of a method to identify microclimates that may potentially be suitable for planting white pine blister rust resistant seedlings. The method uses a high-resolution water balance model that incorporates fine-scale terrain and soil survey data to downscale relatively coarse climate grid cell data to biologically relevant scales. The "downscaling" is achieved by accounting for the influence of topoedaphic features (slope, aspect, and soil water holding capacity) on temperature and precipitation to produce biologically relevant indicators of climate: actual evapotranspiration, an estimate of plant water use, and climatic water deficit, a measure of evaporative demand and drought stress. This method revealed the potential for wide variability within a single climate grid cell at the study site based on topoedaphic variation and site properties that modify the grid cell climate when considering water balance variables. This variability can be leveraged to inform planting site selection by identifying small-scale features—potential climate microrefugia—that minimize drought stress under projections of climate that may be unfavorable at macroclimate scale. The microsite features that were identified as potential microrefugia tended to include northern aspects, minimizing climatic water deficit, and high water holding capacity soils,

maximizing actual evapotranspiration. These microsites can potentially minimize projected drought stress as well as year-to-year variability in growing conditions that can promote tree longevity. The microclimate maps can be used to select planting sites based on projected future conditions, not just historical ones.

Implications for whitebark pine conservation and management

The findings of this research are of great practical value to land managers interested in whitebark pine conservation, which benefits from efficient use of costly and limited resources of time, funding, and disease-resistant seedlings. Climate projections and ecological responses to future climate are inherently uncertain, a fact recognized by adaptive management frameworks such as Resist-Accept-Direct (RAD) (Lynch et al., 2021; Williams and Brown, 2024). This research provides data-driven insights that can support these strategies across multiple spatial scales.

The broad-scale maps of white pine blister rust disease hazard (Chapter 3) and wildfire risk (Chapter 2) allow managers to prioritize resources based on specific threats. Areas with low projected risk from these major threats can be prioritized for *Resist* strategies, such as focusing on protecting existing stands. Conversely, locations with high projected risk might lead managers to *Accept* ecological change or to *Direct* the system towards the desired future conditions, perhaps by prioritizing other locations or by considering strategies such as assisted migration to more favorable areas. Furthermore, maps of white pine blister rust and fire danger can be interpreted in tandem to identify areas with combined high or low risks across multiple threats.

These broad-scale hazard maps can help select priority areas for conservation and within these areas the planting microsite selection model based high-resolution water balance can be used to better understand site suitability at spatial scales relevant to individual trees. The high-resolution water balance planting microsite model identifies microrefugia that allow

hedging against climate uncertainty by targeting locations with potentially more stable climatic conditions that might be more resilient to future climate variability and extremes. Within areas targeted for *Resist* or *Direct* conservation actions, the planting microsite model can identify specific planting locations that buffer seedlings from drought stress or interannual climatic variability. Targeting plantings to these optimal planting microsites can maximize the likelihood of establishment and survival of costly and limited disease resistant whitebark pine seedlings. This method allows for evaluation of planting sites based on explicit consideration of climate at fine scales to the end of the century, not just based on historical climate conditions which may not reflect the suitability of the climate in the future as seedlings mature.

This research provides probabilistic assessments of risk to threats such as white pine blister rust, wildfire, and drought which can support decision-making under adaptive frameworks such as RAD that also include other factors in addition to climate threats. These data-driven insights into climate-linked risks across spatial scales can help inform management decisions and optimize allocation of limited time, funding, and disease resistant seedling resources to increase the likelihood of successful, long-term whitebark pine conservation outcomes.

Limitations and future research

Study limitations

Uncertainty in available historic and projected climate data is a limiting factor across all the work presented here. Some of this uncertainty comes from the application of gridded climate data, which is provided at spatial and temporal scales that present issues for some ecological applications such as models of individual organism response or susceptibility. Available gridded climate data products also have inherent bias in areas of complex terrain where weather stations are sparse, such as the mountainous, subalpine habitat of whitebark pine, which affects the accuracy of temperature and precipitation due to processes such as

lapse-rate effects (Tercek et al., 2021a) and orographic rainfall (Lin et al., 2001). Furthermore, models trained on historic climate data in this analysis are subject to assumptions of stationarity which assumes that the underlying spatial processes will interact with novel future climates as they did with the historical climate.

The white pine blister rust study was limited by available monitoring data. Because monitoring is performed at coarser time steps (4 years) than the time span at which white pine blister rust infection occurs (a single August/September basidiospore transmission period), this study was limited to analyzing conditions over broad temporal scales that may miss important white pine blister rust infection dynamics such as wave years where spikes in certain climatic factors promote higher-than-normal infection rates. In addition, while the monitoring dataset assembled for the study broadly covers whitebark pine's distribution in CONUS, there are areas where monitoring data was not available as well as areas where monitoring data was available, but climate data facilitating the creation of projections was not.

Ecological processes are inherently complex and present many challenges to efforts to model them. Some factors may be impossible to accurately account for in models, such as presence of alternate hosts for white pine blister rust infection or the human component of wildfire behavior. These unmodeled processes introduce another source of uncertainty in this work.

The high-resolution water balance model presents a powerful tool to select ideal planting microsites, but its predictions have not been validated against actual planting outcomes. This model can be used to guide planting within fire or white pine blister rust refugia, however this use is limited by uncertainty in the broad-scale models of those factors, resulting in great part from uncertainty in the direction of future anthropogenic greenhouse gas emissions—whether humanity chooses a path of lowered emissions as predicted in the RCP4.5 scenario or where emissions continue to rise as the RCP8.5 scenario predicts.

Future research directions

These findings and limitations reveal avenues for productive future work.

The high-resolution water balance model should be validated with field monitoring and planting trials to build confidence in its predictions. In addition, the accuracy of the model could be improved by incorporating refinements of other fine-scale processes that affect the water balance such as shade, downslope water flow, and snow accumulation.

This work can be integrated to assess broad-scale risk from white pine blister rust and wildfire as well as fine-scale site suitability for whitebark pine. Other major threats to whitebark pine such as mountain pine beetle should be integrated into this work to allow for a more thorough vulnerability assessment of whitebark pine and all of its threats.

The model of climatic drivers of white pine blister rust infection in whitebark pine has several avenues for improvement. Longitudinal data could refine the temporal aspect of infection to more biologically relevant scales. In addition, the work should be extended to the full range of whitebark pine in Canada if a suitable gridded climate data product can be developed that allows projections of white pine blister rust disease hazard.

The wildfire ignition danger rating system models only one aspect of wildfire behavior—ignition—but does not consider wildfire spread or severity which also have ecological effects. This model could also be further evaluated against existing wildfire danger models.

This work could be improved by refinements to gridded climate data. Climate products with higher resolution and improvements in accuracy and precision in mountainous terrain could resolve many of the limitations of applying these data in areas of complex, mountainous terrain. Until broad-scale climate data is available with better accuracy in areas of complex terrain, methods such as the use of temperature sensor networks present a solution to improve the accuracy of existing climate products for smaller regions (Holden et al., 2016).

Overall conclusions

Whitebark pine, a foundational and keystone species of western North American subalpine ecosystems, faces existential threats from climate-mediated disturbances which are driving its rapid decline. Successful conservation of whitebark pine requires understanding how climate change will impact the species. Explicit consideration of potential future climate is essential for successful management and conservation of long-lived, climate-sensitive species like whitebark pine. This work allows multi-scale and climate-informed estimates of risks to whitebark pine under future climates as well as tools to plan management at both coarse and fine scales. While whitebark pine faces grave and potentially intensifying future threats, this work provides quantified assessments and projections of some of its major threats, offering tools to inform management and promoting successful conservation of this iconic tree species.

CUMULATIVE REFERENCES CITED

Abatzoglou, J. T. (2013). Development of gridded surface meteorological data for ecological applications and modelling. *International Journal of Climatology*, 33(1):121–131. https://onlinelibrary.wiley.com/doi/abs/10.1002/joc.3413.

Abatzoglou, J. T., Battisti, D. S., Williams, A. P., Hansen, W. D., Harvey, B. J., and Kolden, C. A. (2021). Projected increases in western US forest fire despite growing fuel constraints. *Communications Earth & Environment*, 2(1):1–8. https://www.nature.com/articles/s43247-021-00299-0.

Abatzoglou, J. T. and Brown, T. J. (2012). A comparison of statistical downscaling methods suited for wildfire applications. *International Journal of Climatology*, 32(5):772–780. https://onlinelibrary.wiley.com/doi/abs/10.1002/joc.2312.

Abatzoglou, J. T. and Williams, A. P. (2016). Impact of anthropogenic climate change on wildfire across western US forests. *Proceedings of the National Academy of Sciences*, 113(42):11770–11775. https://www.pnas.org/doi/full/10.1073/pnas.1607171113.

Agee, J. (1998). The Landscape Ecology of Western Forest Fire Regimes. *Northwest Science*, 72:24–34. https://digitalcommons.usu.edu/barkbeetles/315.

Anderson, S. C., Ward, E. J., English, P. A., Barnett, L. A. K., and Thorson, J. T. (2024). sdmTMB: An R package for fast, flexible, and user-friendly generalized linear mixed effects models with spatial and spatiotemporal random fields. *bioRxiv : the preprint server for biology*, 2022.03.24.485545.

Bartoń, K. (2025). MuMIn: Multi-model inference. Technical report. https://CRAN.R-project.org/package=MuMIn.

Behnke, R., Vavrus, S., Allstadt, A., Albright, T., Thogmartin, W. E., and Radeloff, V. C. (2016). Evaluation of downscaled, gridded climate data for the conterminous United States. *Ecological Applications*, 26(5):1338–1351. https://www.jstor.org/stable/24818120.

Bentz, B., Campbell, E., Gibson, K., Kegley, S., Logan, J., and Six, D. (2011). Mountain pine beetle in high-elevation five-needle white pine ecosystems. *In: Keane, Robert E.; Tomback, Diana F.; Murray, Michael P.; Smith, Cyndi M., eds. The future of high-elevation, five-needle white pines in Western North America: Proceedings of the High Five Symposium. 28-30 June 2010; Missoula, MT. Proceedings RMRS-P-63. Fort Collins, CO: U.S. Department of Agriculture, Forest Service, Rocky Mountain Research Station. p. 78-84.*, 63:78–84. https://www.fs.usda.gov/research/treesearch/38203.

Bentz, B., Logan, J., and Amman, G. (1991). Temperature Dependent Development of the Mountain Pine Beetle and Simulation of Its Phenology. *The Bark Beetles, Fuels, and Fire Bibliography*, 123.

Bentz, B. J., Duncan, J. P., and Powell, J. A. (2016). Elevational shifts in thermal suitability for mountain pine beetle population growth in a changing climate. *Forestry: An International Journal of Forest Research*, 89(3):271–283. https://doi.org/10.1093/forestry/cpv054.

Bisigato, A. J., Hardtke, L., and del Valle, H. F. (2013). Soil as a capacitor: Considering soil water content improves temporal models of productivity. *Journal of Arid Environments*, 98:88–92. https://www.sciencedirect.com/science/article/pii/S0140196313001389.

Boer, M. M., Nolan, R. H., Resco De Dios, V., Clarke, H., Price, O. F., and Bradstock, R. A. (2017). Changing Weather Extremes Call for Early Warning of Potential for Catastrophic Fire. *Earth's Future*, 5(12):1196–1202. https://agupubs.onlinelibrary.wiley.com/doi/10.1002/2017EF000657.

Bower, A. D. and Aitken, S. N. (2008). Ecological genetics and seed transfer guidelines for Pinus albicaulis (Pinaceae). *American Journal of Botany*, 95(1):66–76.

Breheny, P. and Burchett, W. (2017). Visualization of regression models using visreg. *The R Journal*, 9(2):56–71.

Buotte, P. C., Hicke, J. A., Preisler, H. K., Abatzoglou, J. T., Raffa, K. F., and Logan, J. A. (2016). Climate influences on whitebark pine mortality from mountain pine beetle in the Greater Yellowstone Ecosystem. *Ecological Applications*, 26(8):2507–2524. https://onlinelibrary.wiley.com/doi/10.1002/eap.1396.

Burns, K. S., Tinkham, W. T., Leddy, K. A., Schoettle, A. W., Jacobi, W. R., and Stewart, J. E. (2023). Interactions between white pine blister rust, bark beetles, and climate over time indicate vulnerabilities to limber pine health. *Frontiers in Forests and Global Change*, 6. https://www.frontiersin.org/articles/10.3389/ffgc.2023.1149456.

Campbell, E. M. and Antos, J. A. (2000). Distribution and severity of white pine blister rust and mountain pine beetle on whitebark pine in British Columbia. *Canadian Journal of Forest Research*, 30(7):1051–1059. https://cdnsciencepub.com/doi/10.1139/x00-020.

Cawson, J. G., Collins, L., Parks, S. A., Nolan, R. H., and Penman, T. D. (2024). Atmospheric dryness removes barriers to the development of large forest fires. *Agricultural and Forest Meteorology*, 350:109990. https://www.sciencedirect.com/science/article/pii/S0168192324001059.

Chang, T., Hansen, A. J., and Piekielek, N. (2014). Patterns and Variability of Projected Bioclimatic Habitat for Pinus albicaulis in the Greater Yellowstone Area. *PLoS ONE*, 9(11):e111669. https://www.ncbi.nlm.nih.gov/pmc/articles/PMC4221071/.

Christensen, N. L., Agee, J. K., Brussard, P. F., Hughes, J., Knight, D. H., Minshall, G. W., Peek, J. M., Pyne, S. J., Swanson, F. J., Thomas, J. W., Wells, S., Williams, S. E., and Wright, H. A. (1989). Interpreting the Yellowstone Fires of 1988. *BioScience*, 39(10):678–685. https://www.jstor.org/stable/1310998.

Coop, J. D., Parks, S. A., Stevens-Rumann, C. S., Crausbay, S. D., Higuera, P. E., Hurteau, M. D., Tepley, A., Whitman, E., Assal, T., Collins, B. M., Davis, K. T., Dobrowski, S., Falk, D. A., Fornwalt, P. J., Fulé, P. Z., Harvey, B. J., Kane, V. R., Littlefield, C. E., Margolis, E. Q., North, M., Parisien, M.-A., Prichard, S., and Rodman, K. C. (2020). Wildfire-Driven Forest Conversion in Western North American Landscapes. *BioScience*, 70(8):659–673. https://academic.oup.com/bioscience/article/70/8/659/5859066.

de Groot, W. J., Wotton, B. M., and Flannigan, M. D. (2015). Chapter 11 - Wildland Fire Danger Rating and Early Warning Systems. In Shroder, J. F. and Paton, D., editors, *Wildfire Hazards, Risks and Disasters*, pages 207–228. Elsevier, Oxford. https://www.sciencedirect.com/science/article/pii/B9780124104341000117.

Dilts, T. E., Weisberg, P. J., Dencker, C. M., and Chambers, J. C. (2015). Functionally relevant climate variables for arid lands: A climatic water deficit approach for modelling desert shrub distributions. *Journal of Biogeography*, 42(10):1986–1997. https://onlinelibrary.wiley.com/doi/abs/10.1111/jbi.12561.

Dingman, S. L. (2015). *Physical Hydrology*. Waveland Press, Inc, Long Grove, Illinois, third edition.

Dobrowski, S. Z. (2011). A climatic basis for microrefugia: The influence of terrain on climate. *Global Change Biology*, 17(2):1022–1035. https://onlinelibrary.wiley.com/doi/abs/10.1111/j.1365-2486.2010.02263.x.

Dudney, J., Willing, C. E., Das, A. J., Latimer, A. M., Nesmith, J. C. B., and Battles, J. J. (2021). Nonlinear shifts in infectious rust disease due to climate change. *Nature Communications*, 12(1):5102. https://www.nature.com/articles/s41467-021-25182-6.

Dudney, J. C., Nesmith, J. C. B., Cahill, M. C., Cribbs, J. E., Duriscoe, D. M., Das, A. J., Stephenson, N. L., and Battles, J. J. (2020). Compounding effects of white pine blister rust, mountain pine beetle, and fire threaten four white pine species. *Ecosphere*, 11(10):e03263. https://onlinelibrary.wiley.com/doi/abs/10.1002/ecs2.3263.

Dyer, J. M. (2019). A GIS-Based Water Balance Approach Using a LiDAR-Derived DEM Captures Fine-Scale Vegetation Patterns. *Remote Sensing*, 11(20):2385. https://www.mdpi.com/2072-4292/11/20/2385.

Eidenshink, J., Schwind, B., Brewer, K., Zhu, Z.-L., Quayle, B., and Howard, S. (2007). A Project for Monitoring Trends in Burn Severity. *Fire Ecology*, 3(1):3–21. https://fireecology.springeropen.com/articles/10.4996/fireecology.0301003.

Farguell, A., Jolly, W., Koul, A., Moon, Y., and Kochanski, A. K. (2025). Toward Fast Spatial NFDRS Calculations. In *2025 AMS Denver Summit*. AMS. https://ams.confex.com/ams/2025Summit/meetingapp.cgi/Paper/460517.

Fick, S. E. and Hijmans, R. J. (2017). WorldClim 2: New 1-km spatial resolution climate surfaces for global land areas. *International Journal of Climatology*, 37(12):4302–4315. https://onlinelibrary.wiley.com/doi/abs/10.1002/joc.5086.

Franklin, J., Davis, F. W., Ikegami, M., Syphard, A. D., Flint, L. E., Flint, A. L., and Hannah, L. (2013). Modeling plant species distributions under future climates: How fine scale do climate projections need to be? *Global Change Biology*, 19(2):473–483. https://onlinelibrary.wiley.com/doi/abs/10.1111/gcb.12051.

Geils, B. W., Hummer, K. E., and Hunt, R. S. (2010). White pines, *Ribes* , and blister rust: A review and synthesis. *Forest Pathology*, 40(3-4):147–185. https://onlinelibrary.wiley.com/doi/10.1111/j.1439-0329.2010.00654.x.

Ghelardini, L., Luchi, N., Pecori, F., Pepori, A. L., Danti, R., Della Rocca, G., Capretti, P., Tsopelas, P., and Santini, A. (2017). Ecology of invasive forest pathogens. *Biological Invasions*, 19(11):3183–3200. https://doi.org/10.1007/s10530-017-1487-0.

Gillingham, P. K., Huntley, B., Kunin, W. E., and Thomas, C. D. (2012). The effect of spatial resolution on projected responses to climate warming. *Diversity and Distributions*, 18(10):990–1000. https://onlinelibrary.wiley.com/doi/abs/10.1111/j.1472-4642.2012.00933.x.

Goddard, L. and Gershunov, A. (2020). Impact of El Niño on Weather and Climate Extremes. In *El Niño Southern Oscillation in a Changing Climate*, chapter 16, pages 361–375. American Geophysical Union (AGU). https://onlinelibrary.wiley.com/doi/abs/10.1002/9781119548164.ch16.

Goeking, S. A. and Izlar, D. K. (2018). Pinus albicaulis Engelm. (Whitebark Pine) in Mixed-Species Stands throughout Its US Range: Broad-Scale Indicators of Extent and Recent Decline. *Forests*, 9(3):131. https://www.mdpi.com/1999-4907/9/3/131.

Gotelli, N. J. and Ellison, A. M. (2013). *A Primer of Ecological Statistics*. Sinauer Associates, Inc., Publishers, Sunderland, Massachusetts, second edition edition.

Graham, M. H. (2003). CONFRONTING MULTICOLLINEARITY IN ECOLOGICAL MULTIPLE REGRESSION. *Ecology*, 84(11):2809–2815. http://doi.wiley.com/10.1890/02-3114.

Greater Yellowstone Whitebark Pine Monitoring Working Group (2011). Interagency Whitebark Pine Monitoring Protocol for the Greater Yellowstone Ecosystem, Version 1.1.

Hansen, A. J., East, A., Keane, R. E., Lavin, M., Legg, K., Holden, Z., Toney, C., and Alongi, F. (2021). Is whitebark pine less sensitive to climate warming when climate tolerances of juveniles are considered? *Forest Ecology and Management. 493: 19221.*, 493:19221. http://www.fs.usda.gov/treesearch/pubs/62425.

Hernández, F. (2020). Ecological Discord and the Importance of Scale in Scientific Inquiry. *The Journal of Wildlife Management*, 84(8):1427–1434. https://onlinelibrary.wiley.com/doi/abs/10.1002/jwmg.21942.

Hernangómez, D. (2023). Using the tidyverse with terra objects: The tidyterra package. *Journal of Open Source Software*, 8(91):5751. https://doi.org/10.21105/joss.05751.

Hijmans, R. J. (2024). *Terra: Spatial Data Analysis*. https://CRAN.R-project.org/package=terra.

Hoff, R. J. (1992). *How to Recognize Blister Rust Infection on Whitebark Pine*. U.S. Department of Agriculture, Forest Service, Intermountain Research Station. http://dx.doi.org/10.2737/INT-RN-406.

Holden, Z. A., Abatzoglou, J. T., Luce, C. H., and Baggett, L. S. (2011). Empirical downscaling of daily minimum air temperature at very fine resolutions in complex terrain. *Agricultural and Forest Meteorology*, 151(8):1066–1073. https://www.sciencedirect.com/science/article/pii/S0168192311001080.

Holden, Z. A., Swanson, A., Klene, A. E., Abatzoglou, J. T., Dobrowski, S. Z., Cushman, S. A., Squires, J., Moisen, G. G., and Oyler, J. W. (2016). Development of high-resolution (250 m) historical daily gridded air temperature data using reanalysis and distributed sensor networks for the US Northern Rocky Mountains. *International Journal of Climatology*, 36(10):3620–3632. https://onlinelibrary.wiley.com/doi/abs/10.1002/joc.4580.

Holden, Z. A., Swanson, A., Luce, C. H., Jolly, W. M., Maneta, M., Oyler, J. W., Warren, D. A., Parsons, R., and Affleck, D. (2018). Decreasing fire season precipitation increased recent western US forest wildfire activity. *Proceedings of the National Academy of Sciences*, 115(36):E8349–E8357. https://www.pnas.org/doi/abs/10.1073/pnas.1802316115.

Jackson, S. T., Betancourt, J. L., Booth, R. K., and Gray, S. T. (2009). Ecology and the ratchet of events: Climate variability, niche dimensions, and species distributions. *Proceedings of the National Academy of Sciences*, 106(supplement_2):19685–19692. https://pnas.org/doi/full/10.1073/pnas.0901644106.

Jenkins, M., Jr..Incashola, T., LaFleur, D., Hoang, L., Renwick, K., Schoettle, A., Mellman-Brown, S., Lozeau, J., O'Bennick, K. R., Meyer, E., Anderson, K., Sissons, R., Keane, B., and Jones, B. (2020). Crown of the Continent Ecosystem Whitebark Pine Restoration Strategy: 2019 Pilot - Project Summary. *Crown Managers Partnership (CMP), High Five Working Group (Hi5WG). 8 p.* https://research.fs.usda.gov/treesearch/62150.

Jimenez-Ruano, A., Jolly, W. M., Freeborn, P. H., Vega-Nieva, D. J., Monjaras-Vega, N. A., Briones-Herrera, C. I., and Rodrigues, M. (2022). Spatial predictions of human and natural-caused wildfire likelihood across Montana (USA). *Forests. 13: 1200.*, 13:1200. https://research.fs.usda.gov/treesearch/65053.

Johnson, D. M., McCulloh, K. A., and Reinhardt, K. (2011). The Earliest Stages of Tree Growth: Development, Physiology and Impacts of Microclimate. In Meinzer, F. C., Lachenbruch, B., and Dawson, T. E., editors, *Size- and Age-Related Changes in Tree Structure and Function*, volume 4, pages 65–87. Springer Netherlands, Dordrecht. http://link.springer.com/10.1007/978-94-007-1242-3_3.

Jolly, W. M., Cochrane, M. A., Freeborn, P. H., Holden, Z. A., Brown, T. J., Williamson, G. J., and Bowman, D. M. J. S. (2015). Climate-induced variations in global wildfire danger from 1979 to 2013. *Nature Communications*, 6(1):7537. https://www.nature.com/articles/ncomms8537.

Jolly, W. M., Freeborn, P. H., Bradshaw, L. S., Wallace, J., and Brittain, S. (2024). Modernizing the US National Fire Danger Rating System (version 4): Simplified fuel models and improved live and dead fuel moisture calculations. *Environmental Modelling & Software*, 181:106181. https://www.sciencedirect.com/science/article/pii/S1364815224002421.

Jolly, W. M., Freeborn, P. H., Page, W. G., and Butler, B. W. (2019). Severe Fire Danger Index: A Forecastable Metric to Inform Firefighter and Community Wildfire Risk Management. *Fire*, 2(3):47. https://www.mdpi.com/2571-6255/2/3/47.

Jolly, W. M. and Johnson, D. M. (2018). Pyro-Ecophysiology: Shifting the Paradigm of Live Wildland Fuel Research. *Fire*, 1(1):8. https://www.mdpi.com/2571-6255/1/1/8.

Jorge, A. L., Abatzoglou, J. T., Fleishman, E., Williams, E. L., Rupp, D. E., Jenkins, J. S., Sadegh, M., Kolden, C. A., and Short, K. C. (2025). COVID-19 Fueled an Elevated Number of Human-Caused Ignitions in the Western United States During the 2020 Wildfire Season. *Earth's Future*, 13(4):e2024EF005744. https://onlinelibrary.wiley.com/doi/abs/10.1029/2024EF005744.

Keane, R. E., Tomback, D. F., Aubry, C. A., Bower, A. D., Campbell, E. M., Cripps, C. L., Jenkins, M. B., Mahalovich, M. F., Manning, M., McKinney, S. T., Murray, M. P., Perkins, D. L., Reinhart, D. P., Ryan, C., Schoettle, A. W., and Smith, C. M. (2012). A range-wide restoration strategy for whitebark pine (Pinus albicaulis). Technical Report RMRS-GTR-279, U.S. Department of Agriculture, Forest Service, Rocky Mountain Research Station, Ft. Collins, CO. https://www.fs.usda.gov/treesearch/pubs/40884.

Kearns, H. S. and Jacobi, W. R. (2007). The distribution and incidence of white pine blister rust in central and southeastern Wyoming and northern Colorado. *Canadian Journal of Forest Research*, 37(2):462–472. https://cdnsciencepub.com/doi/full/10.1139/x06-231.

Kearns, H. S. J., Jacobi, W. R., Reich, R. M., Flynn, R. L., Burns, K. S., and Geils, B. W. (2014). Risk of white pine blister rust to limber pine in Colorado and Wyoming, USA. *Forest Pathology*, 44(1):21–38. https://onlinelibrary.wiley.com/doi/abs/10.1111/efp.12065.

Krueger, E. S., Levi, M. R., Achieng, K. O., Bolten, J. D., Carlson, J. D., Coops, N. C., Holden, Z. A., Magi, B. I., Rigden, A. J., and Ochsner, T. E. (2022). Using soil moisture information

to better understand and predict wildfire danger: A review of recent developments and outstanding questions. *International Journal of Wildland Fire*, 32(2):111–132. https://www.publish.csiro.au/wf/WF22056.

LaFrance, B. J., Ray, A. M., Tercek, M. T., Fisher, R. N., and Hossack, B. R. (2024). Amphibian richness, rarity, threats, and conservation prospects across the U.S. National Park System. *npj Biodiversity*, 3(1):1–9. https://www.nature.com/articles/s44185-024-00067-1.

Laufenberg, D., Thoma, D., Hansen, A., and Hu, J. (2020). Biophysical Gradients and Performance of Whitebark Pine Plantings in the Greater Yellowstone Ecosystem. *Forests*, 11(1):119. https://www.mdpi.com/1999-4907/11/1/119.

Lawrence, D. J., Runyon, A. N., Gross, J. E., Schuurman, G. W., and Miller, B. W. (2021). Divergent, plausible, and relevant climate futures for near- and long-term resource planning. *Climatic Change*, 167(3):38. https://doi.org/10.1007/s10584-021-03169-y.

Legendre, P. (1993). Spatial Autocorrelation: Trouble or New Paradigm? *Ecology*, 74(6):1659–1673. https://www.jstor.org/stable/1939924.

Levin, J. (2022). The Whitebark Pine: Endangered Species Protection and Critical Habitat Designation. *Tulane Environmental Law Journal*, 35(1/2):45–68. https://www.jstor.org/stable/27160114.

Levin, S. A. (1992). The Problem of Pattern and Scale in Ecology: The Robert H. MacArthur Award Lecture. *Ecology*, 73(6):1943–1967. https://onlinelibrary.wiley.com/doi/abs/10.2307/1941447.

Liebhold, A. M., Brockerhoff, E. G., Garrett, L. J., Parke, J. L., and Britton, K. O. (2012). Live plant imports: The major pathway for forest insect and pathogen invasions of the US. *Frontiers in Ecology and the Environment*, 10(3):135–143. https://esajournals.onlinelibrary.wiley.com/doi/10.1890/110198.

Lin, Y.-L., Chiao, S., Wang, T.-A., Kaplan, M. L., and Weglarz, R. P. (2001). Some Common Ingredients for Heavy Orographic Rainfall. *Weather and Forecasting*, 16(6):633–660. https://journals.ametsoc.org/view/journals/wefo/16/6/1520-0434_2001_016_0633_scifho_2_0_co_2.xml.

Lindgren, F. (2024). *Fmesher: Triangle Meshes and Related Geometry Tools*. https://CRAN.R-project.org/package=fmesher.

Littell, J. S., McKenzie, D., Wan, H. Y., and Cushman, S. A. (2018). Climate Change and Future Wildfire in the Western United States: An Ecological Approach to Nonstationarity. *Earth's Future*, 6(8):1097–1111. https://onlinelibrary.wiley.com/doi/abs/10.1029/2018EF000878.

Littell, J. S., Peterson, D. L., Riley, K. L., Liu, Y., and Luce, C. H. (2016). A review of the relationships between drought and forest fire in the United States. *Global Change Biology*, 22(7):2353–2369. https://onlinelibrary.wiley.com/doi/10.1111/gcb.13275.

Lorenz, T. J., Sullivan, K. A., Bakian, A. V., and Aubry, C. A. (2011). Cache-Site Selection in Clark's Nutcracker (Nucifraga Columbiana) - Selección de Sitios de Acumulación de Alimento en Nucifraga columbiana. *The Auk*, 128(2):237–247. https://www.jstor.org/stable/10.1525/auk.2011.10101.

Lutz, J. A., van Wagtendonk, J. W., and Franklin, J. F. (2010). Climatic water deficit, tree species ranges, and climate change in Yosemite National Park. *Journal of Biogeography*, 37(5):936–950. https://onlinelibrary.wiley.com/doi/abs/10.1111/j.1365-2699.2009.02268.x.

Lynch, A. J., Thompson, L. M., Beever, E. A., Cole, D. N., Engman, A. C., Hawkins Hoffman, C., Jackson, S. T., Krabbenhoft, T. J., Lawrence, D. J., Limpinsel, D., Magill, R. T., Melvin, T. A., Morton, J. M., Newman, R. A., Peterson, J. O., Porath, M. T., Rahel, F. J., Schuurman, G. W., Sethi, S. A., and Wilkening, J. L. (2021). Managing for RADical ecosystem change: Applying the Resist-Accept-Direct (RAD) framework. *Frontiers in Ecology and the Environment*, 19(8):461–469. https://onlinelibrary.wiley.com/doi/abs/10.1002/fee.2377.

Mancuso, M. (2022). Monitoring white pine blister rust in whitebark pine communities on the Sawtooth National Forest, Idaho: 2021 results. Technical report, Mancuso Botanical Services.

McCaughey, W., Scott, G. L., and Izlar, K. L. (2009). Whitebark Pine Planting Guidelines. *Western Journal of Applied Forestry*, 24(3):163–166. https://academic.oup.com/wjaf/article/24/3/163/4683493.

McCormick, E. L., Dralle, D. N., Hahm, W. J., Tune, A. K., Schmidt, L. M., Chadwick, K. D., and Rempe, D. M. (2021). Widespread woody plant use of water stored in bedrock. *Nature*, 597(7875):225–229.

McCune, B. and Keon, D. (2002). Equations for Potential Annual Direct Incident Radiation and Heat Load. *Journal of Vegetation Science*, 13(4):603–606. https://www.jstor.org/stable/3236745.

McKenzie, D. and Littell, J. S. (2017). Climate change and the eco-hydrology of fire: Will area burned increase in a warming western USA? *Ecological Applications*, 27(1):26–36. https://onlinelibrary.wiley.com/doi/abs/10.1002/eap.1420.

McKinney, S. T., Stewardship, U. S. N. P. S. N. R., and body. Science, i. (2012). Monitoring white pine (pinus albicaulis, P. balfouriana, P. flexilis) community dynamics in the pacific west region - klamath, sierra nevada, and upper columbia basin networks. Standard operating procedures. Version 1.0 (appendix a to narrative version 1.0). In *Monitoring White Pine (Pinus Albicaulis, P. Balfouriana, P. Flexilis) Community Dynamics in the*

Pacific West Region - Klamath, Sierra Nevada, and Upper Columbia Basin Networks. Standard Operating Procedures. Version 1.0 (Appendix a to Narrative Version 1.0), Natural Resource Report ; NPS/PWR/NRR–2012/533. U.S. Department of the Interior, National Park Service, Natural Resource Stewardship and Science, Fort Collins, Colorado.

McMaster, G. S. and Wilhelm, W. W. (1997). Growing degree-days: One equation, two interpretations. *Agricultural and Forest Meteorology*, 87(4):291–300. https://www.sciencedirect.com/science/article/pii/S0168192397000270.

Meyn, A., White, P. S., Buhk, C., and Jentsch, A. (2007). Environmental drivers of large, infrequent wildfires: The emerging conceptual model. *Progress in Physical Geography: Earth and Environment*, 31(3):287–312. https://journals.sagepub.com/doi/10.1177/0309133307079365.

Mielke, K. P., Claassen, T., Busana, M., Heskes, T., Huijbregts, M. A. J., Koffijberg, K., and Schipper, A. M. (2020). Disentangling drivers of spatial autocorrelation in species distribution models. *Ecography*, 43(12):1741–1751. https://onlinelibrary.wiley.com/doi/abs/10.1111/ecog.05134.

Miller, C. and Urban, D. L. (2000). Connectivity of forest fuels and surface fire regimes. *Landscape Ecology*, 15(2):145–154. http://link.springer.com/10.1023/A:1008181313360.

Morelli, T. L., Daly, C., Dobrowski, S. Z., Dulen, D. M., Ebersole, J. L., Jackson, S. T., Lundquist, J. D., Millar, C. I., Maher, S. P., Monahan, W. B., Nydick, K. R., Redmond, K. T., Sawyer, S. C., Stock, S., and Beissinger, S. R. (2016). Managing Climate Change Refugia for Climate Adaptation. *PLOS ONE*, 11(8):e0159909. https://journals.plos.org/plosone/article?id=10.1371/journal.pone.0159909.

Moudrý, V., Keil, P., Gábor, L., Lecours, V., Zarzo-Arias, A., Barták, V., Malavasi, M., Rocchini, D., Torresani, M., Gdulová, K., Grattarola, F., Leroy, F., Marchetto, E., Thouverai, E., Prošek, J., Wild, J., and Šímová, P. (2023). Scale mismatches between predictor and response variables in species distribution modelling: A review of practices for appropriate grain selection. *Progress in Physical Geography: Earth and Environment*, 47(3):467–482. https://doi.org/10.1177/03091333231156362.

National Whitebark Pine Restoration Plan (2021). Whitebark Pine Treatment Pricing List. https://whitebarkfound.org/wp-content/uploads/2021/04/NWPRP-Treatment-cost-list_3_15_21.pdf.

Nelder, J. A. (1977). A Reformulation of Linear Models. *Journal of the Royal Statistical Society. Series A (General)*, 140(1):48–77. https://www.jstor.org/stable/2344517.

Neumann, M., Mues, V., Moreno, A., Hasenauer, H., and Seidl, R. (2017). Climate variability drives recent tree mortality in Europe. *Global change biology*, 23(11):4788–4797. https://www.ncbi.nlm.nih.gov/pmc/articles/PMC5633074/.

Norment, C. J. (1991). Bird use of forest patches in the subalpine forest-alpine tundra ecotone of the Beartooth Mountains, Wyoming. *Northwest science.*, 65(1).

Northwest Knowledge Network (2025). REACCH METDATA (GRIDMET) meterological by variable—1979 to CurrentYear (version 4.6.11). http://thredds.northwestknowledge.net:8080/thredds/reacch_climate_MET_catalog.html.

Olsen, L. R. and Zachariae, H. B. (2024). *Cvms: Cross-Validation for Model Selection*. https://CRAN.R-project.org/package=cvms.

Omernik, J. M. (1987). Ecoregions of the Conterminous United States. *Annals of the Association of American Geographers*, 77(1):118–125. https://doi.org/10.1111/j.1467-8306.1987.tb00149.x.

Oudin, L., Moulin, L., Bendjoudi, H., and Ribstein, P. (2010). Estimating potential evapotranspiration without continuous daily data: Possible errors and impact on water balance simulations. *Hydrological Sciences Journal*, 55(2):209–222. https://doi.org/10.1080/02626660903546118.

Paysen, T. E., Ansley, R. J., Brown, J. K., Gottfried, G. J., Haase, S. M., Harrington, M. G., Narog, M. G., Sackett, S. S., and Wilson, R. C. (2000). Fire in western shrubland, woodland, and grassland ecosystems. *Wildland fire in ecosystems: Effects of fire on flora*, 2:121–59.

Pebesma, E. (2018). Simple Features for R: Standardized Support for Spatial Vector Data. *The R Journal*, 10(1):439–446. https://doi.org/10.32614/RJ-2018-009.

Pontius, R. G. and Parmentier, B. (2014). Recommendations for using the relative operating characteristic (ROC). *Landscape Ecology*, 29(3):367–382. https://doi.org/10.1007/s10980-013-9984-8.

QGIS Development Team (2024). *QGIS Geographic Information System*. https://www.qgis.org.

R Core Team (2024). *R: A Language and Environment for Statistical Computing*. R Foundation for Statistical Computing, Vienna, Austria. https://www.R-project.org/.

Rammer, W., Braziunas, K. H., Hansen, W. D., Ratajczak, Z., Westerling, A. L., Turner, M. G., and Seidl, R. (2021). Widespread regeneration failure in forests of Greater Yellowstone under scenarios of future climate and fire. *Global Change Biology*, 27(18):4339–4351. https://onlinelibrary.wiley.com/doi/10.1111/gcb.15726.

Ray, A. M., Hossack, B. R., Gould, W. R., Patla, D. A., Spear, S. F., Klaver, R. W., Bartelt, P. E., Thoma, D. P., Legg, K. L., Daley, R., Stephen Corn, P., and Peterson, C. R. (2022). Multi-species amphibian monitoring across a protected landscape: Critical reflections on 15 years of wetland monitoring in Grand Teton and Yellowstone national

parks. *Ecological Indicators*, 135:108519. https://www.sciencedirect.com/science/article/pii/S1470160X21011845.

Righetto, A. J., Faes, C., Vandendijck, Y., and Ribeiro, P. J. (2020). On the choice of the mesh for the analysis of geostatistical data using R-INLA. *Communications in Statistics - Theory and Methods*, 49(1):203–220. https://www.tandfonline.com/doi/full/10.1080/03610926.2018.1536209.

Riley, K. L., Abatzoglou, J. T., Grenfell, I. C., Klene, A. E., Heinsch, F. A., Riley, K. L., Abatzoglou, J. T., Grenfell, I. C., Klene, A. E., and Heinsch, F. A. (2013). The relationship of large fire occurrence with drought and fire danger indices in the western USA, 1984–2008: The role of temporal scale. *International Journal of Wildland Fire*, 22(7):894–909. https://www.publish.csiro.au/wf/WF12149.

Rochefort, R., Bivin, M., Boetsch, J., Acker, S., and Whiteaker, L. (2010). Alpine and subalpine vegetation monitoring in the north coast and cascades network natural resource data series NPS/NCCN/NRDS-2015/746. Technical report.

Rollins, M. G. (2009). LANDFIRE: A nationally consistent vegetation, wildland fire, and fuel assessment. *International Journal of Wildland Fire*, 18(3):235–249. https://www.publish.csiro.au/wf/WF08088.

Running, S. W. (2006). Is Global Warming Causing More, Larger Wildfires? *Science*, 313(5789):927–928. https://www.science.org/doi/10.1126/science.1130370.

Rust, S. K. and Gurvich, D. (2018). Whitebark Pine Monitoring in Grandmother Mountain Wilderness Study Area. Technical report.

Schloerke, B., Cook, D., Larmarange, J., Briatte, F., Marbach, M., Thoen, E., Elberg, A., and Crowley, J. (2024). *GGally: Extension to 'Ggplot2'*. https://CRAN.R-project.org/package=GGally.

Scott, G. L. and McCaughey, W. W. (2006). Whitebark Pine Guidelines for Planting Prescriptions. *In: Riley, L.E.; Dumroese, R.K.; Landis, T.D., tech. coords. 2006. National Proceedings: Forest and Conservation Nursery Associations - 2005. Proc. RMRS-P-43. Fort Collins, CO: U.S. Department of Agriculture, Forest Service, Rocky Mountain Research Station. p. 84-90*, 043. https://www.fs.usda.gov/research/treesearch/26661.

Shanahan, E., Irvine, K. M., Thoma, D., Wilmoth, S., Ray, A., Legg, K., and Shovic, H. (2016). Whitebark pine mortality related to white pine blister rust, mountain pine beetle outbreak, and water availability. *Ecosphere*, 7(12):e01610. https://onlinelibrary.wiley.com/doi/abs/10.1002/ecs2.1610.

Shanahan, E., Wright, W. J., and Irvine, K. M. (2021). Adaptive monitoring in action: Reconsidering design-based estimators reveals underestimation of whitebark pine disease prevalence in the Greater Yellowstone Ecosystem. *Journal of Applied Ecology*, 58(5):1079–1089. https://onlinelibrary.wiley.com/doi/abs/10.1111/1365-2664.13837.

Shepherd, B., Krakowski, J., Moody, R., Reid, I., Murray, M., Stafl, N., Sissons, R., Alger, G., Park, J., McLellan, C., Schwarz, C., and Smith, C. (2024). Climate dominates geographic influences on whitebark pine and limber pine trends and landscape patterns in Canada. *Canadian Journal of Forest Research*, 55:1–19.

Shmueli, G. (2010). To Explain or to Predict? *Statistical Science*, 25(3). https://projecteuclid.org/journals/statistical-science/volume-25/issue-3/To-Explain-or-to-Predict/10.1214/10-STS330.full.

Six, D. L. and Newcomb, M. (2005). A rapid system for rating white pine blister rust incidence, severity, and within-tree distribution in whitebark pine. *Northwest Science*, 79(2-3):189–195.

Smith-Mckenna, E. K., Resler, L. M., Tomback, D. F., Zhang, H., and Malanson, G. P. (2013). Topographic influences on the distribution of white pine blister rust in Pinus albicaulis treeline communities. *Écoscience*, 20(3):215–229. https://doi.org/10.2980/20-3-3599.

Sniezko, R. A., Johnson, J. S., Kegley, A., and Danchok, R. (2024). Disease resistance in whitebark pine and potential for restoration of a threatened species. *PLANTS, PEOPLE, PLANET*, 6(2):341–361. https://onlinelibrary.wiley.com/doi/abs/10.1002/ppp3.10443.

Sniezko, R. A. and Liu, J.-J. (2023). Prospects for developing durable resistance in populations of forest trees. *New Forests*, 54(4):751–767. https://doi.org/10.1007/s11056-021-09898-3.

Soil Survey Staff, Natural Resources Conservation Service, U. S. D. o. A. (2024). Soil survey geographic (SSURGO) database. https://www.nrcs.usda.gov/conservation-basics/natural-resource-concerns/soil/citing-our-databases.

Stephenson, N. (1998). Actual evapotranspiration and deficit: Biologically meaningful correlates of vegetation distribution across spatial scales. *Journal of Biogeography*, 25(5):855–870. https://onlinelibrary.wiley.com/doi/abs/10.1046/j.1365-2699.1998.00233.x.

Stephenson, N. L. (1990). Climatic Control of Vegetation Distribution: The Role of the Water Balance. *The American Naturalist*, 135(5):649–670. https://www.jstor.org/stable/2462028.

Tercek, M. and Rodman, A. (2016). Forecasts of 21st Century Snowpack and Implications for Snowmobile and Snowcoach Use in Yellowstone National Park. *PLOS ONE*, 11(7):e0159218. https://journals.plos.org/plosone/article?id=10.1371/journal.pone.0159218.

Tercek, M. T., Gross, J. E., and Thoma, D. P. (2023). Robust projections and consequences of an expanding bimodal growing season in the western United States. *Ecosphere*, 14(5):e4530. https://onlinelibrary.wiley.com/doi/abs/10.1002/ecs2.4530.

Tercek, M. T., Rodman, A., Woolfolk, S., Wilson, Z., Thoma, D., and Gross, J. (2021a). Correctly applying lapse rates in ecological studies: Comparing temperature observations and gridded data in Yellowstone. *Ecosphere*, 12(3):e03451. https://onlinelibrary.wiley.com/doi/abs/10.1002/ecs2.3451.

Tercek, M. T., Thoma, D., Gross, J. E., Sherrill, K., Kagone, S., and Senay, G. (2021b). Historical changes in plant water use and need in the continental United States. *PLOS ONE*, 16(9):e0256586. https://journals.plos.org/plosone/article?id=10.1371/journal.pone.0256586.

Thoma, D. P., Munson, S. M., Irvine, K. M., Witwicki, D. L., and Bunting, E. L. (2016). Semi-arid vegetation response to antecedent climate and water balance windows. *Applied Vegetation Science*, 19(3):413–429. https://onlinelibrary.wiley.com/doi/abs/10.1111/avsc.12232.

Thoma, D. P., Munson, S. M., and Witwicki, D. L. (2019a). Landscape pivot points and responses to water balance in national parks of the southwest US. *Journal of Applied Ecology*, 56(1):157–167. https://onlinelibrary.wiley.com/doi/abs/10.1111/1365-2664.13250.

Thoma, D. P., Shanahan, E. K., and Irvine, K. M. (2019b). Climatic Correlates of White Pine Blister Rust Infection in Whitebark Pine in the Greater Yellowstone Ecosystem. *Forests*, 10(8):666. https://www.mdpi.com/1999-4907/10/8/666.

Thoma, D. P., Tercek, M. T., Schweiger, E. W., Munson, S. M., Gross, J. E., and Olliff, S. T. (2020). Water balance as an indicator of natural resource condition: Case studies from Great Sand Dunes National Park and Preserve. *Global Ecology and Conservation*, 24:e01300. https://www.sciencedirect.com/science/article/pii/S2351989420308416.

Thornthwaite, C. W. (1948). An Approach toward a Rational Classification of Climate. *Geographical Review*, 38(1):55–94. https://www.jstor.org/stable/210739.

Thornton, P. E., Thornton, M. M., Mayer, B. W., Wilhelmi, N., Wei, Y., Devarakonda, R., and Cook, R. B. (2014). Daymet: Daily Surface Weather Data on a 1-km Grid for North America, Version 2. *ORNL DAAC*. https://daac.ornl.gov/cgi-bin/dsviewer.pl?ds_id=1219.

Tomback, D. (2011). The Magnificent High-Elevation Five-Needle White Pines: Ecological Roles and Future Outlook Why the High Five Pines? *The Future of High-elevation, Five-needle White Pines in Western North America: Proceedings of the High Five Symposium*.

Tomback, D. F., Arno, S. F., and Keane, R. E., editors (2001). *Whitebark Pine Communities: Ecology and Restoration*. Island Press, Washington.

Tomback, D. F., Hoffman, LA., and Sund, S. K. (1990). Coevolution of whitebark pine and nutcrackers: Implications for forest regeneration. *USDA Forest Service, General Technical Report INT*, 270:118–129.

Tomback, D. F., Keane, R. E., Schoettle, A. W., Sniezko, R. A., Jenkins, M. B., Nelson, C. R., Bower, A. D., DeMastus, C. R., Guiberson, E., Krakowski, J., Murray, M. P., Pansing, E. R., and Shamhart, J. (2022). Tamm review: Current and recommended management practices for the restoration of whitebark pine (Pinus albicaulis Engelm.), an imperiled high-elevation Western North American forest tree. *Forest Ecology and Management*, 522:119929. https://www.sciencedirect.com/science/article/pii/S0378112721010203.

Turner, M. G., Braziunas, K. H., Hansen, W. D., Hoecker, T. J., Rammer, W., Ratajczak, Z., Westerling, A. L., and Seidl, R. (2022). The magnitude, direction, and tempo of forest change in Greater Yellowstone in a warmer world with more fire. *Ecological Monographs*, 92(1):e01485. https://onlinelibrary.wiley.com/doi/abs/10.1002/ecm.1485.

United States Forest Service. White Pine Blister Rust and its threat to to High Elevation White Pines. https://www.fs.usda.gov/rm/highelevationwhitepines/Threats/blister-rust-threat.htm.

U.S. Geological Survey (2020). WY FEMA East B9 2019. https://portal.opentopography.org/usgsDataset?dsid=WY_FEMA_East_B9_2019.

Van Arsdel, E. P. (1961). *The Climatic Distribution of Blister Rust on White Pine in Wisconsin*. Number 87. Forest Service, US Department of Agriculture.

Van Arsdel, E. P., Riker, A. J., and Patton, R. F. (1956). The effects of temperature and moisture on the spread of White Pine blister rust. *Phytopathology*, 46(6):307–318 pp.

Viney, N. R. (1991). A Review of Fine Fuel Moisture Modelling. *International Journal of Wildland Fire*, 1(4):215–234. https://www.publish.csiro.au/wf/wf9910215.

Wang, Z., Wang, T., and Zhang, Y. (2019). Interplays between State and Flux Hydrological Variables across Vadose Zones: A Numerical Investigation. *Water*, 11(6):1295. https://www.mdpi.com/2073-4441/11/6/1295.

Westerling, A. L., Turner, M. G., Smithwick, E. A. H., Romme, W. H., and Ryan, M. G. (2011). Continued warming could transform Greater Yellowstone fire regimes by mid-21st century. *Proceedings of the National Academy of Sciences*, 108(32):13165–13170. https://www.pnas.org/doi/full/10.1073/pnas.1110199108.

Wickham, H. (2016). *Ggplot2: Elegant Graphics for Data Analysis*. Springer-Verlag New York. https://ggplot2.tidyverse.org.

Wickham, H., Averick, M., Bryan, J., Chang, W., McGowan, L. D., François, R., Grolemund, G., Hayes, A., Henry, L., Hester, J., Kuhn, M., Pedersen, T. L., Miller, E., Bache, S. M., Müller, K., Ooms, J., Robinson, D., Seidel, D. P., Spinu, V., Takahashi, K., Vaughan, D., Wilke, C., Woo, K., and Yutani, H. (2019). Welcome to the tidyverse. *Journal of Open Source Software*, 4(43):1686.

Williams, B. K. and Brown, E. D. (2024). Managing ecosystems with resist–accept–direct (RAD). *Methods in Ecology and Evolution*, 15(5):796–805. https://onlinelibrary.wiley.com/doi/abs/10.1111/2041-210X.14309.

Young, D. J. N., Slaton, M. R., and Koltunov, A. (2023). Temperature is positively associated with tree mortality in California subalpine forests containing whitebark pine. *Ecosphere*, 14(2):e4400. https://onlinelibrary.wiley.com/doi/abs/10.1002/ecs2.4400.

Zacharakis, I. and Tsihrintzis, V. A. (2023). Environmental Forest Fire Danger Rating Systems and Indices around the Globe: A Review. *Land*, 12(1):194. https://www.mdpi.com/2073-445X/12/1/194.

Zeileis, A. and Grothendieck, G. (2005). Zoo: S3 Infrastructure for Regular and Irregular Time Series. *Journal of Statistical Software*, 14:1–27. https://doi.org/10.18637/jss.v014.i06.

Zotarelli, L., Dukes, M., Romero, C., Migliaccio, K., and Morgan, K. (2024). Step by step calculation of the penman-monteith evapotranspiration (FAO-56 method): AE459, 2/2010. *EDIS*, 2010.

Zscheischler, J., Michalak, A. M., Schwalm, C., Mahecha, M. D., Huntzinger, D. N., Reichstein, M., Berthier, G., Ciais, P., Cook, R. B., El-Masri, B., Huang, M., Ito, A., Jain, A., King, A., Lei, H., Lu, C., Mao, J., Peng, S., Poulter, B., Ricciuto, D., Shi, X., Tao, B., Tian, H., Viovy, N., Wang, W., Wei, Y., Yang, J., and Zeng, N. (2014). Impact of large-scale climate extremes on biospheric carbon fluxes: An intercomparison based on MsTMIP data. *Global Biogeochemical Cycles*, 28(6):585–600. https://onlinelibrary.wiley.com/doi/abs/10.1002/2014GB004826.